2019

UTILIZATION OF VARIOUS METHODS AND A LANDSAT NDVI/GOOGLE EARTH ENGINE PRODUCT FOR CLASSIFYING IRRIGATED LAND COVER

Andrew Nemecek
University of Montana, Missoula

Let us know how access to this document benefits you.

Recommended Citation

UTILIZATION OF VARIOUS METHODS AND A LANDSAT NDVI/GOOGLE

EARTH ENGINE PRODUCT FOR CLASSIFYING IRRIGATED LAND COVER

By

ANDREW JOHN BROWN NEMECEK

Associate of Life Sciences, Maricopa Community Colleges, Phoenix, Arizona, 2013
Bachelor of Science in Applied Biological Sciences, Arizona State University, Phoenix, Arizona, 2015

Thesis

presented in partial fulfillment of the requirements
for the degree of

Master of Science in Geography

The University of Montana
Missoula, MT

January 2019

Approved by:

Scott Whittenburg, Dean
Graduate School

Dr. David Shively, Chair
Geography

Dr. Anna Klene
Geography

Dr. Nathaniel Robinson
Franke College of Forestry and Conservation

Nemecek, Andrew, M.S., December 2018
   Geography

Utilization of Various Methods and a Landsat NDVI/Google Earth Engine Product for Classifying Irrigated Land Cover

Dr. David Shively, Chair

Methods for classifying irrigated land cover are often complex and not quickly reproducible. Further, moderate resolution time-series datasets have been consistently utilized to produce irrigated land cover products over the past decade, and the body of irrigation classification literature contains no examples of subclassification of irrigated land cover by irrigation method. Creation of geospatial irrigated land cover products with higher resolution datasets could improve reliability, and subclassification of irrigation by method could provide better information for hydrologists and climatologists attempting to model the role of irrigation in the surface-ground water cycle and the water-energy balance. This study summarizes a simple, reproducible methodology using 30-meter resolution Landsat NDVI data for classifying irrigated land cover in semi-arid western Montana by leveraging the rising availability of machine learning algorithms in geographic information systems (GIS) software programs to compare results from models constructed using Decision Trees, Random Forest, and principal components analysis. Finally, this study was an attempt to subclassify irrigated land cover into a geospatial layer that distinguishes center pivot irrigation systems from other methods. The Random Forest model was the best model for classifying irrigated land cover, validating its recent use for classifying irrigated land cover in other studies. Further, the NDVI dataset that interpolates cloud and cloud shadow pixels with a user-specified climatology provided a time-series dataset with sufficient spatial and temporal resolution for time-series irrigated land cover classification at the basin and growing season scales. This dataset provides a viable alternative to coarse resolution products often used for creation of geospatial irrigated area datasets at larger scales and an opportunity to create small-scale irrigated area datasets that provide more detailed information. Finally, subclassification of irrigation by method was unsuccessful, but availability of small-scale evapotranspiration datasets and a time-series green index dataset without cloud contamination could improve models.

TABLE OF CONTENTS

FIGURES

TABLES

INTRODUCTION

Global hunger has been in decline, but recent evidence suggests a rise, with an estimated one of nine people currently undernourished (Food and Agriculture Organization 2018). However, as the global population increases from approximately 7 billion to between 8 and 10 billion by 2050 (Lutz and Samir 2010), experts expect global income levels to rise (Rask and Rask 2010) resulting in greater food consumption (Kearney 2010). Since irrigation increases crop yields per unit cultivated area (Schürkmann, Biewald and Rolinski 2014), irrigation will play a major role in increasing food production for rising global demand. Conversion from dryland farming to irrigation and expansion of irrigation into previously uncultivated areas results in dramatic climatic, hydrologic and habitat disturbances. Some sources observe that the rate of irrigated land cover expansion is decreasing (Wada et al. 2013; Brown and Pervez 2014; Deines, Kendall and Hyndman 2017). However, Bruinsma (2003) expects area equipped for irrigation to expand and 60% of all land with irrigation potential to be in use by 2030. Net irrigated land cover may increase or decrease on a global scale, but irrigated land cover change is geospatially dynamic on a regional scale (Brown and Pervez 2014; Deines, Kendall and Hyndman 2017) due to economic influences, climate, water policy and cropping decisions (Deines, Kendall and Hyndman 2017). Irrigated land cover expansion and contraction is a form of land use change, and land use change is expected to have a profound effect on changes in biodiversity (Sala et al. 2000). Further, irrigation contributes to dramatic changes to the hydrologic systems on which humans are dependent. The World Bank (2018) estimates that 70% of global water withdrawals are for agriculture. As anthropogenic effects on hydrologic processes result in aquifer depletion and reduced stream flows (Postel 2003; Lauffenburger et al. 2018), hydrologists are beginning to better understand the ground and surface water connection

(Winter et al. 1998; Hill and Walter 2003). Additionally, irrigation forces several changes in the regional energy-water balance such as surface moisture and temperature (Weare and Du 2008). Finally, evidence suggests climate change is currently driving changes in hydrologic systems as well as regional fluctuations in temperature and precipitation, and global temperatures are expected to substantially rise as precipitation patterns drastically change (Intergovernmental Panel on Climate Change 2014). Wada et al. (2013) and Lauffenburger et al. (2018) expect climate change to increase irrigation water demand, and Lauffenburger et al. (2018) provide evidence for increasing annual evapotranspiration with a warming climate, further straining hydrologic systems (e.g., reduced groundwater recharge) on which food production depends.

Geospatial irrigation datasets are important for: water-energy budget modeling (Boucher, Myhre and Myhre 2004), modeling irrigation water demand under various climate change scenarios (Wada et al. 2013), irrigation water use and river reach water balance models (Ozdogan et al. 2006; Peña Arancibia et al. 2016), gaining insight into food security risks (Thenkabail and Wu 2012), water managers (Deines, Kendall and Hyndman 2017) and understanding behavior of producers (Deines, Kendall and Hyndman 2017). The US Department of Agriculture's (USDA) National Agriculture Statistics Service (NASS) documents county-level irrigation area in the Census of Agriculture (USDA 2018), and county-level statistics may be available from other sources. However, these statistics do not contain spatial information, and availability of regional agricultural maps or geospatial datasets is inconsistent.

Study Summary

For most irrigated land area classifications, data preprocessing is an important step. Further, data inputs are often numerous and potentially not readily available to all researchers. Also, for most recent studies, researchers use moderate resolution datasets, usually Moderate

Resolution Imaging Spectroradiometer (MODIS) products. Additionally, methodologies are often complex with sometimes dozens of steps, requiring highly skilled researchers to implement, and the software they use is not always clearly stated and/or widely utilized. Finally, no studies attempt to classify irrigation by method (e.g., surface/sprinkler or center-pivot/other method) using only time-series spectral data and automated image analysis. Different irrigation methods are associated with variable irrigation efficiencies (Howell 2003; Irmak et al. 2011) and evapotranspiration rates (Montana Department of Natural Resources and Conservation (MDNRC) 2013). Therefore, geospatial irrigation datasets that distinguish irrigation by method are potentially useful for regional hydrologic and climate models.

Due to the complex nature of the methodology required to classify irrigation on a global scale and the moderate resolution of global and continental scale geospatial irrigated land datasets, water managers, hydrologists, climatologists and geospatial analysts may want to use a simplified process and/or create these layers at a regional level. For this study, a simple process is defined as one that requires the following: (1) minimal data inputs, (2) minimal data preprocessing, (3) readily available data sources, (4) widely utilized software and (5) relatively simple image analysis models that users with basic GIS skills can implement.

The study described here tested the viability of various classifiers for irrigation classification, including machine learning algorithms (i.e., Decision Tree and Random Forest) and principal component analysis (PCA), on the Upper Clark Fork River Basin (UCFRB) of western Montana (Figure 1) using a newly available, high-resolution (30-meter), climatology-interpolated Google Earth Engine/Landsat NDVI product (Robinson et al. 2017). The aims of this study are:

1. determine which of the tested classification methods are most accurate or suitable at the study site, a semi-arid river basin;

2. develop a simple process for generating binary irrigated/unirrigated land cover maps that are applicable at least regionally (western Montana) and, perhaps, across the American West (this includes testing the viability of the Robinson et al. (2017) dataset for time-series irrigated land cover classification);

3. and attempt classification of irrigation by method (center pivot/other method) using only time-series NDVI data.

To develop a simple process, the viability of the Robinson et al. (2017) dataset for time-series irrigated area classification was tested. Use of this product requires minimal data preprocessing (i.e., projecting, integer-to-float conversion, downscaling and masking). Also, the product is readily available and easily downloadable (Figure 2 - https://ndvi.ntsg.umt.edu/), and its high resolution offers higher potential for accuracy than products generated from MODIS sensors. The only additional data inputs are a digital elevation model (DEM), land-cover product and public lands dataset, all of which are also readily available and easily downloadable (Montana State Library 2018a). Additionally, the software programs, ArcGIS and TerrSet were used to perform all analyses because they are prevalent and widely utilized at universities and/or government agencies. Finally, by automating the preprocessing workflow with arcpy and using the ArcGIS and TerrSet graphical user interfaces, a methodology was designed which is implementable by those with a basic to moderate geographic information systems skillset. This study demonstrates that proper masking, quality ground truth data and time-series NDVI data are

keys for producing regional geospatial irrigation datasets, and climate data is potentially not

necessary at the watershed or basin scale in the arid or semi-arid American West.
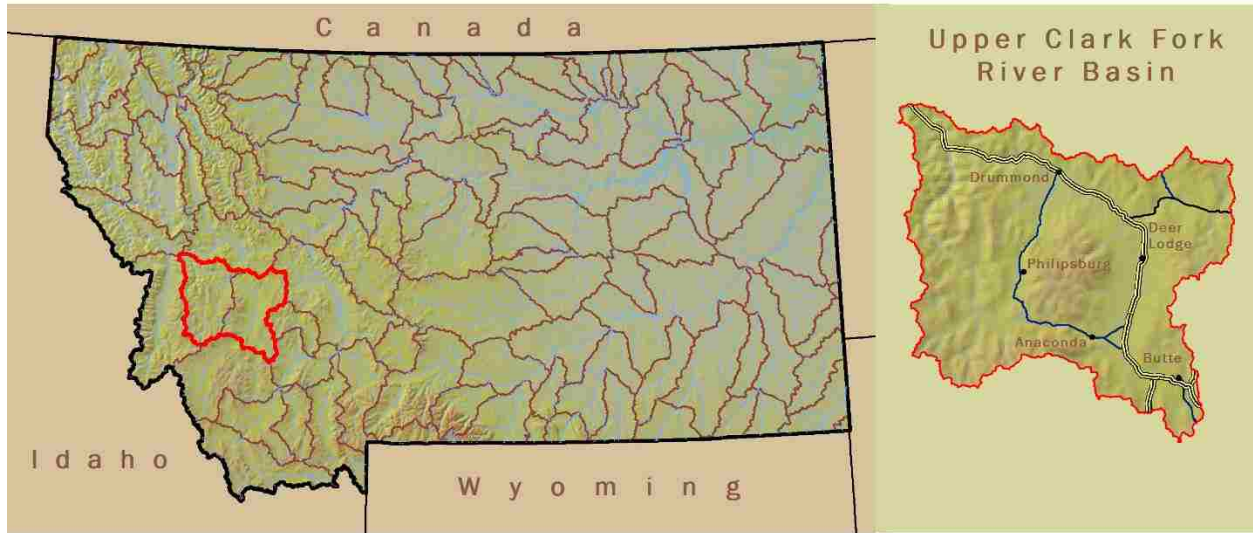
Figure 1: Study area.
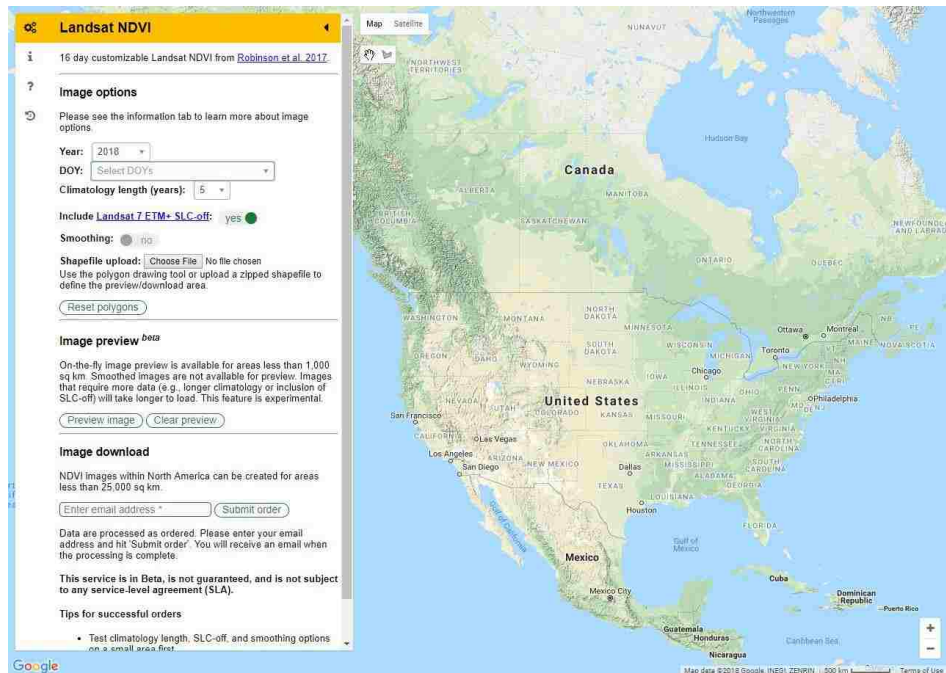
Figure 2: Robinson et al. (2017) NDVI data download page
(https://ndvi.ntsg.umt.edu/).

5

LITERATURE REVIEW

Analysis Techniques for Classifying Irrigated Areas

     Analysis techniques (i.e., models) used for creating geospatial irrigated land cover maps range from visual interpretation of imagery to complex supervised machine learning classifications. Prior to the development of digital image analysis techniques, visual interpretation of aerial or satellite imagery was the only imagery analysis option (Heimes and Luckey 1980; Thelin and Heimes 1987; MDNRC 2018). In the 1980s, Heimes and Luckey (1980) and Thelin and Heimes (1987) determined that leveraging satellite imagery was most effective for spatially extensive regions and that other methods were "too costly" and "time consuming."

     Since the 1980s, irrigated land cover classification using digital image analysis techniques has become increasingly complex. Early techniques include: separation of pixels with small digital numbers in the red band and large numbers in the infrared band into the irrigated class (Heimes and Luckey 1980; Thelin and Heimes 1987), tasseled cap with brightness-greenness decision rules (Eckhardt, Verdin and Lyford1990), supervised maximum likelihood classification (Barbosa, Casterdad and Herrero 1996) and threshold normalized difference vegetation index (NDVI) decision rule classifiers (Dappen 2003; Ozdogan et al. 2006), a predecessor to Decision Trees. Thenkabail et al. (2005) and Thenkabail et al. (2009) increased the complexity of irrigation classification by exploring various digital image analysis techniques including tasseled cap, single-date spectral angle, multi-date spectral angle, space-time spiral curves (STSCs) and development of temporal signatures. With their NDVI threshold Decision Tree, Thenkabail et al. (2009) were among the earliest researchers to explore machine learning in irrigated land classification. Irrigated land cover classification continued to evolve

following Thenkabail et al. (2005). However, some simple methods have persisted. Tian et al. (2007) questioned the necessity of complex techniques such as spectral angle mapping by comparing accuracies of the threshold NDVI method and spectral angle mapping, and Pervez and Brown (2010) also applied the NDVI threshold technique. Thenkabail et al. (2007) and Biggs et al. (2007) explored subpixel classification of irrigated areas. Finally, within the past decade, machine learning algorithms became the primary method for producing geospatial irrigation datasets (Ozdogan and Gutman 2008; Thenkabail and Wu 2012; Pervez, Budde and Rowland 2014; Salmon et al. 2015; Ambika, Wardlow and Mishra 2016; Peña-Arancibia et al. 2016; Deines, Kendall and Hyndman 2017). However, statistical techniques for classifying irrigated land cover that do not employ machine learning continue to improve and also increase in complexity (Chen et al. 2018).

Model Data

Researchers use a variety of spectral data products as model inputs for creation of geospatial irrigation datasets. Each product has its own temporal and spatial resolutions and requires some degree of preprocessing, ranging from virtually no preprocessing, for some of the latest products, to a high degree of preprocessing. Spectral products are either single images or time-series composites and multispectral or downloaded as NDVI images or converted to other indices. Additional inputs often include climate and topographical data.

Earlier studies used low temporal (one to several time steps from a growing season)/high spatial resolution (30 meters) Landsat (Heimes and Luckey 1980; Thelin and Heimes 1987; Barbosa, Casterdad and Herrero 1996; Dappen 2003; Ozdogan et al. 2006; Tian, Xie and Keller 2007), Systeme Probatoire d'Observation de la Terre (SPOT) (Eckhardt, Verdin and Lyford 1990) and/or IKONOS (Tian, Xie and Keller 2007) data for analyses varying in complexity and

achieved high accuracies. Landsat satellites have at least a 16-day return interval for every location on Earth, but atmospheric (for earlier Landsat sensors) and cloud (for all Landsat sensors) contamination reduce the usability of many Landsat images and thus the effective temporal resolution of Landsat datasets. Heimes and Luckey (1980) and Thelin and Heimes (1987) digitally analyzed only a single growing-season Landsat image. Eckhardt, Verdin and Lyford (1990) used two time-step images from each of their study's two growing seasons. Barbosa, Casterdad and Herrero (1996) used two time-step images from one growing season. Dappen (2003) used three growing-season images. Ozdogan et al. (2006) used a single image from the height of multiple growing seasons. Finally, Tian et al. (2007) used five images from a three growing seasons.

Products from earlier studies required extensive preprocessing including radiometric corrections (Eckhardt, Verdin and Lyford 1990; Barbosa, Casterdad and Herrero 1996; Ozdogan et al. 2006), atmospheric corrections (Barbosa, Casterdad and Herrero 1996; Tian, Xie and Keller 2007) and geometric corrections (Dappen 2003). Radiometric normalization was a common preprocessing step (Eckhardt, Verdin and Lyford 1990; Ozdogan et al. 2006). Barbosa, Casterdad and Herrero (1996) calculated surface reflectance since Landsat Surface Reflectance (SR) products were not available. Finally, Barbosa, Casterdad and Herrero (1996) and Tian et al. (2007) performed dark-object subtraction, an atmospheric correction.

In the previous two decades, MODIS products became the standard for irrigation classification studies. The use of MODIS sacrifices spatial resolution, and the reasons for the shift to MODIS are not definitive, but the increase in study-area size and the availability of cloud-corrected MODIS that increased temporal resolutions might explain the transition. Earlier studies utilizing high-resolution imagery as model data inputs focused on either an irrigation

district (Barbosa, Casterdad and Herrero 1996), agricultural areas in a US county (Tian, Xie and Keller 2007), US state-level regions (Eckhardt, Verdin and Lyford 1990; Dappen 2003), or a national region (Ozdogan et al. 2006). Study areas for studies that utilize MODIS as model data inputs are river basins (Thenkabail, Schull and Turral 2005; Biggs et al. 2007; Peña-Arancibia et al. 2016), the conterminous US (Ozdogan and Gutman 2008; Pervez and Brown 2010), entire nations (Thenkabail and Wu 2012; Pervez, Budde and Rowland 2014; Ambika, Wardlow and Mishra 2016), and Earth (Thenkabail et al. 2007; Thenkabail et al. 2009 and Salmon et al. 2015). Preprocessing is a characteristic of some studies utilizing MODIS (Thenkabail, Schull and Turral 2005; Pervez and Brown 2010; Pervez, Budde and Rowland 2014), but discussion of preprocessing in recent studies using MODIS data has receded (Ambika, Wardlow and Mishra 2016; Peña-Arancibia et al. 2016). Thenkabail et al. (2005) downloaded a MODIS product as an atmospherically corrected estimate of surface reflectance and then applied cloud corrections and additional aerosol corrections. Pervez and Brown (2010) and Pervez, Budde and Rowland (2014) applied temporal smoothing to minimize disturbances from cloud contamination, atmospheric perturbations, variable viewing geometry of the sensor and imperfect sensor calibration. However, most researchers have not applied radiometric, atmospheric or cloud corrections on downloaded MODIS datasets (Biggs et al. 2007; Ozdogan and Gutman 2008; Thenkabail and Wu 2012; Ambika, Wardlow and Mishra 2016; Peña-Arancibia et al. 2016). Biggs et al. (2007) utilized a pre-calibrated dataset that was cloud corrected using the maximum NDVI method. Ozdogan and Gutman (2008) utilized the Nadir Bidirectional Reflectance Distribution Function (BRDF) MODIS dataset, which is cloud screened, atmospherically corrected and corrected for view- and illumination-angle effects. Thenkabail and Wu (2012) utilized a dataset normalized to surface reflectance but did not discuss cloud corrections. Finally,

Ambika, Wardlow and Mishra (2016) and Peña-Arancibia et al. (2016) did not discuss any corrections.

The products derived from MODIS sensors on the Terra and Aqua satellites that are used for irrigation classification studies are either 8- or 16-day temporal resolution products and 250- or 500-meter spatial resolution products. Thenkabail et al. (2005), Biggs et al. (2007) Ozdogan and Gutman (2008) and Salmon et al. (2015) used 8-day, 500-meter products. Later MODIS studies used 16-day 250-meter products (Pervez, Budde and Rowland 2014; Ambika, Wardlow and Mishra 2016), a monthly 250-meter product (Peña-Arancibia et al. 2016) or 250-meter maximum NDVI value composites (Pervez and Brown 2010; Thenkabail and Wu 2012). Thenkabail and Wu (2012) utilized Landsat and MODIS datasets, combining Landsat-derived biophysical and climate data with time-series MODIS data into a single mega file data cube (MFDC) which they subsequently resampled and inputted into a model. Finally, one global irrigation classification study did not use MODIS. Instead, it utilized 10-kilometer Advanced Very High Resolution Radiometer and 1-kilometer SPOT products as model data inputs to create the Global Irrigated Area Map (GIAM) (Thenkabail et al. 2009).

In addition to spectral data, researchers use climate data, biophysical vegetation data, topographic data, land cover data and other data as inputs for irrigation classification models. Non-spectral data inputs are used for masking, which requires incorporating them into classification workflows, but non-spectral data are also inputted into models. Thenkabail et al. (2009) combined the Global 30 Arc-Second Elevation Dataset, rainfall data, forest cover data and Japanese Earth Resources Satellite Synthetic Aperture Radar data with spectral data inputs into a 159-layer MFDC. The MFDC was the data used for a complex multi-stage classification procedure supplemented by multiple secondary data sources for masking, training and validation.

The process began with masking and progressed through image segmentation, unsupervised ISOCLASS clustering, generation of class spectra, spectral matching, grouping of similar classes, class identification and labeling, identification with bi-spectral plots and STSCs, Decision Tree classification and, finally, validation. Thenkabail and Wu (2012) combined biomass, leaf area index, chlorophyll absorption, moisture sensitivity, thermal emissivity, elevation and slope data with time-series MODIS data for their model. Finally, Salmon et al. (2015) inputted MODIS-derived land-surface temperature data, WORLDCLIM climate data, climate moisture index data, average annual moisture index data, agroecozone maps and hemispheric code index data with spectral data into their Decision Tree model.

A recent study in the Great Plains region signals a shift back to high-resolution Landsat imagery for creation of geospatial irrigated land datasets. Deines, Kendall and Hyndman (2017) transformed Landsat SR imagery products from November 1998 to October 2016 to multiple indices and inputted those images with DEMs, total plant available water storage data, precipitation data, potential evapotranspiration data and Palmer Drought Severity Index data into a Random Forest model. Landsat SR products are the highest quality Landsat products, accounting for artifacts from the atmosphere, illumination and viewing geometry (US Department of the Interior (USDI) 2018a; USDI 2018b). They are ready for time-series analysis upon downloading. However, they are not cloud corrected, and cloud correction is a common characteristic of MODIS data.

Masking

Masks eliminate areas that are not irrigable from irrigation classifications, thus reducing potential for model errors. Land cover masks eliminate classes that are spectrally similar with irrigation but not irrigable (e.g., coniferous forest). They also eliminate classes that are

nominally, and perhaps spectrally, not confused with irrigation (e.g., water). Researchers often mask irrigable areas such as meadows, riparian areas, wetlands and rangeland from their analyses (Dappen 2003; Tian, Xie and Keller 2007; Pervez and Brown 2010; Pervez, Budde and Rowland 2014; Salmon et al. 2015; Ambika, Wardlow and Mishra 2016; Deines, Kendall and Hyndman 2017). However, due to the irrigable nature of meadows, riparian areas, rangeland and other classes, including these classes in areas-of-interest makes analyses suitable for monitoring spatial change in irrigated land cover, and excluding them makes irrigation classification analyses more dependent on the quality of land cover products. The quality and age of land cover data used for masking may determine if irrigable (potentially irrigated) areas are omitted from the area-of-interest in error. However, researchers can eliminate some areas from irrigation classifications with reasonable confidence that they are not eliminating irrigable pixels from analyses. Areas with slope > 20% are not irrigable and are often masked (Pervez, Budde and Rowland 2014; Ambika, Wardlow and Mishra 2016). Finally, public land that usually protects high-elevation, less-productive areas (e.g., US Forest Service (USFS) coniferous forest land) is not irrigable and thus eligible for masking, but researchers should only remove public land from analyses after careful consideration. For example, in western Montana, USFS land generally protects not irrigable high-elevation coniferous forest and alpine areas.

Although several studies include non-agricultural land cover in their areas-of-interest (Thenkabail and Wu 2012, Salmon et al. 2015; Deines, Kendall and Hyndman 2017), thus allowing models to distinguish between agricultural and non-agricultural land cover, many researchers attempt to completely mask non-agricultural land cover from their study areas (Dappen 2003; Pervez and Brown 2010; Salmon et al. 2015; Ambika, Wardlow and Mishra 2016). However, other studies target specific areas such as forest cover (Thenkabail et al. 2009;

12

Pervez, Budde and Rowland 2014; Deines, Kendall and Hyndman 2017), rangeland (Pervez,

Budde and Rowland 2014), wetlands (Deines, Kendall and Hyndman 2017), desert (Tian, Xie

and Keller 2007), urban/residential areas (Tian, Xie and Keller 2007; Deines, Kendall and

Hyndman 2017), roads (Tian, Xie and Keller 2007), and fallow land (Tian, Xie and Keller 2007).

Researchers also commonly use topographical data for masking. Biggs et al. (2007) masked

elevations > 630 meters, and Pervez, Budde and Rowland (2014) and Ambika, Wardlow and

Mishra (2016) masked slope > 20%. Ozdogan and Gutman (2008) and Thenkabail et al. (2009)

used climate data for masking. Finally, other criteria also determine eligibility for masking such

as spectrally-mixed areas (Biggs et al. 2007).

Training and Validation Data

      Training and validation data are key components for irrigated land cover classification.

Field-verified training and validation data collected for specific studies were important before

existing datasets became widely available. Visual field verification was a common early method

for generating training and validation data (Dappen 2003; Thenkabail, Schull and Turral 2005;

Ozdogan and Gutman 2006; Biggs et al. 2007; Tian, Xie and Keller 2007). Ozdogan and

Gutman (2006) supplemented visual field verification via interviews with farmers. Random and

systematic sampling in large regions is costly, and some areas are practically inaccessible due to

rough terrain, lack of roads, etc. (Thenkabail, Schull and Turral 2005). Thenkabail, Schull and

Turral (2005) stratified sampling by access through roads and foot paths and randomized by

locating sites every few minutes. At each point, they recorded photos, land cover class based on

the Anderson et al. (1976) system, percentage of land cover type, crop type, crop pattern, crop

calendar and water source. As the availability of field-verified data increased, the need to

perform study-specific field verifications decreases. Thenkabail et al. (2009) used existing

global field-verified datasets, thus eliminating the need to collect field data for their study. Pervez and Brown (2010) used existing field-verified data from California Department of Water Resources and University of North Dakota.

As high-resolution imagery became widely available and existing remotely-sensed products improved, researchers shifted to visually interpreting imagery and using existing land cover products, agricultural statistics, climate data and irrigated area maps. Thenkabail and Wu (2012) used only high-resolution imagery for training and validation. Ozdogan and Gutman (2008) used high-resolution imagery, existing irrigated area maps, climate data, state reports and the internet for training and validation. Pervez, Budde and Rowland (2014) used high-resolution imagery and surface-temperature data for both training and validation. Salmon et al. (2015) used Google Earth imagery with land cover data, ecological zone data, the GIAM and time-series climate data to train and validate. Ambika, Wardlow and Mishra (2016) used land cover and ecological zone data, existing spectral profile data, agricultural statistics and high-resolution imagery. Peña-Arancibia et al. (2016) used Landsat to select training pixels and agricultural statistics for validation. Deines, Kendall and Hyndman (2017) used crop maps and National Aerial Imagery Program and Landsat imagery to train their model and agricultural statistics, water use data and randomly generated points to validate their classifications.

Output Classes and Accuracies

The number of classes in geospatial irrigation datasets varies widely. Binary products are those with irrigated/unirrigated classes, and non-binary products have either multiple irrigated and/or unirrigated classes. A binary product could include multiple irrigated subclasses (Thenkabail et al. 2009). However, most products are simple irrigated/unirrigated outputs (Dappen 2003; Ozdogan et al. 2006; Tian, Xie and Keller 2007; Ozdogan and Gutman 2008;

Pervez and Brown 2010; Pervez, Budde and Rowland 2014; Peña-Arancibia et al. 2016; Deines, Kendall and Hyndman 2017).

Non-binary products are common. Unirrigated classes in non-binary products include water, herbaceous rangeland and dry cropland (Heimes and Luckey 1980; Thelin and Heimes 1987), an unknown class (Eckhardt, Verdin and Lyford 1990), rainfed crops (Thenkabail and Wu 2012; Salmon et al. 2015), other (Thenkabail and Wu 2012) and, finally, non-irrigated and non-cropland (Ambika, Wardlow and Mishra 2016). Irrigated classes in non-binary products include the simple irrigated class (Heimes and Luckey 1980; Thelin and Heimes 1987; Eckhardt, Verdin and Lyford 1990; Barbosa, Casterdad and Herrero 1996; Biggs et al. 2007; Thenkabail and Wu 2012; Ambika, Wardlow and Mishra 2016), irrigated and supplemental irrigation (Thenkabail, Schull and Turral 2005) and irrigated and paddy croplands (Salmon et al. 2015).

Methods for assessing product accuracy are variable, and accuracies are wide ranging. Error/confusion matrices are the most common accuracy assessment tool (Eckhardt, Verdin and Lyford 1990; Barbosa, Casterdad and Herrero 1996; Dappen 2003; Ozdogan et al. 2006; Thenkabail, Schull and Turral 2005; Tian, Xie and Keller 2007; Thenkabail et al. 2007; Ozdogan and Gutman 2008; Thenkabail et al. 2009; Pervez and Brown 2010; Thenkabail and Wu 2012; Salmon et al. 2015; Deines, Kendall and Hyndman 2017). Heimes and Luckey (1980) and Thelin and Heimes (1987) did not quantify their accuracies, instead relying on visual interpretation. Overall accuracies > 90% from error matrices are common (Eckhardt, Verdin and Lyford 1990; Ozdogan et al. 2006; Thenkabail, Schull and Turral 2005; Tian, Xie and Keller 2007; Thenkabail et al. 2009; Pervez and Brown 2010; Thenkabail and Wu 2012; Deines, Kendall and Hyndman 2017). Accuracies within single studies can vary by region. Ozdogan and Gutman (2008) achieved 87% overall accuracy in the western US and 79% in the eastern

US, and Pervez and Brown (2010) achieved overall accuracies of 92% in California and 75% in the Great Plains region, suggesting that irrigated area classifications are more accurate in the arid or semi-arid western US. Finally, accuracies can vary widely across classes. Thenkabail et al. (2005) mapped many classes, achieving a range of 56-100% accuracy across all classes, but most of their classes were 80-100% accurate.

Validation methods other than error matrices included comparisons with agricultural statistics, comparisons with existing geospatial irrigation datasets, pixel-window methods for subpixel classifications, Bayesian prior-probability validations and STSCs. Biggs et al. (2007) measured different degrees of correctness over each pixel. Thenkabail et al. (2007) compared their acreage estimates with agricultural statistics using linear regression. Pervez et al. (2014) made simple acreage estimate comparisons with national and global irrigated land cover datasets and further made comparisons with a secondary Landsat-based classification. Salmon et al. (2015) applied a Bayesian method by estimating prior probabilities for the presence of irrigated, rainfed and paddy croplands and performed cross validation with existing datasets. Ambika, Wardlow and Mishra (2016) compared their estimates with agricultural statistics and utilized STSCs for validation. Finally, Peña-Arancibia et al. (2016) and Deines, Kendall and Hyndman (2017) compared their estimates with agricultural statistics.

METHODS & STUDY AREA

Study Area

The UCFRB is part of the Clark Fork watershed, which contributes to the northern headwaters of the Columbia River system in Montana (Figure 3). The UCFRB is 9559 km^2 and dominated by USFS land in its mountainous areas. Public and private land covers its foothills
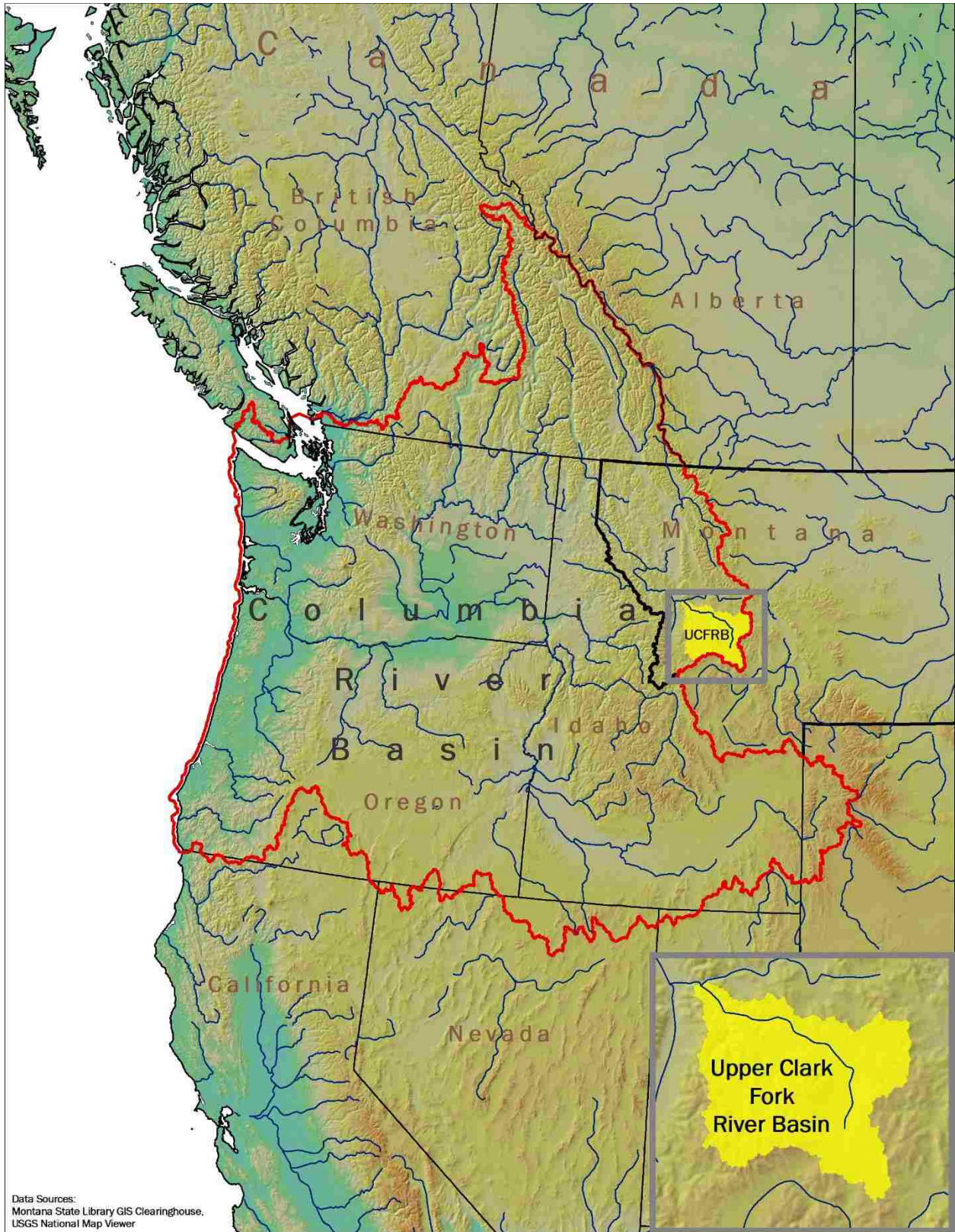
Figure 3: Position of the study area in the Columbia River Basin.

and valleys where irrigated forage/hay is the dominant crop. The Clark Fork River is the largest by volume in Montana, sustaining ecosystems, agriculture, recreation, and water for other human-related beneficial uses. The Clark Fork begins near Butte, Montana where Silver Bow and Warm Springs Creeks merge.

The UCFRB was selected as a study region for several reasons. Producers in the UCFRB utilize a wide array of irrigation practices including flood irrigation and multiple forms of sprinkler irrigation (hand line, center pivot, etc.). Most crop production from the basin is forage (i.e., grass, hay, alfalfa) (USDA 2014), thus narrowing the range of spectral variability attributable to crop species. Further, the UCFRB is characteristic of western Montana river basins as it contains a patchwork of "surficial" (alluvial) aquifers (Montana State Library 2018b), potentially exacerbating the role played by irrigation in the hydrologic cycle (Winter et al. 1998). Finally, the UCFRB is within 100 miles of Missoula, Montana, where most of this research initiated, making it a convenient location for field verification.

Defining Irrigation

For this study, irrigation is defined as the artificial application of water to crops at least once during the growing season. Harvests do not affect the definition of irrigation. Although, including harvest as a definitional criterion may increase the accuracy of classifications because harvests are associated with abrupt declines in NDVI, and model algorithms may better distinguish between irrigated and unirrigated land cover if they are only trained with irrigated points associated with harvest. However, including harvests as a requirement or criterion would exclude pasture irrigated only for grazing.

Models

In the past decade, machine learning algorithms have become the primary classifier for irrigated land cover classifications. Decision Trees were the first machine learning algorithms used for irrigation classification (Ozdogan and Gutman 2008; Thenkabail et al. 2009; Thenkabail and Wu 2012; Pervez et al. 2014; Salmon et al. 2015; Ambika, Wardlow and Mishra 2016). Decision Trees are non-parametric supervised learning models that utilize either expert-knowledge- or algorithm-derived Boolean decision rules for classification. They form a tree-like structure, beginning at the root and proceeding through branches which split from nodes (decision rules) and terminate at leaves (decisions/classes). Each case (i.e., pixel) is processed through this tree). More recently, researchers are utilizing Random Forests (Peña-Arancibia et al. 2016; Deines, Kendall and Hyndman 2017), an ensemble learning method which constructs multiple decision trees of variable structure through which each pixel is run. The mode of classes output from all trees is the class assigned to a pixel, or the output is probabilistic (proportions of trees allocating pixels to each class). Principal Component Analysis is a statistical technique used to explain variance among predictor variables in n-dimensional space. Though the literature review did not uncover the use of PCA for irrigation classification, the method was thought to have promise for distinguishing irrigated lands relative to all other land cover classes based on a predicted high rate of variance of spectral signatures, and so was also employed.

For this study, the Random Forest model (Breiman 2001) was utilized to test the viability of the Robinson et al. (2017) dataset for irrigation classification. The Rocky Mountain Research Station (RMRS) Raster Utility (https://www.fs.fed.us/rm/raster-utility/) ArcGIS add-in toolbar Random Forest model (Hogland and Anderson 2017) was used to conduct the three analyses for

both irrigated/unirrigated and center pivot/other method classifications (a total of 6 analyses). After the initial series of classifications, Random Forests were also employed to mitigate the issue of misclassified pixels on the edges of analysis areas. Peña-Arancibia et al. (2016) and Deines, Kendall and Hyndman (2017) used Random Forests for their irrigated land cover classifications. The second model was the C4.5 Decision Tree (Quinlan 1993) and was applied in TerrSet to perform a single analysis, the analysis with the most accurate results of the six random-forest tested analyses, for a binary irrigated/unirrigated classification. Ozdogan and Gutman (2008) and Salmon et al. (2015) used the C4.5 Decision Tree algorithm for their irrigated land cover classifications. Finally, a PCA with RMRS tools using data from the Random Forest analysis that yielded the most accurate results was performed to determine if PCA is a viable analysis for irrigation classification.

Data

The availability of highly preprocessed, free and downloadable Landsat SR data and MODIS products have made image corrections a less time-consuming or non-existent step in irrigation classification. However, clouds and cloud shadows still present a problem for Landsat-based time-series analyses which require clear pixels at every location for each time step of the pixels' spectro-temporal profiles. Most irrigation classifications use complete time-series datasets, and if researchers select individual time-step images for their analysis, they select clear images. Pre-applied cloud corrections make MODIS datasets appealing for irrigation classification. Most researchers creating geospatial irrigated land datasets in the past two decades used 250- or 500-meter MODIS data as the primary spectral inputs to their models. Product accuracies will increase if use of Landsat SR data for irrigation classification becomes

the standard, but cloud-corrected Landsat SR time-series composite datasets are not available for download by the public.

A new Landsat-derived dataset (Robinson et al. 2017) produced by transforming Landsat SR products into an interpolated 16-day NDVI composite dataset is free and downloadable (https://ndvi.ntsg.umt.edu/). The interpolation process depends on the quality band included with each SR scene. This quality band includes pixel data quality flag information, and Robinson et al. (2017) utilized that pixel quality information to create their product covering the conterminous US with Google Earth Engine. Their program calculates a mean NDVI at a location using all clear pixels from overlapping images at that location. If no pixels within a 16-day timeframe at a location are clear, then the program populates the pixel digital number at that location using a climatology-interpolated value. The program calculates climatology as the median NDVI of clear and water-and-snow pixels over the same 16-day period from previous years. The user specifies climatology length (e.g., 2 years, 5 years, etc.) before downloading data. If climatology data is not available for the specified climatology length, then the pixel is filled with a no-data value. Each 16-day composite image contains no cloud or cloud shadow.

Land cover and topographical data is common in masking. An updated Northwest ReGAP project land cover product downloaded from Montana State Library (2018a) was used to mask target land cover classes, and a slope mask was also employed. The baseline Northwest ReGAP product is derived from Landsat imagery obtained between 1999 and 2001. The product uses the Anderson et al. (1976) land cover class system and was last updated in December 2015. The slope mask was created using the 1/3 arc-second resolution National Elevation Dataset DEMs downloaded from the National Map Viewer (US Geological Survey (USGS) 2018). Finally, to mask USFS land, a public lands dataset downloaded from the Montana State Library

(MSL) GIS Clearinghouse (MSL 2018a) was used. The public lands dataset is derived from the Montana Cadastral Parcel layer created for the Montana Department of Revenue.

NDVI

The most common index used for irrigation classification is the NDVI (Dappen 2003; Ozdogan et al. 2006; Thenkabail, Schull and Turral 2005; Biggs et al. 2007; Thenkabail et al. 2007; Tian, Xie and Keller 2007; Thenkabail et al. 2009; Thenkabail and Wu 2012; Pervez and Brown 2010; Pervez, Budde and Rowland 2014; Ambika, Wardlow and Mishra 2016; Peña-Arancibia et al. 2016; Deines, Kendall and Hyndman 2017). Other recent studies incorporate a variety of indices such as the Green Index (Ozdogan and Gutman 2008; Deines, Kendall and Hyndman 2017), Enhanced Vegetation Index (Salmon et al. 2015; Deines, Kendall and Hyndman 2017), Normalized Difference Wetness Index (Salmon et al. 2015; Deines, Kendall and Hyndman 2017) and Normalized Difference Infrared Index (Salmon et al. 2015).

Tucker (1979) demonstrated the utility of using red and NIR linear combinations to monitor green leaf area and biomass. Since that demonstration, NDVI, calculated as

$$\frac{NIR - Red}{NIR + Red},$$

is the most popular index for monitoring vegetation (Robinson et al. 2017). Schwartz (1994) demonstrated that NDVI is useful for monitoring vegetation phenology, and Wiegand, Everitt and Richardson (1992) showed correlation of NDVI with crop yield. Average growing season NDVI values are also highly correlated with growing-season precipitation across multiple land-cover types (Wang, Rich and Price 2003). Finally, researchers have used NDVI to successfully classify irrigated land cover for over a decade (Dappen 2003; Ozdogan et al. 2006; Thenkabail, Schull and Turral 2005; Biggs et al. 2007; Thenkabail et al. 2007; Tian, Xie and Keller 2007; Thenkabail et al. 2009; Thenkabail and Wu 2012; Pervez and Brown 2010; Pervez, Budde and

Rowland 2014; Ambika, Wardlow and Mishra 2016; Peña-Arancibia et al. 2016; Deines,

Kendall and Hyndman 2017).

Masks and Preprocessing

The preprocessing and masking workflow (outlined in Figure 4) was mostly scripted in

arcpy to promote efficiency, consistency, and to produce a repeatable workflow for other

applications.
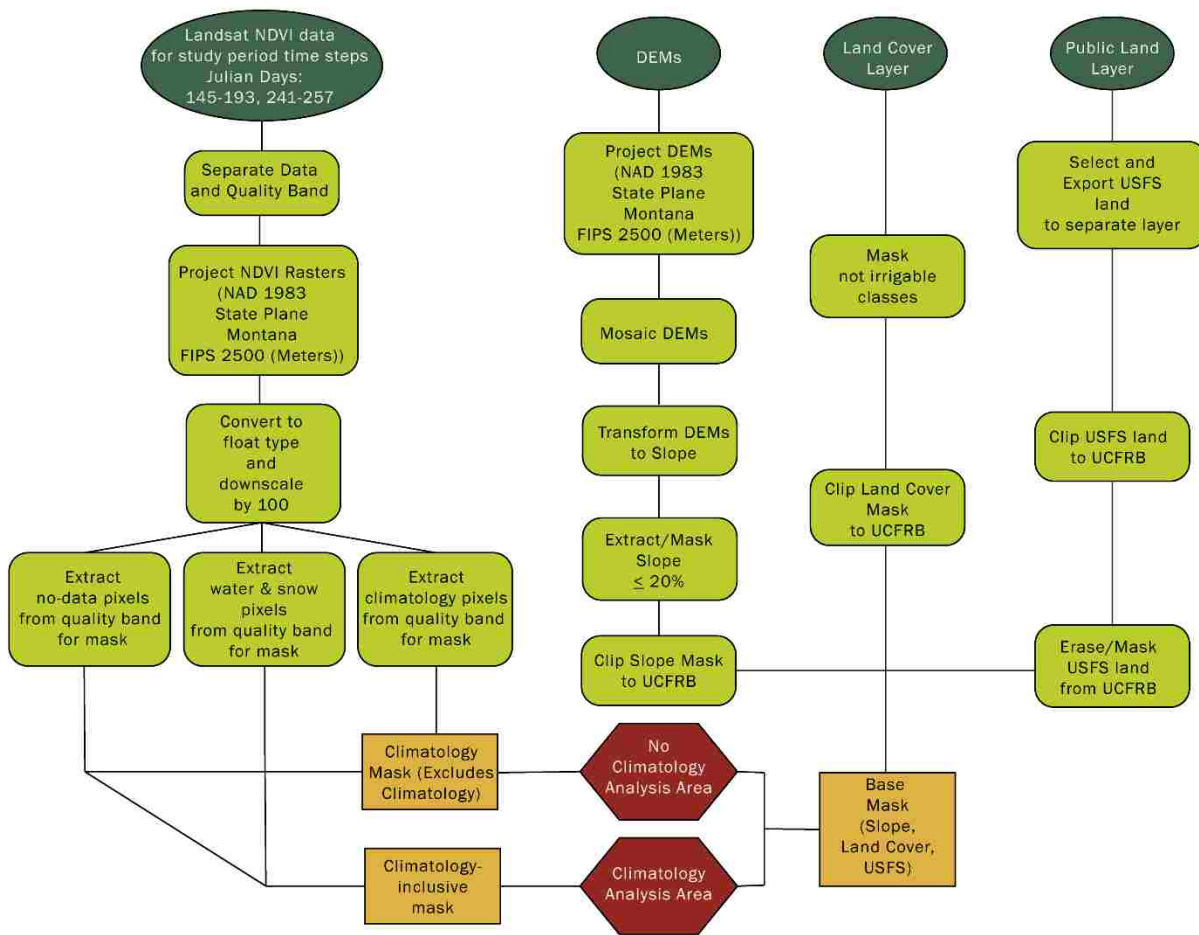
Figure 4: Preprocessing and masking workflow.

The DEM, converted to slope percentage, was used to mask areas with slope > 20%, and the

Montana public lands layer was used for masking USFS land. Finally, the land cover layer was

used to mask five classes (Table 1) and further remove any classes with $\leq$ 1000 pixels in the study area because they were not adequately represented in the study area and were difficult to sample. Land cover class masking was performed to eliminate areas that may be spectrally similar to irrigated land cover but are not irrigable (e.g., coniferous forest, water, etc.). Not irrigable classes that are spectrally similar with irrigated land are the most important to mask. Due to the potential irrigability of meadows, riparian areas, rangeland and other classes, including these classes in analysis areas makes analyses suitable for monitoring spatial change in irrigated land cover over time. Since these areas are irrigable, exclusion of them via a land cover

Table 1: Land cover product classes used to delineate analysis areas.

Class (level 2 – USDI (1976))	Masking status (masked/not masked)
Open Water	Masked
Cliff, Canyon and Talus	
Alpine Sparse and Barren	
Conifer dominated forest and woodland	
Alpine Grassland and Shrubland	
Developed	Not masked
Mining and Resource Extraction	
Agriculture	
Bluff, Badland and Dune	
Deciduous dominated forest and woodland	
Mixed deciduous/coniferous forest and woodland	
Scrub and Dwarf Shrubland	
Deciduous Shrubland	
Sagebrush Steppe	
Montane Grassland	
Lowland/Prairie Grassland	
Introduced Vegetation	
Recently burned	
Harvested Forest	
Floodplain and Riparian	
Forested Marsh	
Depressional Wetland	
Mining and Resource Extraction	
Insect-Killed Forest	

product introduces opportunity to exclude irrigated land cover from final products, because land cover products are not always updated. Once the slope, USFS and land cover masks were created, they were merged into a base mask (Figure 5), which was the mask combined with quality band masks for all subsequent analyses. Finally, following initial classifications, I masked additional classes that models frequently and mistakenly classified as irrigated on the edges of analysis areas. These classes shared spectral characteristics with the irrigated class and/or were under-sampled during training and validation point sampling. Eight level 1 classes within the level 2 Deciduous Shrubland (Northern Rocky Mountain Montane-Foothill Deciduous Shrubland), Sagebrush Steppe (Intermountain Basins Montane Sagebrush Steppe), Montane Grassland (Rocky Mountain Subalpine-Montane Mesic Meadow), Recently Burned (Post-Fire Recovery), Harvested Forest (Tree, Shrub and Grass Regeneration) and Floodplain and Riparian (Northern Rocky Mountain Lower Montane Riparian Woodland and Shrubland) classes were masked from the most accurate Random Forest product to improve results.

The use of the Robinson et al. (2017) dataset eliminates the need for image corrections, and the quality band downloaded with each corresponding image allows for a simple and efficient masking process. The dataset makes Landsat-derived NDVI data available at 16 Julian day intervals. This study utilized 11 time-step data points for the UCFRB from a 2018 study period ranging from Julian dates 97-257 (April 7-September 14). Julian days 145, 161, 177, 193, 241 and 257 were selected as the dates for independent time-step model variables/raster images. A two-year climatology period was established, so the data at climatology pixels may include median NDVI values from 2017 or 2016. Also, the no-smoothing option was selected (for more information about smoothing, see Robinson et al. 2017). Each image was downloaded in the World Geodetic System 1984 geographic coordinate system.

Service Layer Credits: Source: Esri,
DigitalGlobe, GeoEye, Earthstar Geographics,
CNES/Airbus DS, USDA, USGS, AEX,
Getmapping, Aerogrid, IGN, IGP, swisstopo,
and the GIS User Community

Figure 5. Base mask: mask of selected land cover classes, slope and USFS land; analysis area prior to masking climatology, no data and/or water and snow pixels.

Each image's quality band was inspected to assess the proportion of area covered by no-data, water-and-snow, and climatology pixels. Certain images during the 2018 growing season were dominated by either no-data, water-and-snow, climatology pixels, or some combination of those categories in agricultural areas. No-data, water-and-snow and climatology masks from each time step were overlaid, visually inspected, and images with quality-band masks that covered significant portions of agricultural areas from the analysis were removed (Julian days 97, 113,

129 and 225). Finally, day 209 was removed, because a portion of the study area was absent from the data. Therefore, the study period was Julian days 145-193, 241-257. Climatology pixels still covered a large proportion of the study area after removing five of the time steps from the study, suggesting the utility of Robinson et al. (2017) dataset is dependent on the usability of climatology data (Figure 6). For each model, the same study period (i.e., same set of variables) was used for comparison purposes.

Once selected, each time-step NDVI raster of the study period required some simple preprocessing. First, the quality and NDVI bands were separated. Then, each image was projected to the North American Datum 1983 State Plane Montana FIPS 2500 (Meters) projection. Next, each 16-bit, signed-integer NDVI raster was converted to a 32-bit, floating-point raster, and, since Robinson et al. (2017) NDVI values are multiplied by 100, each raster was downscaled by 100. Finally, all no-data pixels, water-and-snow pixels and climatology pixels were extracted to separate no-data, water-and-snow and climatology rasters (Figure 6) to be used for masking with the base mask (Figure 5). As with the climatology locations, any location was considered a no-data and/or a water-and-snow location if any time-step pixel at that location included either a no-data value, water-and-snow value or both in its spectro-temporal profile.

One aim of this study was to test the viability of the Robinson et al. (2017) dataset for time-series irrigated land cover classification, and one important aspect of testing this dataset is to compare accuracies of products generated using climatology data with products generated without use of climatology data. Since, a climatology location is specified if any time-step of its spectro-temporal profile was a climatology pixel, to make this comparison, any pixel with at least one climatology time step was masked prior to one classification but not masked for the

7,721 square kilometers masked

Climatology
Mask

2,576 square kilometers masked

No Data
Mask

283 square kilometers masked

Water & Snow
Mask

Climatology Mask

Climatology Inclusive Mask

8,657 square kilometers masked

2,728 square kilometers masked

Service Layer Credits: Source: Esri, DigitalGlobe, GeoEye, Earthstar Geographics, CNES/Airbus DS, USDA, USGS, AEX, Getmapping, Aerogrid, IGN, IGP, swisstopo, and the GIS User Community
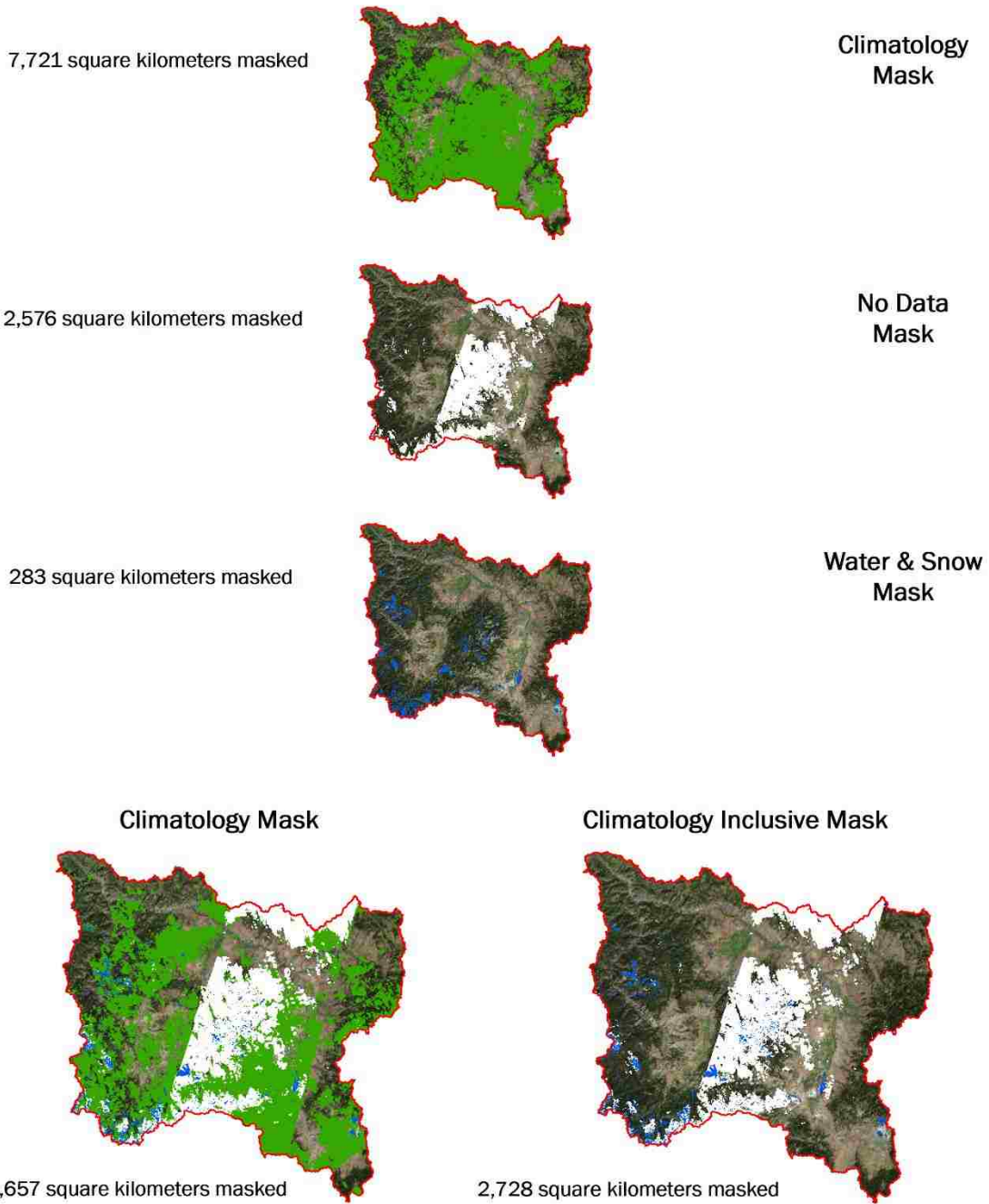
Figure 6. Landsat NDVI quality band masks: no data and water and snow mask later combined with base mask for all analyses (climatology-inclusive mask); climatology mask later combined with base mask and then used to create analysis areas for analyses that exclude climatology pixels (climatology mask).

other two classifications. For the Random Forest models, three classification analyses were conducted for a binary (irrigated/unirrigated (Irrig/Unirrig)) classification, and three classifications for a binary (center pivot/other method (CP/OM)) classification: (1) model training with no-climatology (NoClim) data (base mask, climatology, no-data and water-and-snow pixels masked) followed by classification of NoClim data (train NoClim & classify NoClim), (2) model training with NoClim data followed by classification on climatology (Clim) data (base mask, no-data and water-and-snow pixels masked) (train NoClim & classify Clim) and (3) model training with Clim data followed by classification on Clim data (train Clim & classify Clim) (Table 2). Thus, each Random Forest analysis and the subsequent Decision Tree and PCA analyses are organized and defined by the TVPs and analysis area used for training, the analysis area which was classified and the binary classes of the product (Table 2).

Since Clim data was masked from some analyses and included in others, and center pivot analyses were performed on only irrigated land cover areas produced from Irrig/Unirrig classifications, analysis areas for the defined study period vary (Figure 7). Further, since each analysis was performed for an Irrig/Unirrig and CP/OM classification, initially, a total of six Random Forest analyses were performed for comparison purposes (Table 2). An additional Random Forest analysis was performed following initial classifications to mitigate misclassification issues. This additional Random Forest model was trained with six classes (Developed, Disturbance, Forest, Irrigated, Meadow, Shrub-Grasslands). For the Decision Tree model, only the train Clim & classify Clim data analysis was performed for an Irrig/Unirrig classification (Table 2), since that analysis yielded the best results of the three Random Forest classification analyses, and results from all CP/OM analyses were questionable. Finally, since PCA requires no training data, a simple Clim data analysis was performed (Table 2).

Table 2: Model, training data, classification data and product classes of eight analyses (six Random Forest analysis, one decision tree analysis and one Principal Component Analysis).

Analyses			
Model	**Training Data**	**Classification Data**	**Product Classes**
Random Forest	NoClim	NoClim	Irrig/Unirrig
			CP/OM
	NoClim	Clim	Irrig/Unirrig
			CP/OM
	Clim	Clim	Irrig/Unirrig
			CP/OM
Random Forest	Clim	Clim	Developed, Disturbance, Forest, Irrigated, Meadow, Shrub-Grasslands
Decision Tree	Clim	Clim	Irrig/Unirrig
PCA	NA	Clim	Irrig/Unirrig

(a) NoClim analysis area for training and classification (Irrig/Unirrig)

1,477 square kilometers (15% of study area)

Irrigated NoClim analysis area for training and classification (CP/OM)

339 square kilometers (4% of study area)

(b)

NoClim analysis area for training (Irrig/Unirrig) - 1,477 square kilometers (15% of study area)

Clim analysis area for classification (Irrig/Unirrig) - 2,636 square kilometers (28% of study area)

Irrigated NoClim analysis area for training (CP/OM) - 252 square kilometers (3% of study area)

Irrigated Clim analysis area for classification (CP/OM) - 422 square kilometers (4% of study area)

(c) Clim analysis area for training and classification (Irrig/Unirrig)

2,636 square kilometers (28% of study area)

Irrigated Clim analysis area for training and classification (CP/OM)
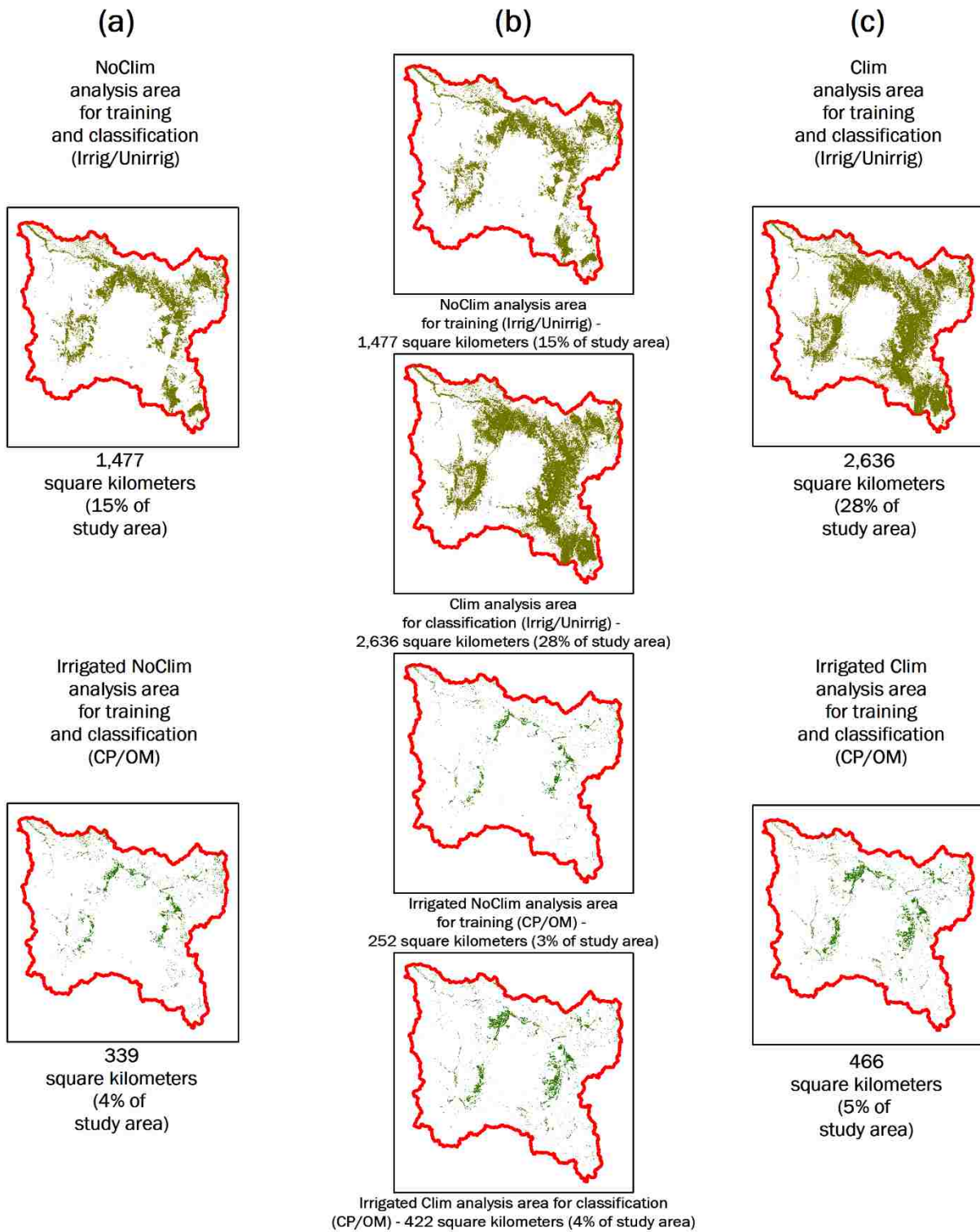
466 square kilometers (5% of study area)

Figure 7. Analysis areas: (a) NoClim training and analysis areas; (b) NoClim training areas and Clim classification areas; (c) Clim training and analysis areas.

31

Training and Validation

Training is a vital step in irrigation classification. Recent studies either use high-resolution imagery and existing datasets exclusively or a combination of field-verified data and other sources. Here, field-verified data and high-resolution imagery from Planet Labs (2018) were used, and separate sampling strategies were employed for irrigated and unirrigated points.

For irrigated points, three strategies for verifying data in the field were employed: opportunistic sampling, expert-knowledge sampling and systematic sampling. Opportunistic sampling was conducted on the Montana State Prison (MSP) Ranch and Clark Fork Coalition Ranch property. When on these properties, if irrigation was observed, points were marked with a handheld GPS unit or using the Google Earth and Adobe Sketch applications. For expert-knowledge sampling, a MSP Ranch Manager marked priority irrigation points in the Google Earth and Adobe Sketch applications. Priority irrigation points were those for which verify through systematic sampling was not practical or not attempted. These included flood-irrigation points and early-season irrigated points. Finally, most training and validation irrigated points were established and sampled through systematic sampling. For this study, systematic sampling was a structured approach to sampling for irrigated points along roads, like the approach employed by Thenkabail et al. (2005). A roads sampling layer was created from a spatial roads dataset (Montana State Library 2018a) that was overlaid on NAIP imagery to identify all public roads intersecting agricultural areas (Figure 8). Each of these roads were transited once (to create equal sampling effort) from June 25, 2018 to August 31, 2018, and active irrigation locations (i.e., sites with visible crop production and irrigation equipment/ditches) were recorded using the Google Earth and Adobe Sketch applications (Figure 9). Flood irrigation was difficult to confirm, because it is easily confused with natural flooding or not observable in tall

vegetation. Following field verification, Planet Labs high-resolution imagery was used to assign

harvest dates to each point for the years 2016-2018. Using Clim data requires interpolating

values from 2017 and 2016 into 2018 time-step data layers. Therefore, the irrigated training and

validation points (TVPs) were organized into two subsets, those verified as irrigated in 2018

only, and those verified as irrigated from 2016-2018. Most points are shared between both

subsets, with the 2018 subset being inclusive, and the 2016-2018 subset being exclusive (Figure

10). Employing all sampling methods, 120 irrigated points for 2018 were retained, and 91

irrigated points for 2016-2018 were retained.

Each point was verified between May and August

2018 (Figure 11) using all three irrigated sampling

strategies (Figure 12). For 2018 (NoClim analysis

points), prior to base masking and climatology,

no-data and water-and-snow pixel masking, 15

flood-irrigated points, 34 hand-line irrigated

points, 16 wheel-line irrigated points and 53

center-pivot irrigated points were retained (Table

3). For 2016-2018 (Clim analysis points), prior to

Figure 8: Roads sampled for irrigated and unirrigated points.

base masking and no-data and water-and-snow pixel masking, nine flood-irrigated points, 25

hand-line irrigated points, 14 wheel-line irrigated points and 41 center-pivot irrigated points were

retained (Table 3). A similar systematic sampling strategy for unirrigated points was employed;

the same roads layer was used to create a 240-meter roads buffer layer to which land cover raster

data were extracted and systematically sampled for each land cover class of the base mask,

generating 205 points for unirrigated sampling.

Figure 9: Screenshot of Google Earth application edited in Adobe Sketch application; showing position of center pivot lateral.

Since the buffer extended 120 meters on each side of the road, all unirrigated sampling points were visible from roads as were all irrigated sampling points (Figure 13). Roads were travelled a second time (post irrigated points sampling) to verify the pre-selected unirrigated points, using the Google Earth and Google Maps applications to navigate to each sampling point and to record a photo and verify land cover (Figure 14). If a point was not clearly and unarguably unirrigated, then it was not included it in the final unirrigated training and validation point subset. Points were excluded from the unirrigated point subset if they were under active irrigation, in a field that appeared irrigated, in a field that was potentially irrigated or within approximately 90 meters of an actively or potentially irrigated field. After sampling, Planet Labs high-resolution imagery was referenced to verify that the point was unirrigated in 2016, 2017 and 2018. If intense green-up in the high-resolution imagery was observed at a point labeled as unirrigated in the field, then it was removed from the unirrigated subset. Following verification, 120 unirrigated points representing 24 land cover classes out of 205 systematically and randomly generated across 27 land cover classes were retained (Figure 15). Unirrigated points were not allocated to subsets. Once

34
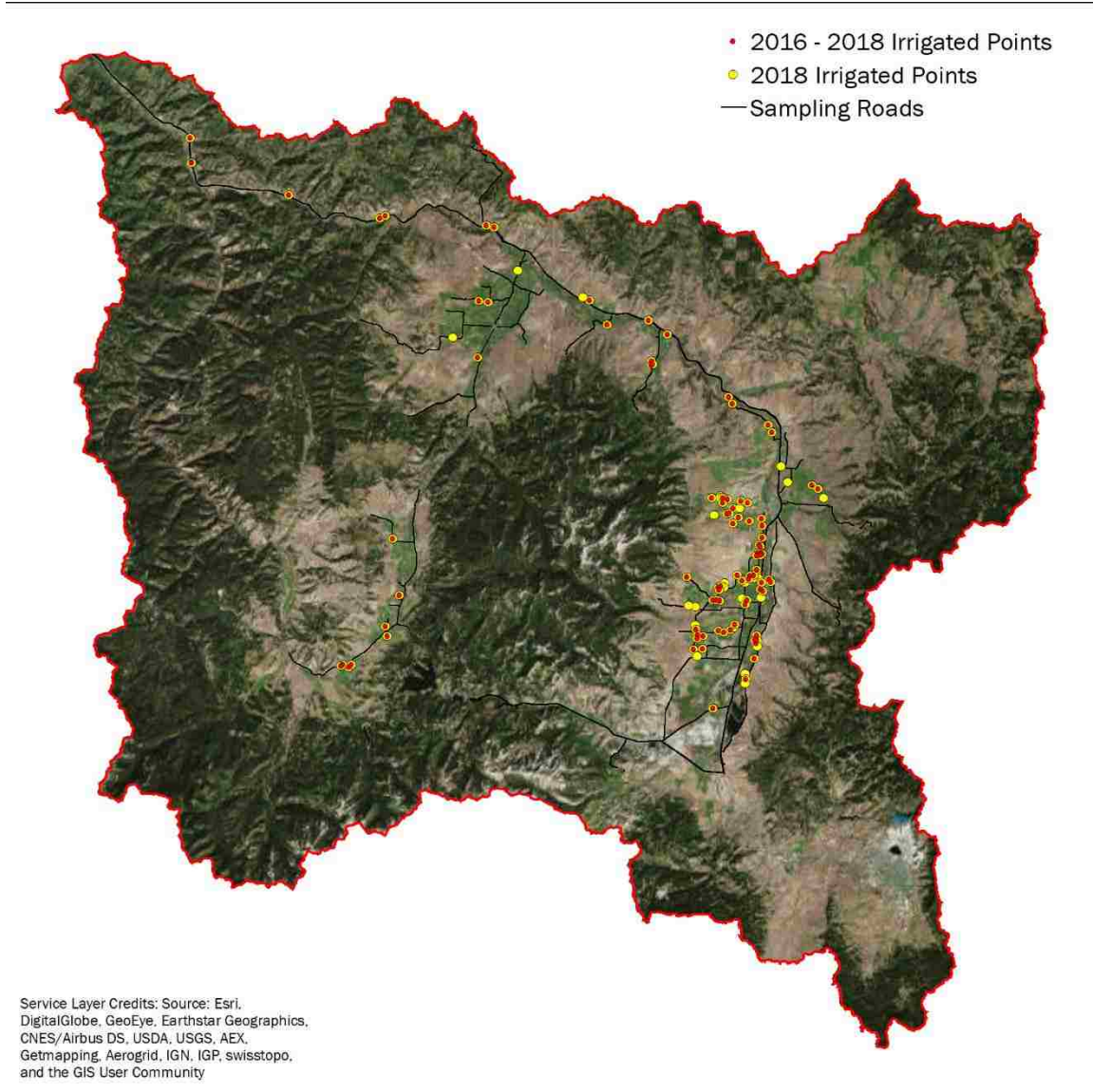
Figure 10: Irrigated training and validation point subsets; two field and Planet Labs verified subsets, one for the 2016-2018 growing seasons and one for the 2018 growing season; the 2018 subset excludes those not verified for all three growing seasons.

unirrigated point verification was completed, the unirrigated points were merged with the 2018

irrigated points subset and then with the 2016-2018 irrigated points subset. Thus, two training

and validation point datasets were created: (1) 2018 irrigated and unirrigated points for NoClim
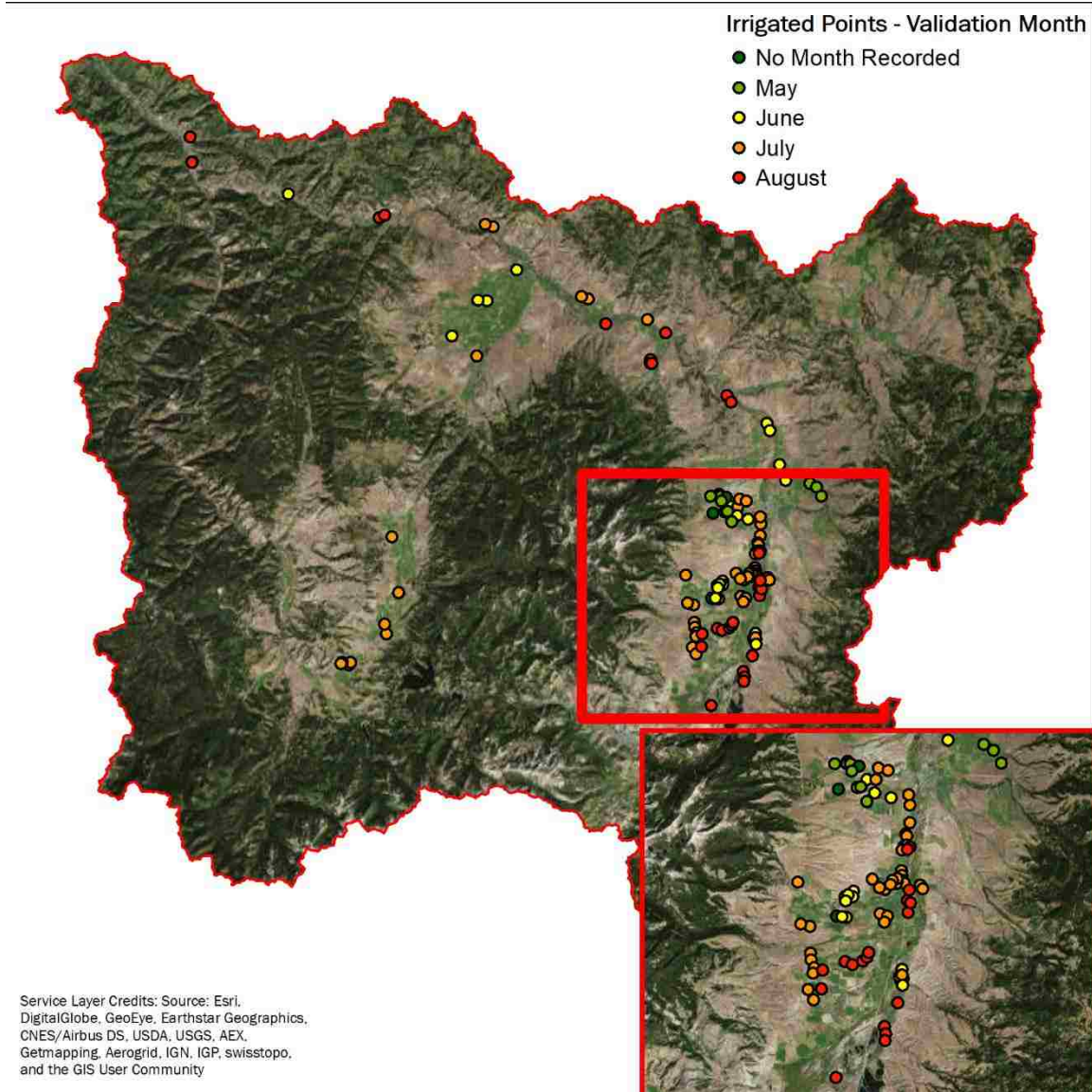
Figure 11: Irrigated points symbolized by field-verification month.

model training and classification analyses and (2) 2016-2018 irrigated and unirrigated points for

Clim model training and classification analyses (Table 3).   Finally, since analysis areas varied

depending upon the analysis being implemented, the total number of TVPs and total number in

each class differed across analyses (Table 3 and Figure 16).

Service Layer Credits: Source: Esri,
DigitalGlobe, GeoEye, Earthstar Geographics,
CNES/Airbus DS, USDA, USGS, AEX,
Getmapping, Aerogrid, IGN, IGP, swisstopo,
and the GIS User Community

Figure 12: Irrigated points symbolized by sampling strategy employed for validation.

Table 3: Training and Validation Points; number of irrigated and unirrigated points, center pivot and other method points and total points in the 2018 subset, used for NoClim training and validation, and 2016-2018 subset, used for Clim training and validation.

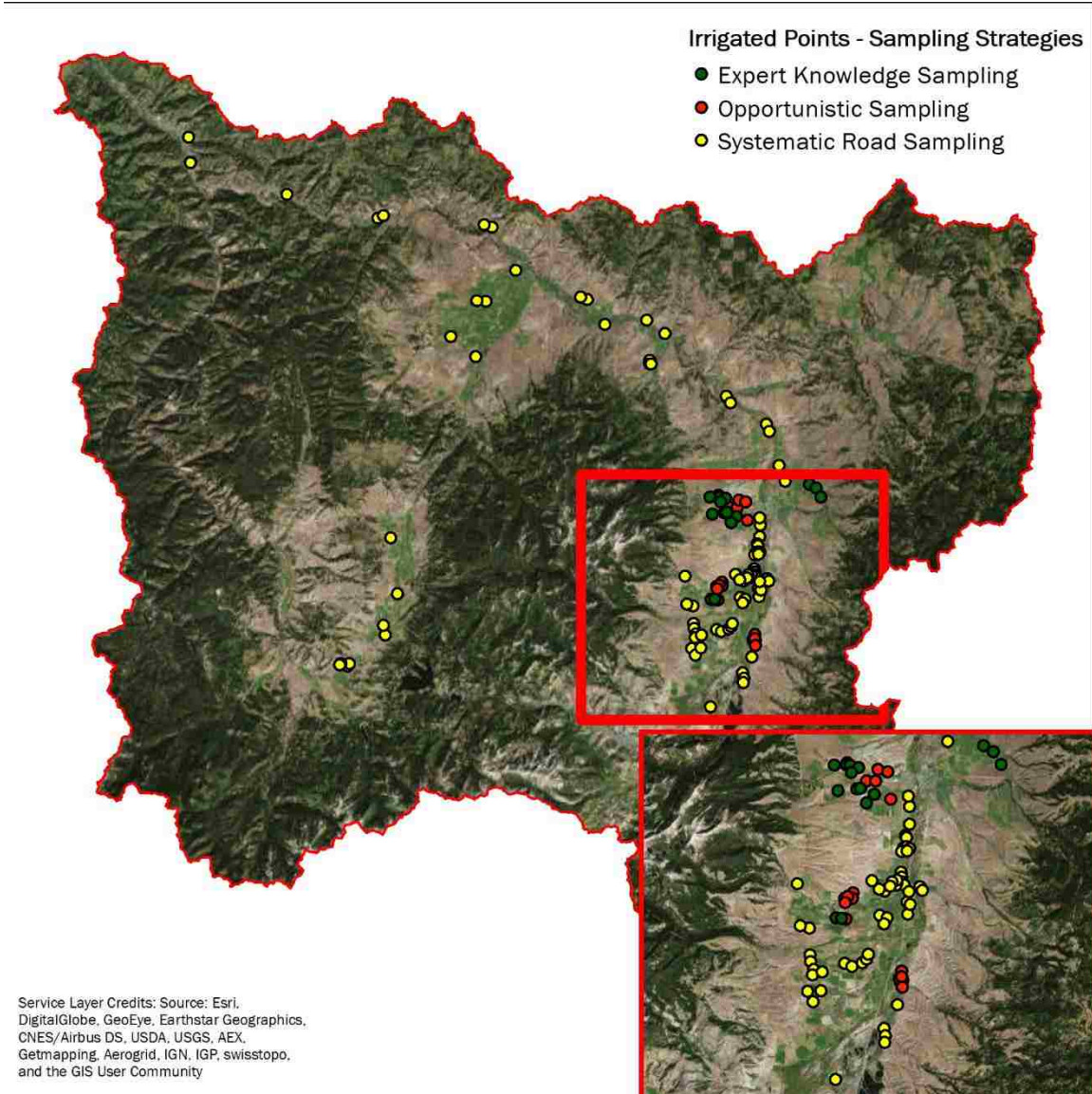| Training and Validation Points					
Analysis areas for each classification	**Number of irrigated points**	**Number of unirrigated points**	**Number of center pivot points**	**Number of other method points**	**Total Number of Points**
2018 – prior to masking	120	120	41	79	240
2016-2018 – prior to masking	91	120	53	38	211
NoClim training and validation/NoClim analysis **Irrig/Unirrig**	67	59	31	36	126
NoClim training and validation/NoClim analysis **CP/OM**	63	0	29	34	63
NoClim training and validation – train NoClim & classify Clim analysis **Irrig/Unirrig**	67	59	31	36	126
NoClim training and validation – train NoClim & classify Clim analysis **CP/OM**	61	0	30	31	61
Clim training and validation/Clim analysis **Irrig/Unirrig**	89	107	39	50	196
Clim training and validation/Clim analysis **CP/OM**	84	0	38	46	84

Figure 13: Unirrigated sampling points with roads buffer.

Figure 14: Land cover validation of foothill and valley grassland area (unirrigated).

Service Layer Credits: Source: Esri,
DigitalGlobe, GeoEye, Earthstar Geographics,
CNES/Airbus DS, USDA, USGS, AEX,
Getmapping, Aerogrid, IGN, IGP, swisstopo,
and the GIS User Community

Figure 15: Unirrigated points retained after validation.

Figure 16. Training and Validation Points: (a) TVPs for Irrig/Unirrig NoClim analysis; (b) TVPs for CP/OM NoClim analysis; (c) TVPS for Irrig/Unirrig train NoClim & classify Clim analysis; (d) TVPs for CP/OM train NoClim & classify Clim analysis; (e) TVPs for Irrig/Unirrig Clim analysis; (f) TVPs for CP/OM Clim analysis.

Modeling

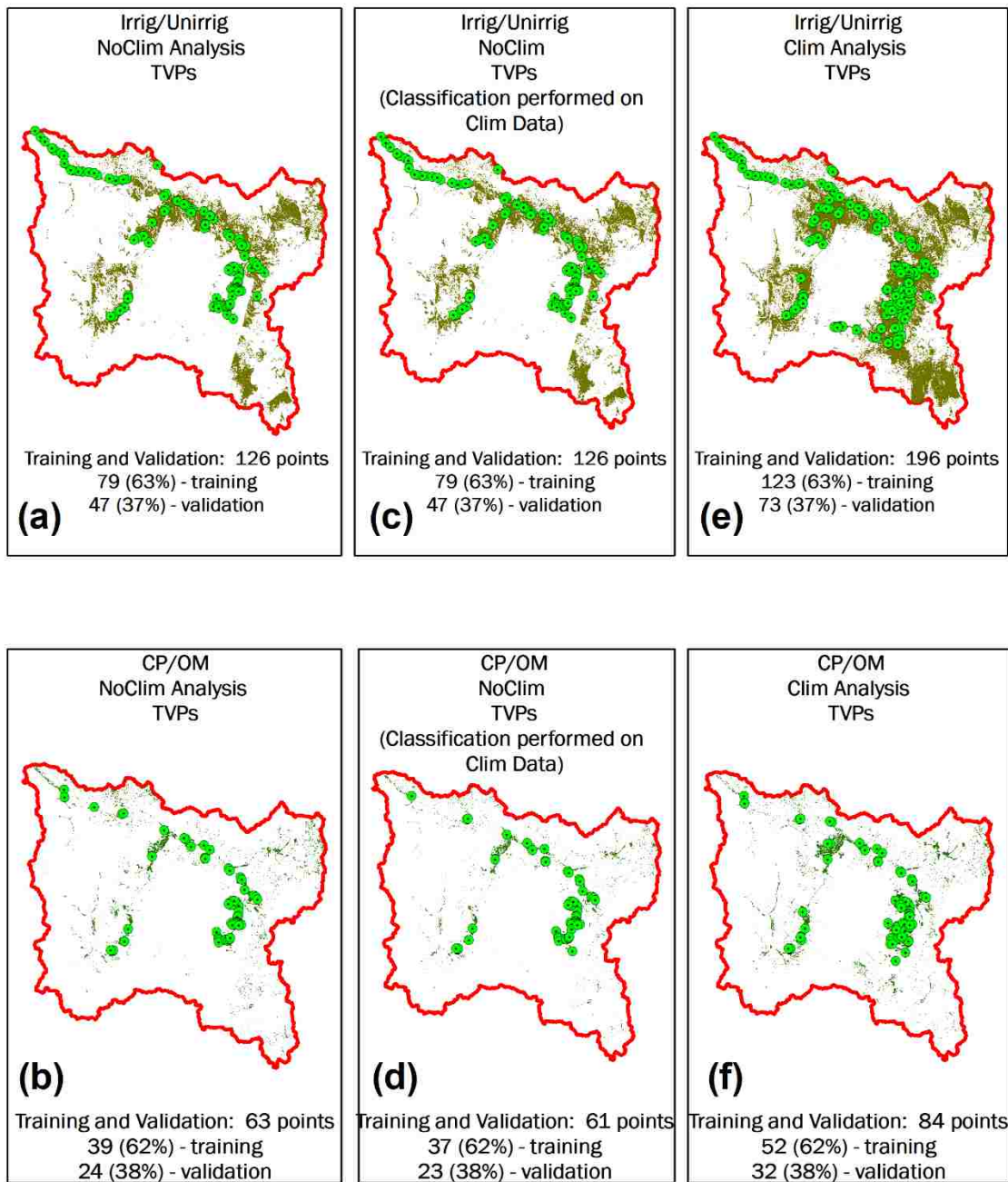Following establishment of analysis areas and TVPs, three Random Forest analyses (Table 2) were performed for an Irrig/Unirrig (stage one), followed by a CP/OM classification (stage two). The Random Forest modeling workflow is outlined in Figures 17, 18, 19 and 20. For each analysis, the NDVI time-series dataset and TVPs were extracted by mask and clipped, respectively, to the analysis area, which varied based on the analysis being performed. Then, the NDVI values from the analysis-area, time-series data were sampled at the training and validation point locations within the analysis area. Subsequently, the points were divided into two subsets, one for training and one for validation. The percentage and number of points in the training and validation subsets also varied across analyses (Table 3 and Figure 16).

Following division of TVPs, the Random Forest model was trained. Model parameters were constant across all analyses, with the number of trees equal to 500, training ratio equal to 0.66 and number of splitting variables equal to two, approximately the square root of the number of independent time-step variables. The Random Forest model used an "internal" out-of-bag (OOB) classification and validation technique, training each tree of the model with 66% of training points and validating each tree of the model with the remaining 34%. The OOB selection of training points for each tree was random with replacement, and the OOB classification error is the proportion of times that validation cases are not equal to their true classes, averaged over all cases. The OOB training and classification process occurs as the Random Forest is constructed and is separate from the post-classification accuracy assessments. Post-classification accuracy assessments are necessary, because training and validation data are not randomly distributed. Variable importance is also determined during the model-training
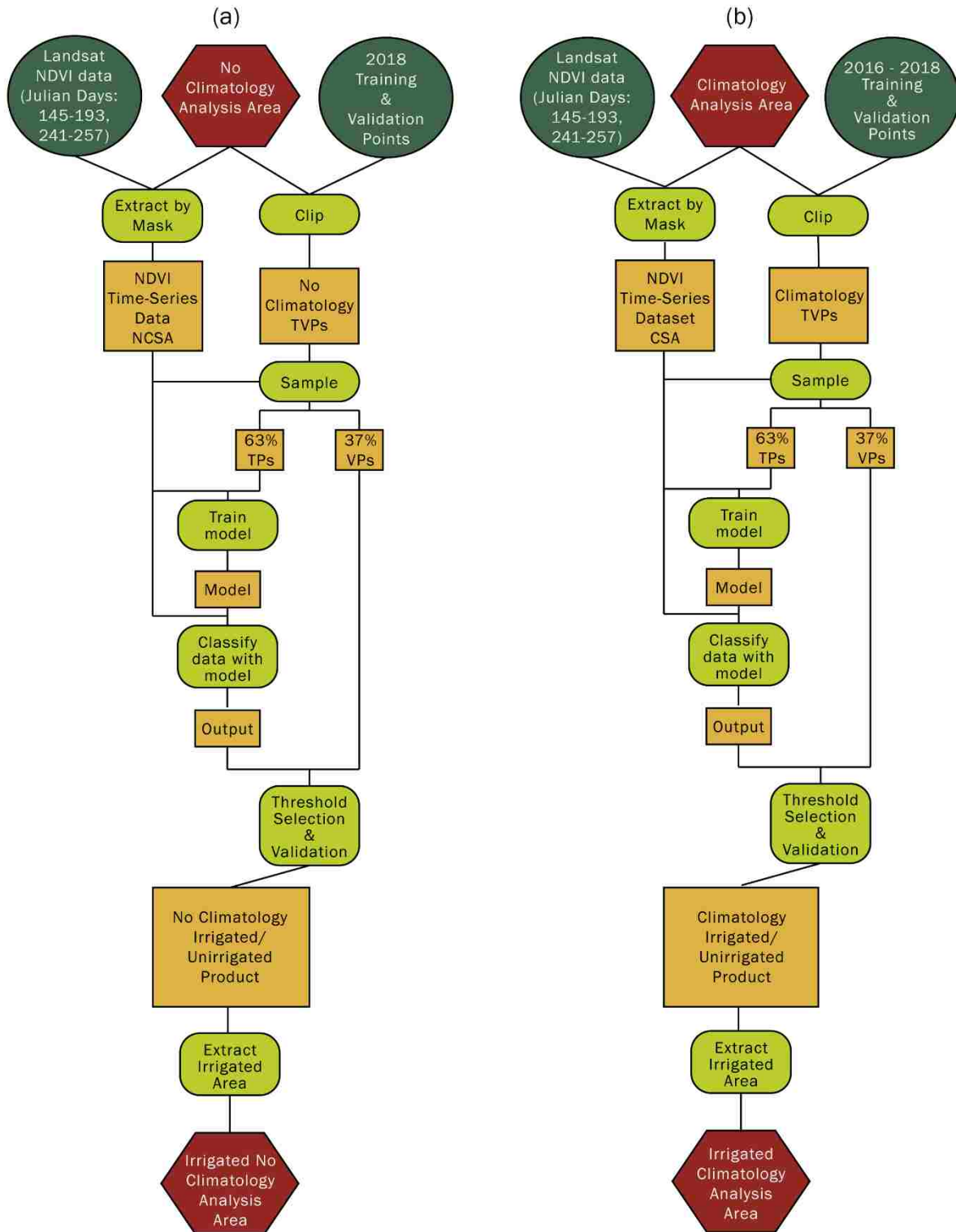
Figure 17. Irrigated/Unirrigated, no climatology and climatology modeling workflows: (a) Irrig/Unirrig, NoClim analysis (stage one); (b) Irrig/Unirrig, Clim analysis (stage one).
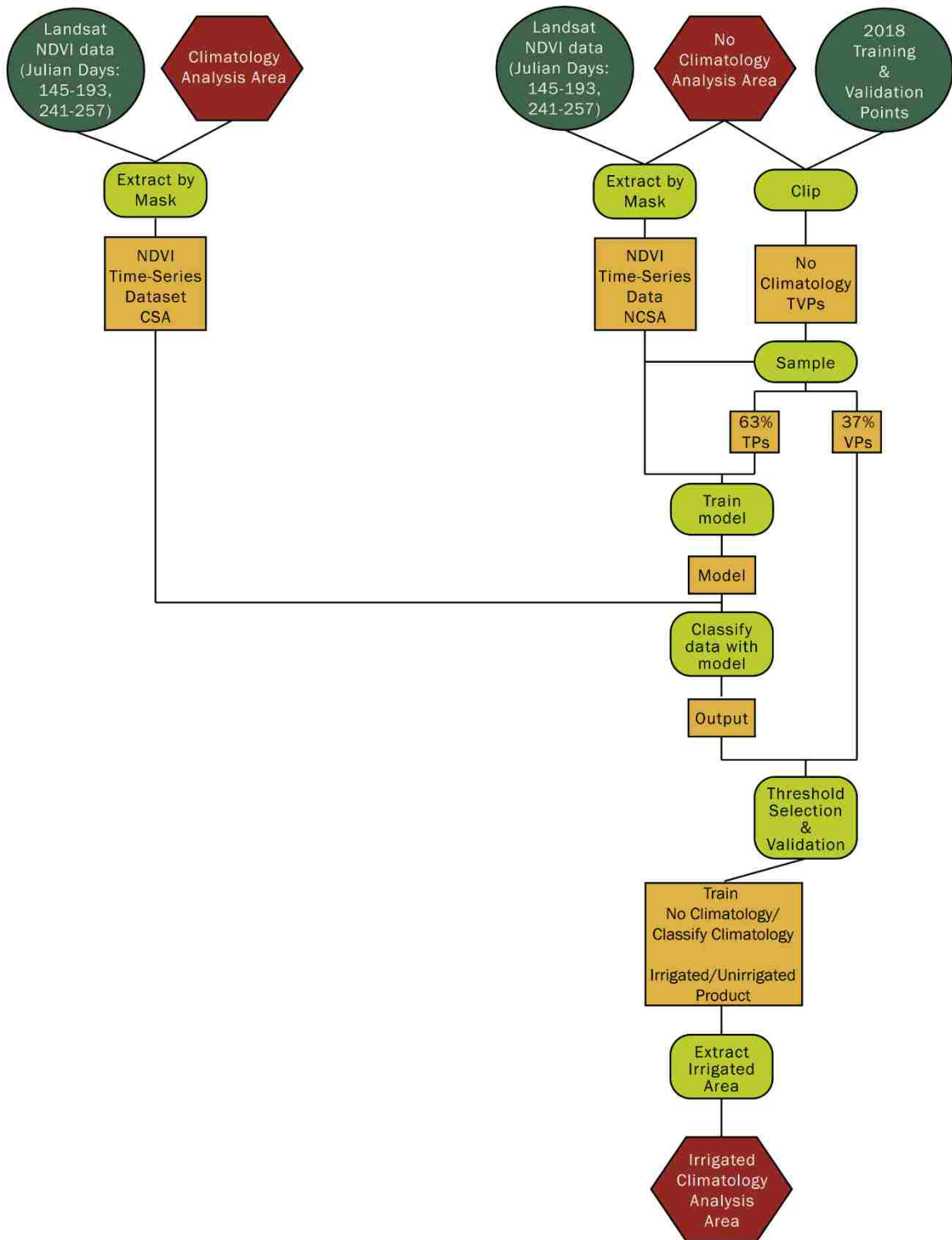
Figure 18: Irrigated/Unirrigated, train no climatology and classify climatology modeling workflow (stage one).

process by formation of a separate model for each independent variable. For each of these models, an independent variable is removed from the Random Forest model and the OOB error values recorded. Variable importance can be assessed by viewing the error value change resulting from the removal of each variable from the model.
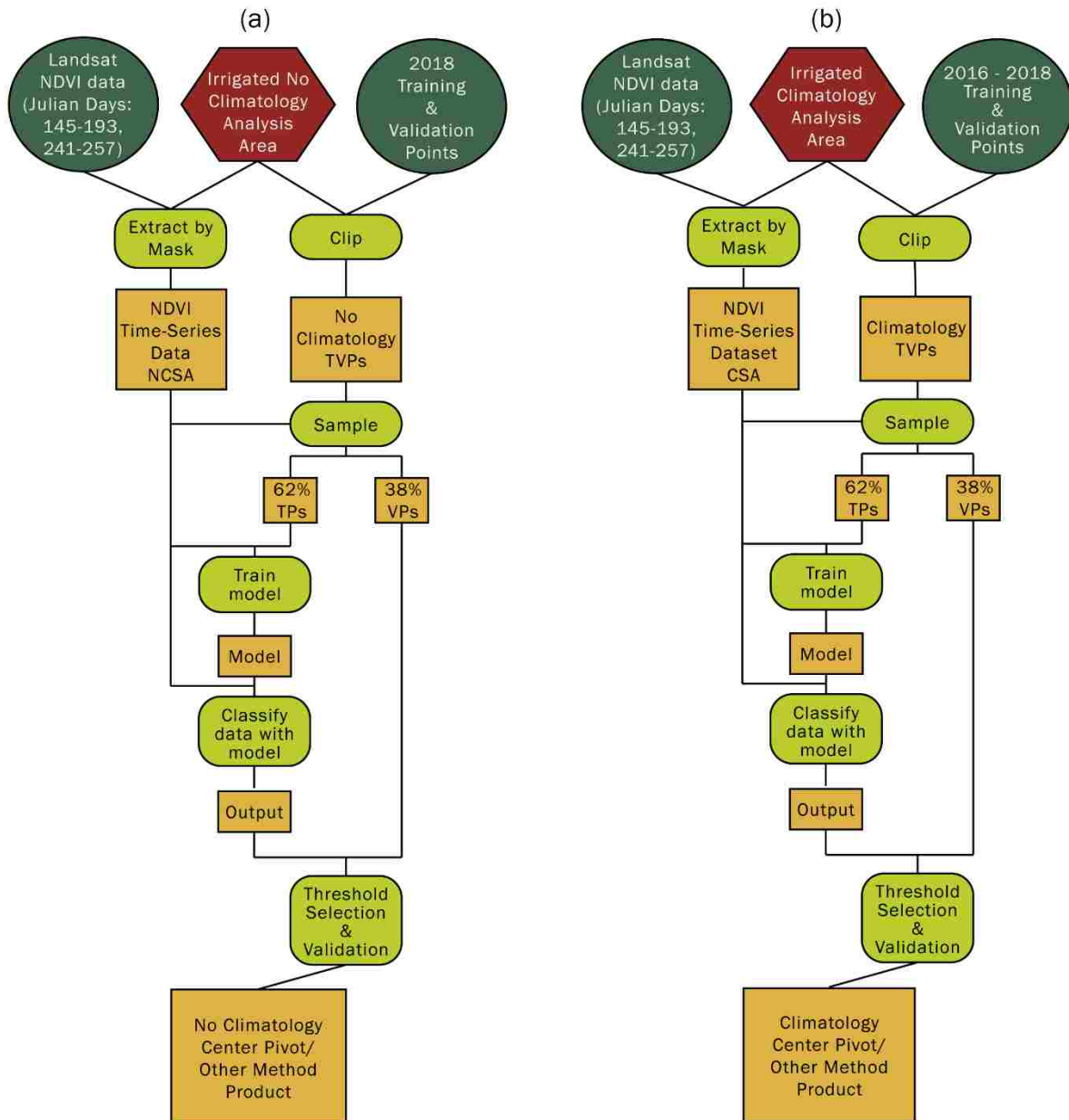
Figure 19. Center pivot/other method, no climatology and climatology modeling workflows: (a) CP/OM NoClim analysis (stage two); (b) CP/OM Clim analysis (stage two).

Following training, classification was performed on the NDVI time-series data extracted to the appropriate analysis area, either Clim or NoClim. The output of the Random Forest model was binary and probabilistic (two bands, one for each class, with a value range from 0-1), representing the proportion of trees that placed a given pixel into either the irrigated or unirrigated class. Due to the probabilistic nature of the output, proportion thresholds were

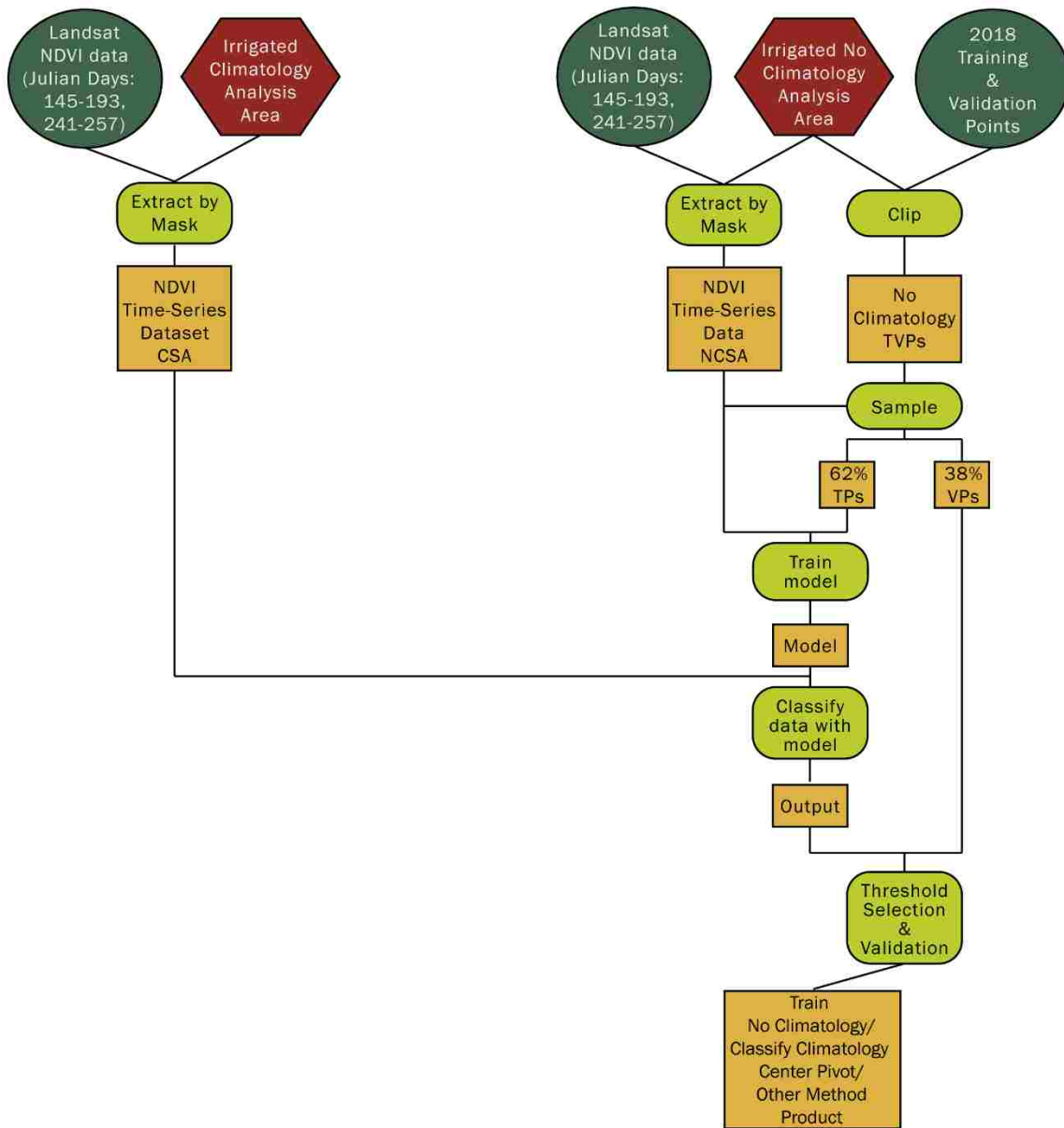**Figure 20: Center pivot/other method, train no climatology and classify climatology modeling workflow (stage two).**

selected, and the model outputs reclassified to make each output binary. Five thresholds of 0.5-0.9 proportions of trees classifying pixels as irrigated (0.1 intervals) were selected, and a binary reclassification (Irrig/Unirrig) was performed to prepare each reclassified output for an accuracy assessment (Table 4). This was followed by an accuracy assessment performed on each binary output created from a different threshold, a total of five binary outputs representing five probabilities of being irrigated. The most accurate threshold was selected, and an Irrig/Unirrig product was produced from a reclassified binary output based on that threshold. Finally, irrigated area from the product was extracted, and this became the analysis area for the subsequent CP/OM analysis for the appropriate analysis area. Following Irrig/Unirrig classifications, a Clim Random Forest model was trained with six classes (Table 2). The threshold approach from initial classifications (Table 4) was applied to the irrigated band of the six-class output and accuracy assessments performed accordingly. Also, since the model was not binary, a highest-position approach was tested to distinguish irrigated from unirrigated land cover. The output from the model was six bands, one irrigated and five unirrigated. Pixels from each band at each location (position) were ranked on probability value from each class's band. The highest proportion of trees classifying a pixel into a class determined the class (Table 4) at that pixel. Following ranking of bands, the six-class output was reclassified to a binary output and accuracy assessments performed accordingly.

A process nearly identical to the Irrig/Unirrig workflow was performed for the subsequent CP/OM stage of each analysis (Figure 19 and Figure 20). Time-series data and points were reduced to analysis areas. Then time-series data were sampled at point locations. Next, the points were divided into training and validation subsets. However, for the CP/OM analyses, all points were irrigated, and classes were center pivot and other method.

Table 4: Tested threshold proportions of trees for all Random Forest analyses.

Random Forest Probabilistic Output Thresholds		
Analysis	**Output Classes**	**Tested Threshold Proportions of Trees Classifying Pixels as Irrigated or Center Pivot**
Train NoClim & Classify NoClim	Irrig/Unirrig	0.5, 0.6, 0.7, 0.8, 0.9
Train NoClim & Classify Clim		
Train Clim & Classify Clim		
Train Clim & Classify Clim	Developed, Disturbance, Forest, Irrigated, Meadow, Shrub-Grasslands	0.5, 0.6, 0.7, 0.8, 0.9
		Highest Position
Train NoClim & Classify NoClim	CP/OM	0.5, 0.6, 0.7
Train NoClim & Classify Clim		
Train Clim & Classify Clim		

The models were trained, and time-series data classified for the analysis areas. Again, this produced a two-band, probabilistic output. However, for the CP/OM analyses, the thresholds for proportion of trees classifying pixels as center pivot pixels were 0.5, 0.6 and 0.7 (three total thresholds) (Table 4). As with the Irrig/Unirrig analyses, a binary, reclassified output was produced representing each threshold probability of pixels being center pivot irrigated. Then accuracy assessments were performed on each binary, reclassified output, and the most accurate output was selected to be the CP/OM product for each analysis.

Following Random Forest analyses, it was determined that the Irrig/Unirrig, train Clim & classify Clim analysis was most accurate. Further, it was determined that CP/OM classification accuracies were poor. Therefore, to compare the Random Forest and Decision Tree models, only a train Clim & classify Clim, Irrig/Unirrig Decision Tree analysis with the same workflow as the train Clim & classify Clim, Irrig/Unirrig Random Forest analysis (Figure 17b) was performed (Table 2). For the Decision Tree analysis, the split type was entropy and auto-pruning was

performed for leaves with < 1% of training points. Finally, only an irrigated, Clim analysis was performed with a PCA model (Table 2) using the ArcGIS RMRS Raster Utility toolbar.

RESULTS

Out-of-Bag Classification Error and Variable Importance

Out-of-bag classification error and variable importance are only quantified for the Random Forest models. Classification errors for Irrig/Unirrig Random Forest models ranged from 0.04 to 0.11, while classification errors for CP/OM Random Forest models ranged from 0.25 to 0.48 (Table 5). The train Clim & classify Clim, Irrig/Unirrig Random Forest model yielded the lowest classification error (classification error = 0.04), and the train Clim & classify Clim, CP/OM model yielded the highest classification error (classification error = 0.48). For the six-class Random Forest model, error was 0.33. The low classification errors of the Irrig/Unirrig models are attributable to the variation between the spectro-temporal profiles of the irrigated and unirrigated classes (Figure 21), and the high classification errors of the CP/OM models are potentially attributable to low variation between the spectro-temporal profiles of the center pivot and other method classes (Figure 21). The greatest variation in spectro-temporal profiles of the center pivot and other method classes is observed for days 177 and 193 (Figure 21), and those are important time-step variables for two of the CP/OM models (Figure 22).

Figure 22 shows classification errors for each model at saturation (all variables included in training) and without each of its six variables. Error values greater than saturation error associated with a time-step variable indicate that removal of that variable increases model error. Those variables associated with error greater than saturation error are the most important model variables.   For the train NoClim & classify NoClim, Irrig/Unirrig model, the day 257 time-step variable is most important (Figure 22a). For the train NoClim & classify NoClim, CP/OM

Table 5: Out-of-bag classification error.

Out-of-Bag Classification Error for Random Forest Models		
Model	**Output Classes**	**Error**
Train NoClim & Classify NoClim	Irrig/Unirrig	0.10
Train NoClim & Classify NoClim	CP/OM	0.25
Train NoClim & Classify Clim	Irrig/Unirrig	0.11
Train NoClim & Classify Clim	CP/OM	0.29
Train Clim & Classify Clim	Irrig/Unirrig	0.04
Train Clim & Classify Clim	Developed, Disturbance, Forest, Irrigated, Meadow, Shrub-Grasslands	0.33
Train Clim & Classify Clim	CP/OM	0.48

model, the day 177 and 193 variables are most important (Figure 22b). These variables are the

time-step variables associated with the most variation in the center pivot and other method

spectro-temporal profiles (Figure 21). The day 145 and 161 variables are most important for the

train NoClim & classify Clim, Irrig/Unirrig model (Figure 22c), and this is notable, because the

same proportion of training points were selected from the same 2018 TVPs subset, and the same

analysis area was sampled as for the train NoClim & classify NoClim, Irrig/Unirrig model. For

the train NoClim & classify Clim, CP/OM model, removal of the day 161 variable increased

error, and so did the removal of the 177 and 193 variables (those associated with the key period

of spectro-temporal profile variation), as they did with the CP/OM model for the train NoClim &

classify NoClim model (Figure 22d). The day 161, 177 and 257 variables were most important

for the train Clim & classify Clim, Irrig/Unirrig model (Figure 22e), and removal of the day 241

and 257 variables from the train Clim & classify Clim, CP/OM model increased error beyond

saturation (Figure 22f), and removal of day 177 and 193 variables from the train Clim & classify

Clim model produced classification error equaling error at saturation (Figure 22f). Finally, for

the six-class Random Forest model, removal of days 145, 193 and 257 increased error beyond its

value at saturation. Variable importance was further investigated by examination of probability

distribution graphs for the most important variables of each model. Probability distribution

graphs were not explored for the six-class Random Forest model. For each model variable, the
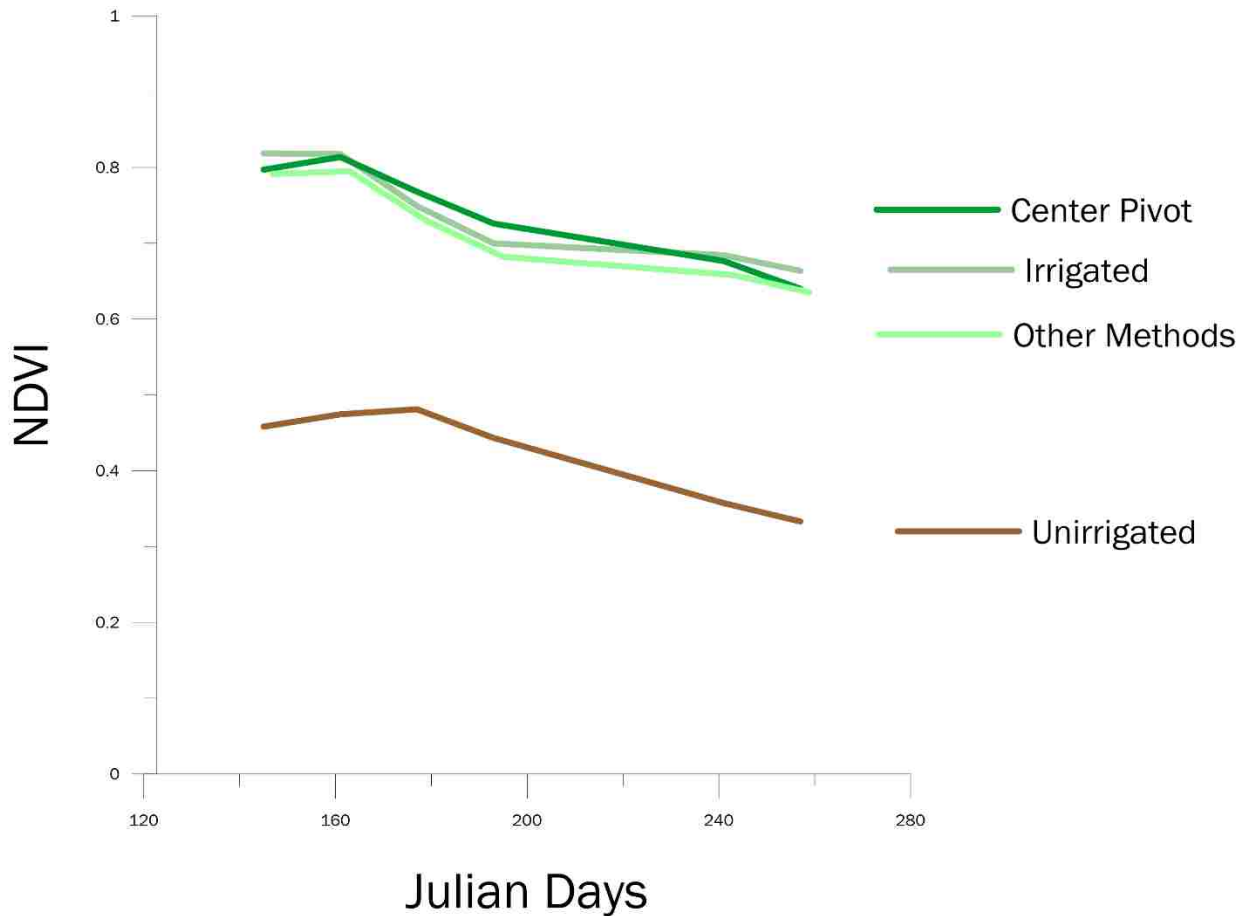
other five

Figure 21: Spectro-temporal profiles for all product classes (derived from 2018 TVPs subset (*n* = 211 points)).

variables were concurrently adjusted from the low to high ends of their ranges, allowing the

investigation of the probability of allocation to each class (i.e., Irrig/Unirrig or CP/OM) for a

single variable's range with all other model variables held constant. Consistently, for each

analysis, Irrig/Unirrig models produced higher probabilities of allocation to the irrigated or

unirrigated classes for their most important variables at the lowest 10% and highest 10% ends of

the ranges of all other model variables (Figure 23, Figure 24 and Figure 25). For example, the
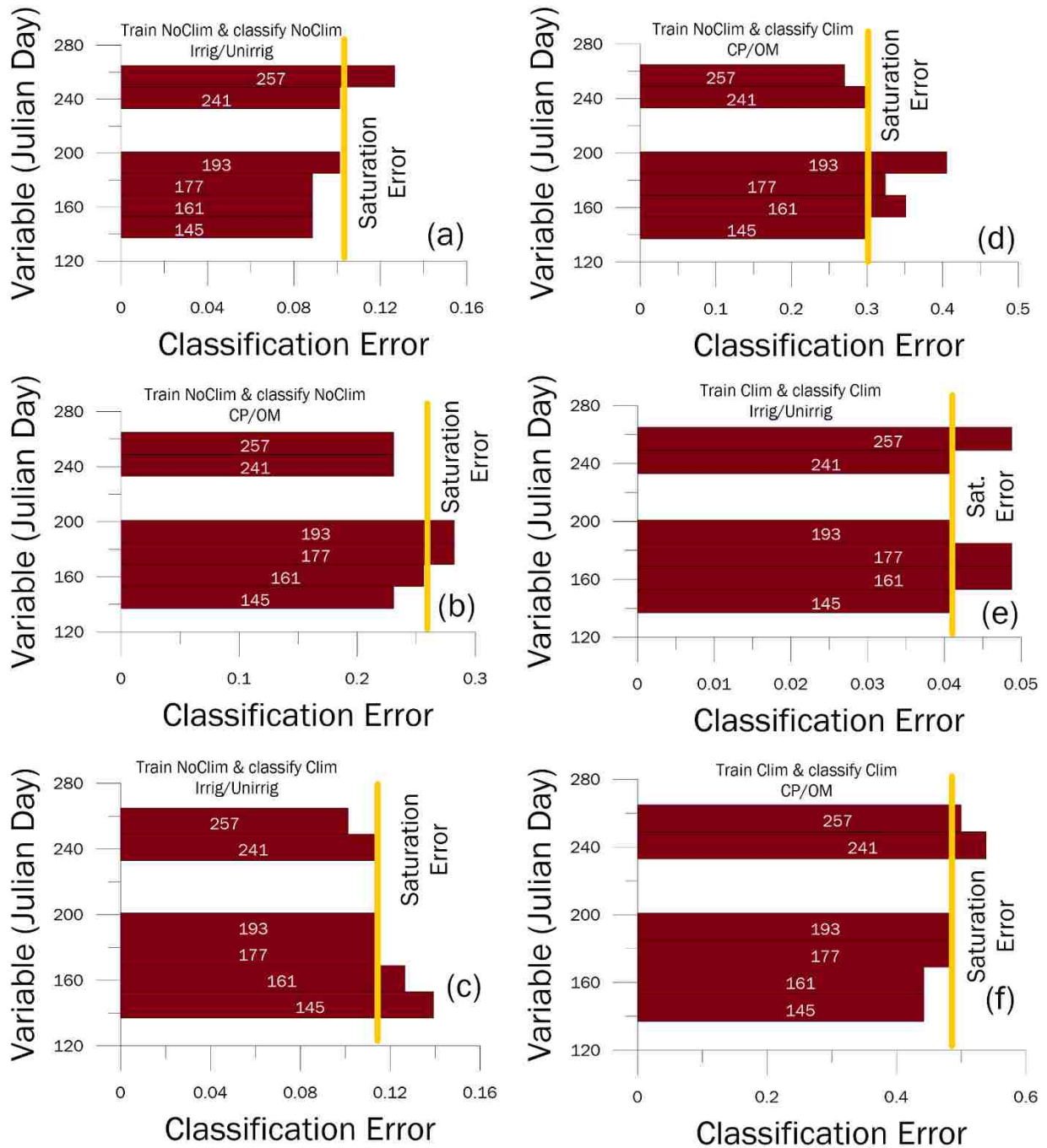
Figure 22. Variable effects on classification error: (a) classification error for train NoClim & classify NoClim, Irrig/Unirrig model at saturation and without each time-step variable; (b) classification error for train NoClim & classify NoClim, CP/OM model; (c) classification error for train NoClim & classify Clim, Irrig/Unirrig model; (d) classification error for train NoClim & classify Clim, CP/OM model; (e) classification error for train NoClim & classify Clim, Irrig/Unirrig model; (f) classification error for train Clim & classify Clim, CP/OM model.

time-step variable 257 probability distribution for the train Clim & classify Clim, Irrig/Unirrig model (the model with the least error), probability of allocation to the irrigated class (proportion of trees classifying pixels as irrigated) ranges from 0.8 – 1 for the range of NDVI values on day 257 (Figure 25f). However, for day 257 of the train Clim & classify Clim, CP/OM model (the model with the most error), the proportion of trees classifying pixels as center pivot ranges from 0.5 - < 0.75 for the range of NDVI values on day 257 (Figure 25j). Finally, investigation of variable importance for the CP/OM model with the lowest classification error reveals that the most important variables (days 177 and 193) demonstrate high proportions of trees classifying pixels as center pivot or other method at the extreme ends of other variable ranges (Figure 26a-e) and at the medians of other variable ranges for time-step variable 193 (Figure 26f). This relationship is potentially explained by the variation between center pivot and other method spectro-temporal profiles at days 177 and 193 (Figure 21). Finally, the distribution of NDVI values for each time step of each analysis may reveal explanations for error and accuracy. Irrig/Unirrig training and analysis areas exhibit broad NDVI distributions and potentially bimodal or trimodal patterns that are more pronounced from days 145-193 (Figure 27 and Figure 28). However, training the model with more classes for an Irrig/Unirrig classification did not appreciably mitigate the issue of misclassified pixels on the edges of analysis areas, and masking target land cover classes improved accuracy and agreement. Conversely, CP/OM training and analysis areas exhibit narrower NDVI distributions (Figure 29 and Figure 30). A key difference between the CP/OM train NoClim & classify NoClim (classification error = 0.25) and train Clim & classify Clim (classification error = 0.48) analyses are the potentially bimodal distributions for the train NoClim & classify NoClim time steps 145-177 (Figure 29). The train Clim & classify
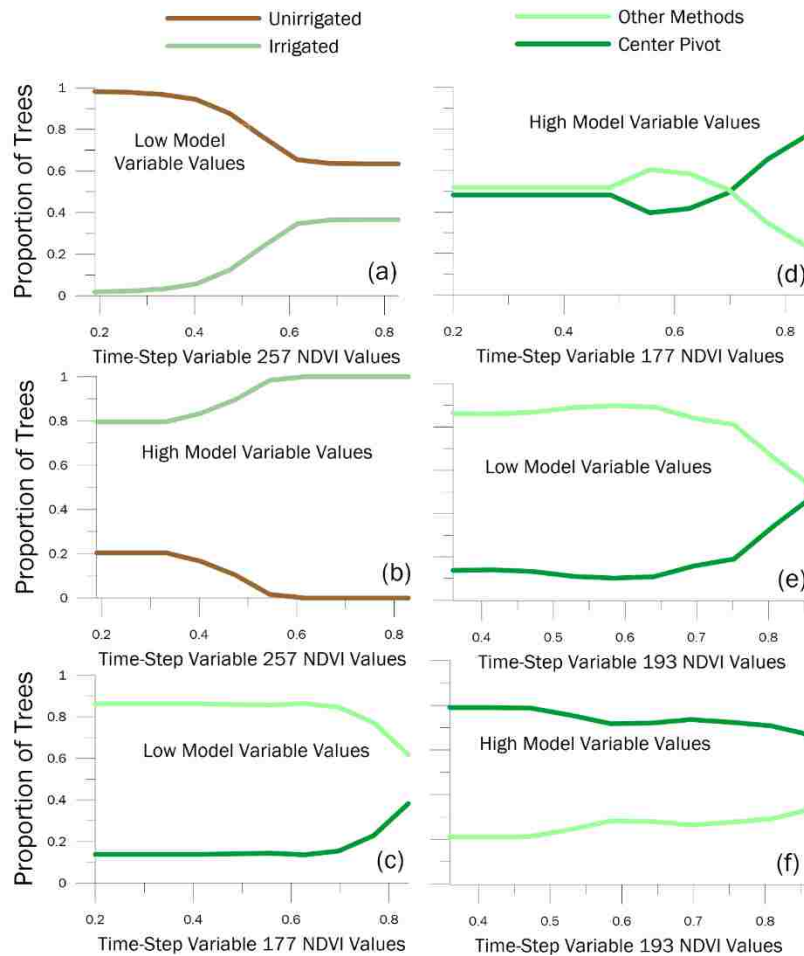
Figure 23. Probability distribution graphs for most important variables for the train NoClim & classify NoClim analyses: (a) Proportion of trees classifying any given pixel as irrigated or unirrigated based on NDVI value on variable-day 257 (i.e., probability distribution) with all other model variables at the low 10% of their range; (b) Irrig/Unirrig probability distribution for variable-day 257 with all other model variables at the high 10% of their range; (c) CP/OM probability distribution for day 177 and low model variable values; (d) CP/OM probability distribution for day 177 and high model variable values; (e) CP/OM probability distribution for day 193 and low model variable values; (f) CP/OM probability distribution for day 193 and high model variable values.

Clim analysis areas have only one potentially bimodal distribution for the earliest time step of

the analysis (Figure 30), suggesting that the potentially bimodal distributions associated with the

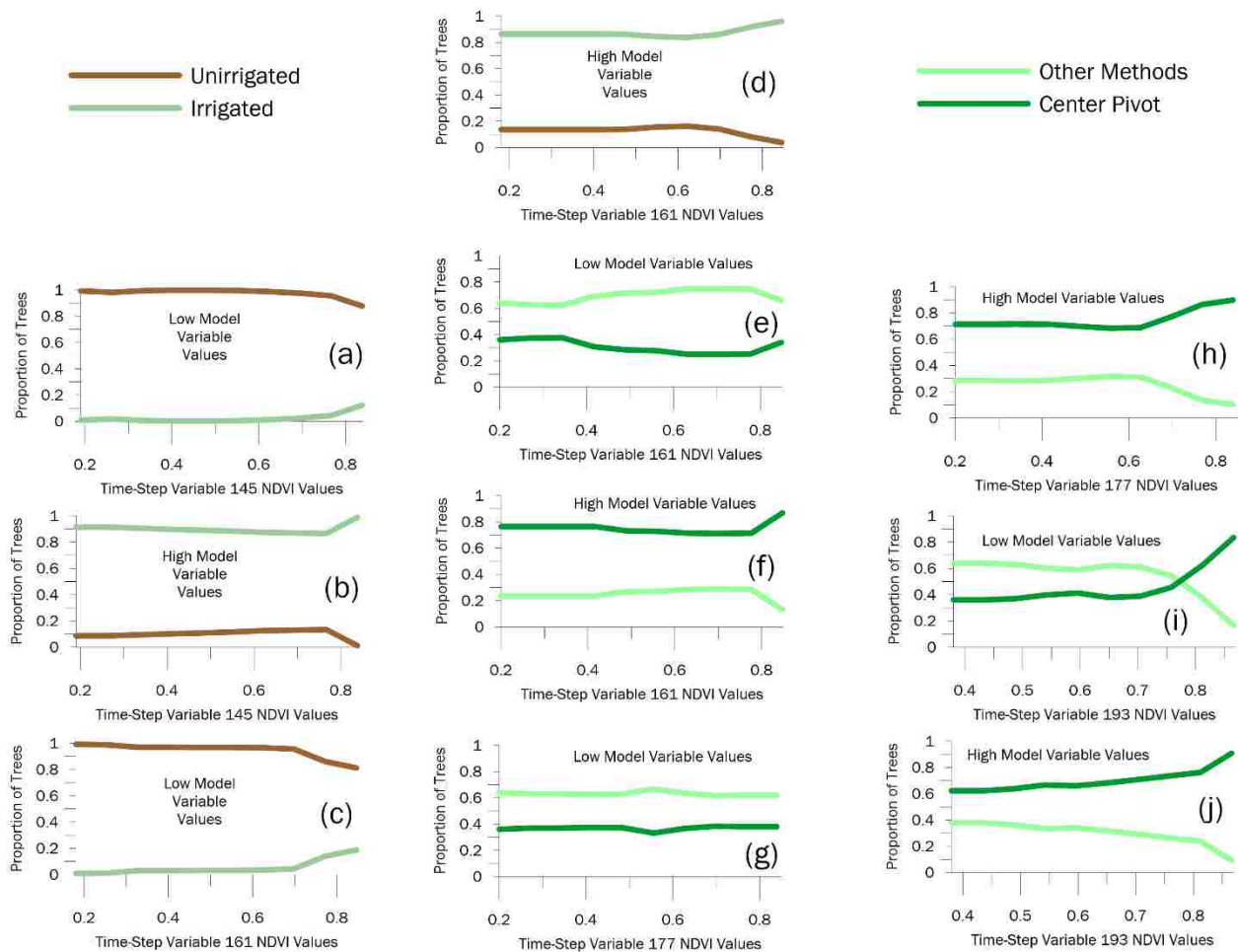NoClim analysis may reduce error.

54

Figure 24. Probability distribution graphs for most important variables for the train NoClim & classify Clim analyses: (a) Irrig/Unirrig probability distribution for day 145 and low model variable values; (b) Irrig/Unirrig probability distribution for day 145 and high model variable values; (c) Irrig/Unirrig probability distribution for day 161 and low model variable values; (d) Irrig/Unirrig probability distribution for day 161 and high model variable values; (e) CP/OM probability distribution for day 161 and low model variable values; (f) CP/OM probability distribution for day 161 and high model variable values; (g) CP/OM probability distribution for day 177 and low model variable values; (h) CP/OM probability distribution for day 177 and high model variable values; (i) CP/OM probability distribution for day 193 and low model variable values; (j) CP/OM probability distribution for day 193 and high model variable values.
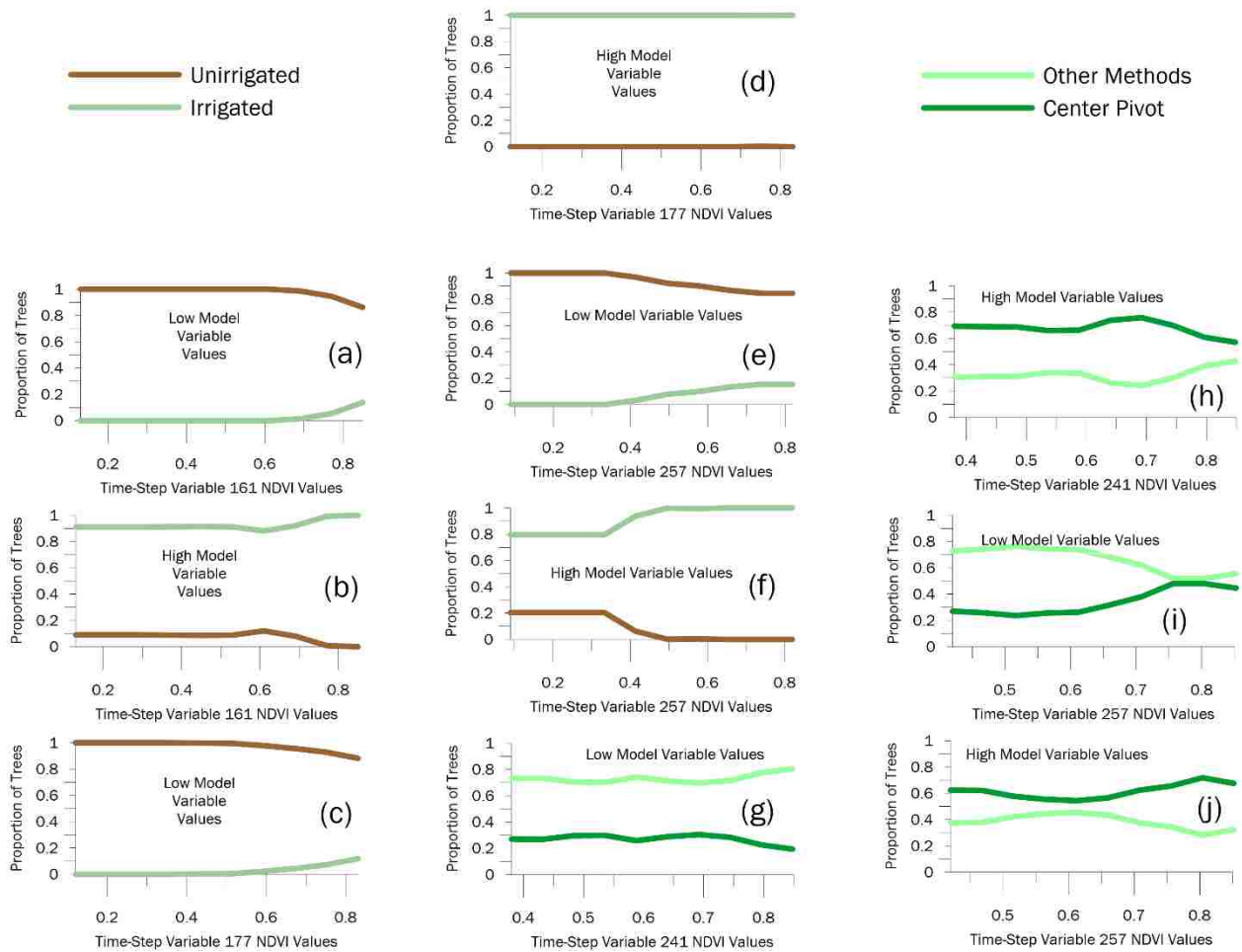
Figure 25. Probability distribution graphs for most important variables for the train Clim & classify Clim analyses: (a) Irrig/Unirrig probability distribution for day 161 and low model variable values; (b) Irrig/Unirrig probability distribution for day 161 and high model variable values; (c) Irrig/Unirrig probability distribution for day 177 and low model variable values; (d) Irrig/Unirrig probability distribution for day 177 and high model variable values; (e) Irrig/Unirrig probability distribution for day 257 and low model variable values; (f) Irrig/Unirrig probability distribution for day 257 and high model variable values; (g) CP/OM probability distribution for day 241 and low model variable values; (h) CP/OM probability distribution for day 241 and high model variable values; (i) CP/OM probability distribution for day 257 and low model variable values; (j) CP/OM probability distribution for day 257 and high model variable values.
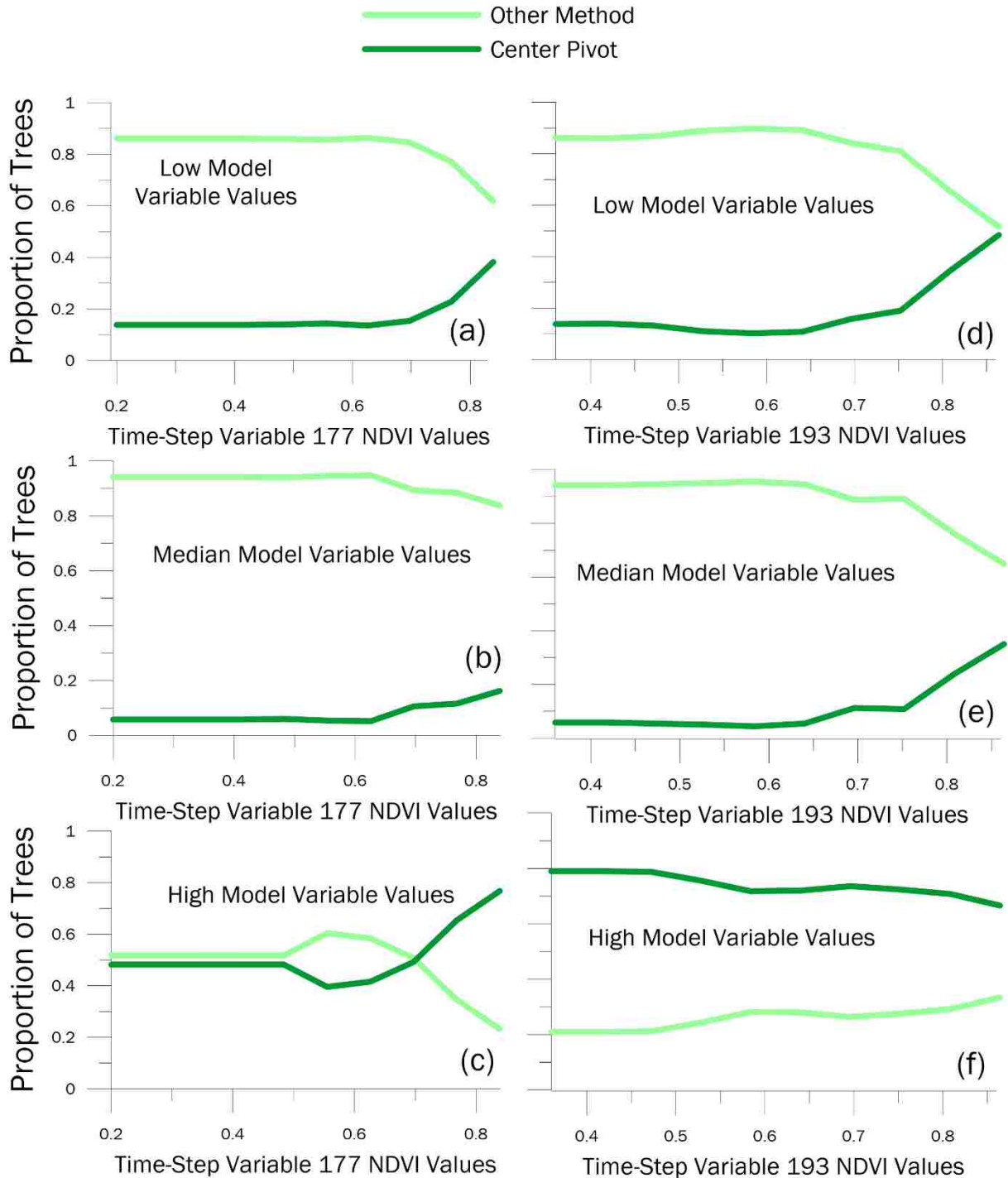
Figure 26. Probability distribution graphs for most important variables for the train NoClim & classify NoClim, CP/OM analysis (including median ranges): (a) CP/OM probability distribution for day 177 and low model variable values; (b) CP/OM probability distribution for day 177 and median model variable values; (c) CP/OM probability distribution for day 177 and high model variable values; (d) CP/OM probability distribution for day 193 and low values; (e) CP/OM probability distribution for day 193 and median values; (f) CP/OM probability distribution for day 193 and high values.

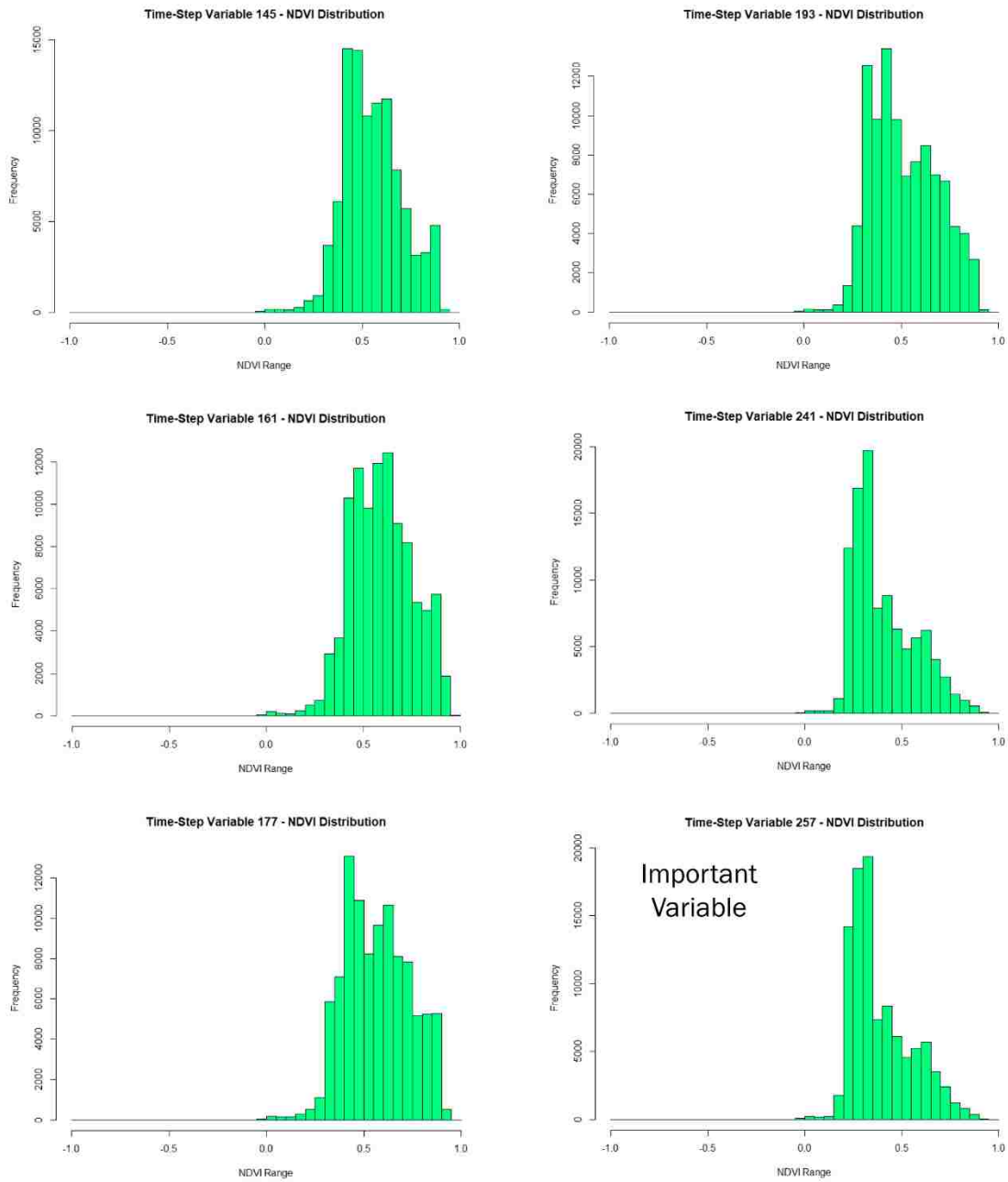**Figure 27: Train NoClim & classify NoClim, Irrig/Unirrig analysis histograms.**
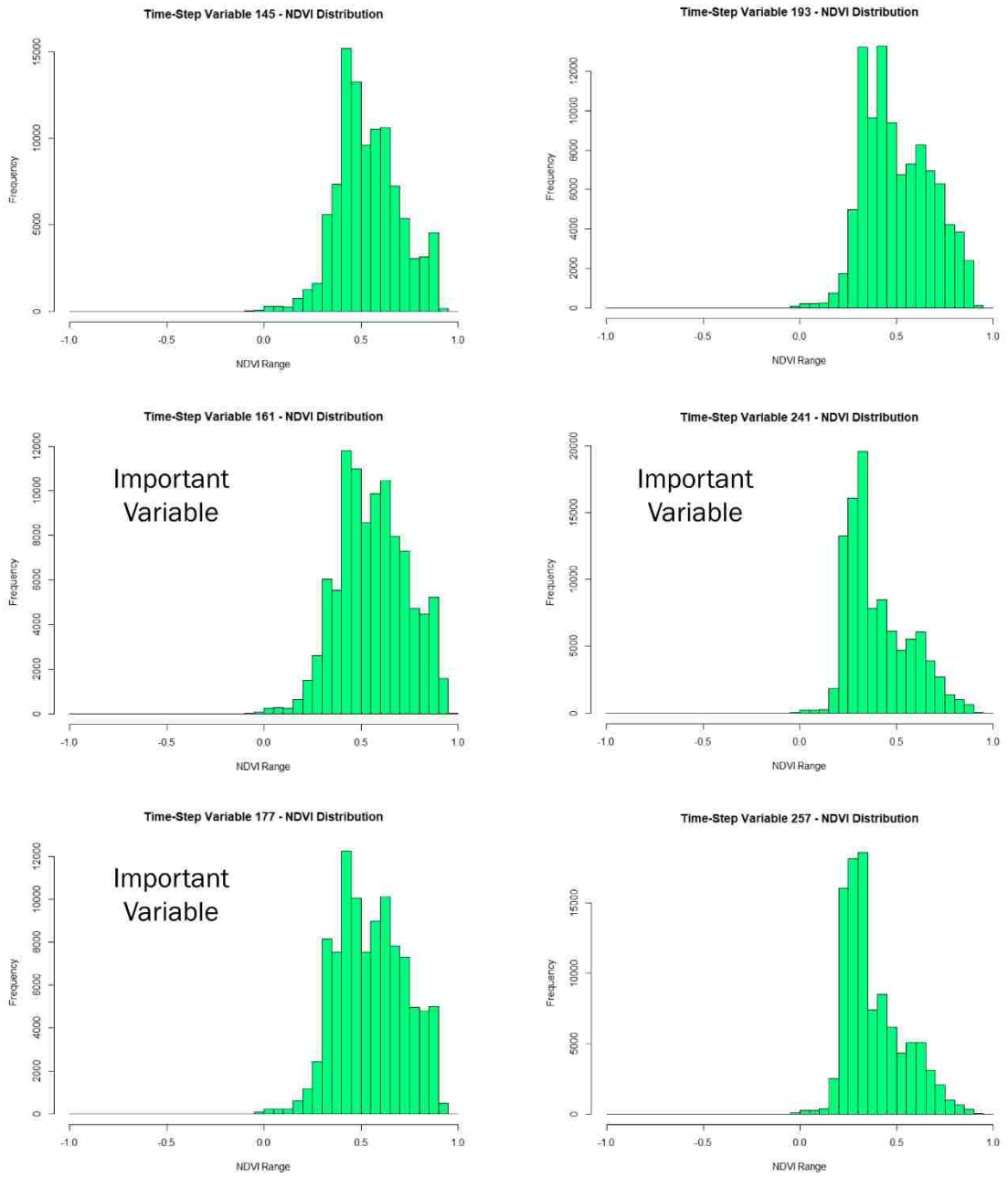
Figure 28: Train Clim & classify Clim, Irrig/Unirrig analysis histograms.
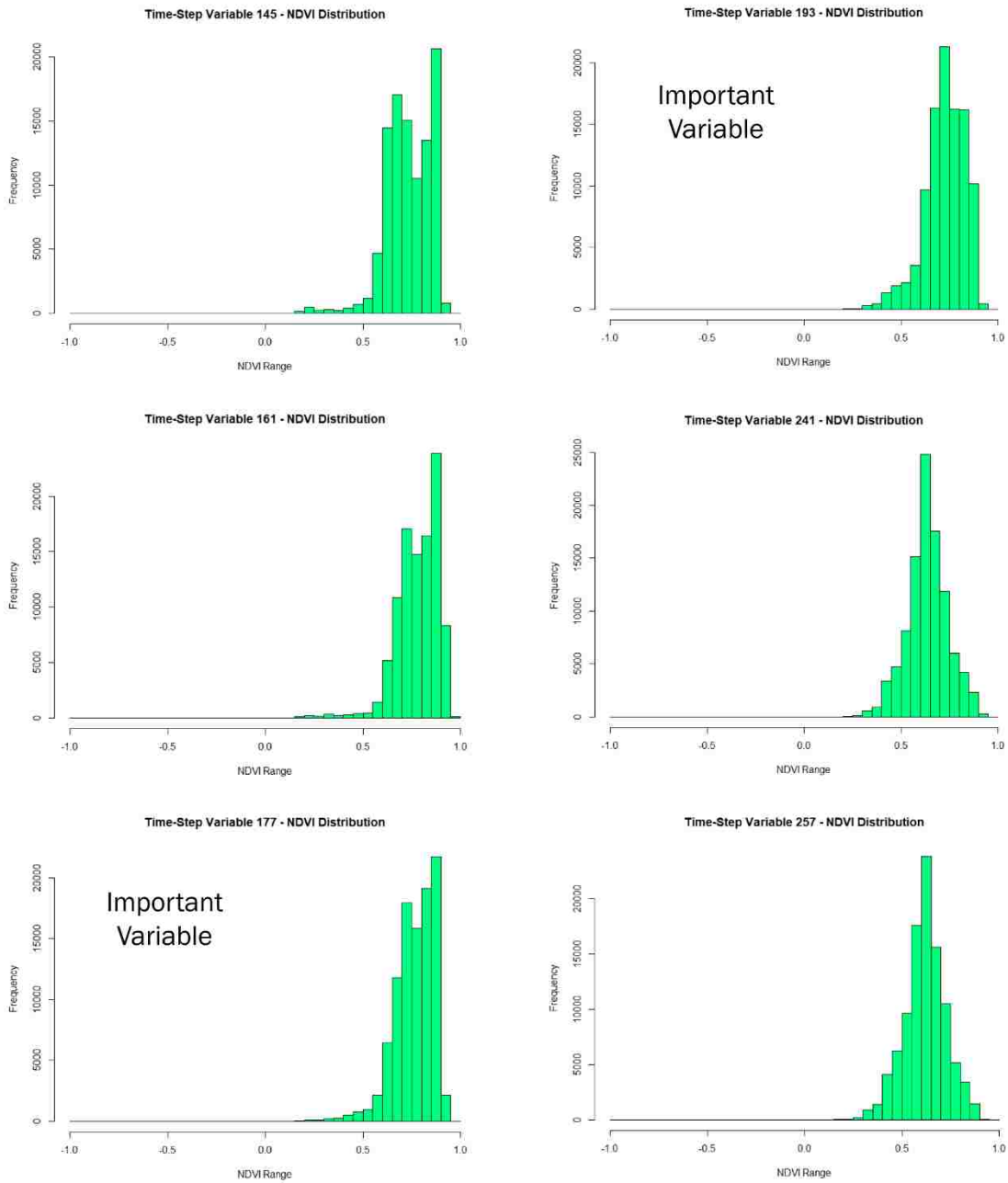
Figure 29: **Train NoClim & classify NoClim, CP/OM analysis histograms.**
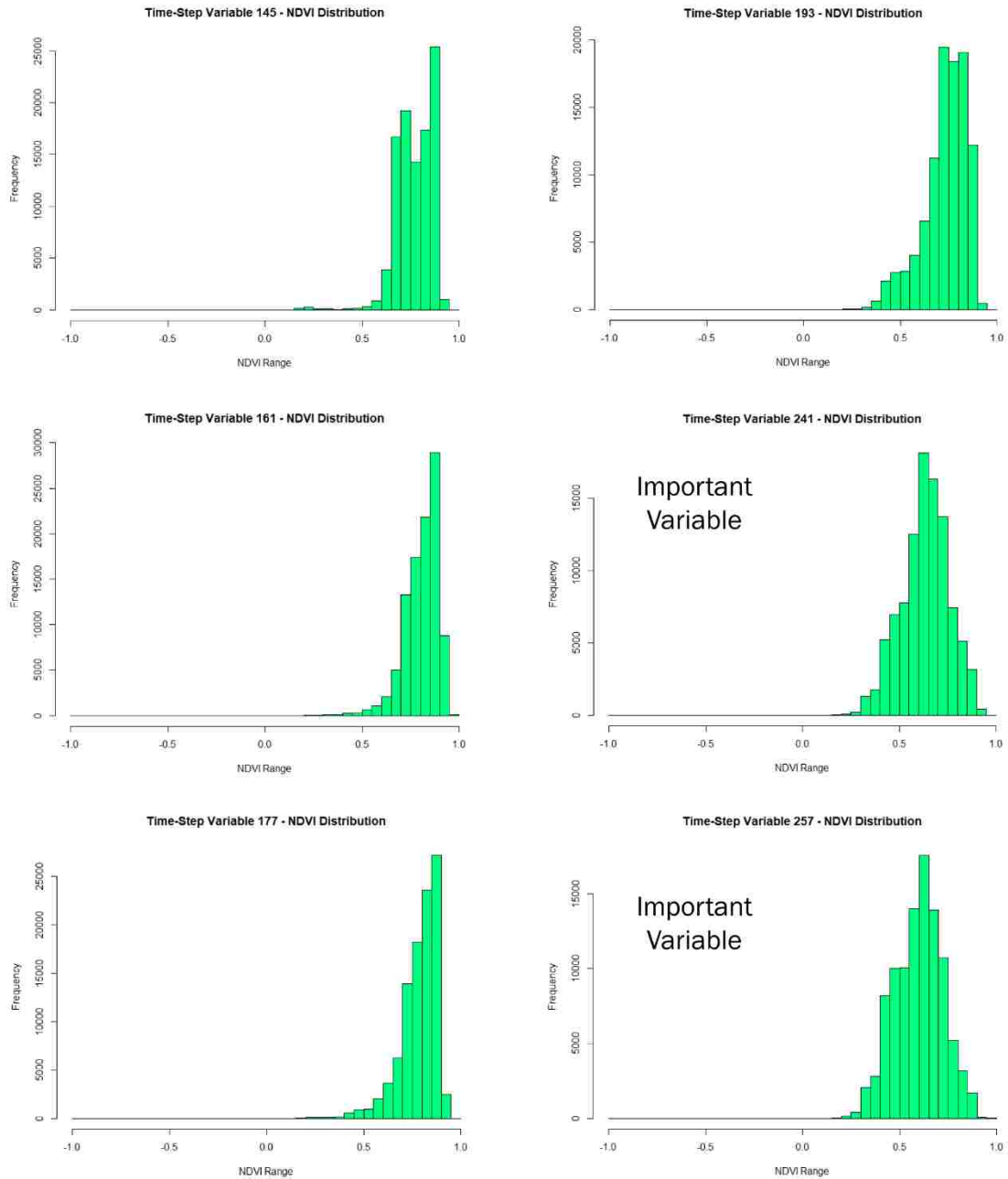
Figure 30: Train Clim & classify Clim, CP/OM analysis histograms.

Accuracy Assessments

Error matrices for all analyses and models were utilized to determine overall model accuracy when used to classify analysis areas and agreement between each product and its corresponding validation points. Agreement was measured by kappa ($\hat{k}$), which is a standardized measurement of the difference in validated outcome between the model (non-random) and the outcome expected from a random assignment of classes to validation points.

Random Forest

Since each model outputted a two-band probabilistic classified raster (i.e., irrigated – band 2 vs. unirrigated – band 1, or center pivot – band 2 vs. other methods – band 1). Threshold proportions of trees classifying pixels as either irrigated or center pivot were selected to form a binary, reclassified output, for which pixels greater than the threshold were either irrigated (for Irrig/Unirrig) or center pivot (for CP/OM). The thresholds 0.5, 0.6, 0.7, 0.8 and 0.9 were tested for the three Irrig/Unirrig analyses and six-class analysis, and the thresholds 0.5, 0.6 and 0.7 were tested for the three CP/OM analyses. For the six-class analysis, the threshold and highest position methods for assigning irrigated/unirrigated status were tested visually and with accuracy assessments. Each threshold was tested with an accuracy assessment, and overall accuracy was used to determine the threshold used for the final product of each analysis. For Irrig/Unirrig and six-class outputs, the 0.5 probability threshold produced the most accurate result all analyses, and for the CP/OM outputs, the 0.5 threshold produced the most accurate results for the train NoClim & classify NoClim and train NoClim & classify Clim analyses. For the train Clim & classify Clim, CP/OM analysis, the 0.6 threshold produced the most accurate result.

Overall accuracies, kappa statistics and class accuracies for the Random Forest models are summarized in Table 6. The most accurate analysis was the train Clim & classify Clim,

Irrig/Unirrig analysis, yielding 92% overall accuracy and almost perfect agreement ($\hat{k} = 0.83$).

The train NoClim & classify NoClim and train NoClim & classify Clim, Irrig/Unirrig analyses

Table 6: Accuracy assessments for all Random Forest analyses.

Accuracy Assessments					
Train NoClim & Classify NoClim Analysis **Accuracy Assessments – proportion/probability irrigated = 0.50, proportion/probability center pivot = 0.50**					
p < 0.01 Overall Accuracy = 0.85 Kappa ($\hat{k}$) = 0.70	**Reference**		*p* = 0.43 Overall Accuracy = 0.58 $\hat{k}$ = 0.16	**Reference**	
	Unirrigated	Irrigated		Other Method	Center Pivot
Mapped Unirrigated	19	3	Other Method	6	5
Mapped Irrigated	4	21	Center Pivot	5	8
Train NoClim & Classify Clim Analysis **Accuracy Assessments – proportion/probability irrigated = 0.50, proportion/probability center pivot = 0.60**					
p < 0.01 Overall Accuracy = 0.87 $\hat{k}$ = 0.75	**Reference**		*p* = 0.22 Overall = 0.61 $\hat{k}$ = 0.23	**Reference**	
	Unirrigated	Irrigated		Other Method	Center Pivot
Mapped Unirrigated	21	6	Other Method	9	7
Mapped Irrigated	0	20	Center Pivot	2	5
Train Clim & Classify Clim Analysis **Accuracy Assessments – proportion/probability irrigated = 0.50, proportion/probability center pivot = 0.60**					
p < 0.01 Overall Accuracy = 0.92 $\hat{k}$ = 0.83	**Reference**		*p* = 0.26 Overall Accuracy = 0.41 $\hat{k}$ = -0.20	**Reference**	
	Unirrigated	Irrigated		Other Method	Center Pivot
Mapped Unirrigated	37	3	Other Method	5	10
Mapped Irrigated	3	30	Center Pivot	9	8

 yielded overall accuracies of 85% and 87%, respectively, and substantial agreement ($\hat{k} = 0.70$ and $\hat{k} = 0.75$, respectively). Further, the six-class train Clim & classify Clim analysis yielded accuracy and agreement equal to the Irrig/Unirrig train Clim & classify Clim analysis regardless of the method used for assigning irrigated or unirrigated status, either threshold or highest position (overall accuracy = 92% and $\hat{k} = 0.83$). Finally, when post-classification masking with a moving 3 x 3 modal window was applied to the Irrig/Unirrig Clim analysis, overall accuracy improved to 94%, and agreement improved to 0.88.

Center pivot/other method accuracies and agreement were considerably lower, with the

train NoClim & classify Clim analysis yielding the highest accuracy, 61%, and fair agreement ($\hat{k}$

= 0.23). The train NoClim & classify NoClim, CP/OM analysis yielded an accuracy of 58% and

slight agreement ($\hat{k}$ = 0.16), and the train Clim & classify Clim analysis yielded an accuracy of

41% and less than chance agreement ($\hat{k}$ = -0.20), the lowest accuracy and agreement of all

analyses.

Decision Tree

Only a train Clim & classify Clim, Irrig/Unirrig Decision Tree analysis was conducted

due to the high accuracy and almost perfect agreement of the Random Forest Clim analysis and

the lack of accuracy and agreement of the CP/OM analyses. Therefore, only a single accuracy

assessment was required (Table 7). The output from the Decision Tree analysis was binary, not

probabilistic, and therefore no threshold selection and testing were necessary. The Decision Tree

analysis yielded an overall accuracy of 89% and substantial agreement ($\hat{k}$ = 0.78).

Table 7: Accuracy assessment for Decision Tree analysis.

Clim Decision Tree Analysis Accuracy Assessment			
p < 0.01 **Overall Accuracy = 0.89** $\hat{k}$ **= 0.78**		**Reference**	
		Unirrigated	Irrigated
Mapped	Unirrigated	37	5
	Irrigated	3	28

PCA

Principal Component Analysis was also performed on Clim data, and PCA does not

require training data. However, the output is unitless. Therefore, threshold selection was

necessary but due to the unitless nature of the output, somewhat arbitrary. The range of values

of all components was 0.04 to 11.82, which was also the range of the first component. Since the

first component explained 97% of the variance (Table 8), the first component was selected to

produce the Irrig/Unirrig PCA product. Various thresholds were selected (i.e., 0, 5 and 7), and

the binary, reclassified outputs (irrigated if pixel value > threshold) of each threshold were

visually assessed and compared with high-resolution imagery to determine which most closely

resembled irrigated areas. A threshold of 7 was selected, and the accuracy of a binary output

produced from a threshold of 7 was tested (Table 9). The overall accuracy was 88%, and

agreement was substantial ($\hat{k} = 0.75$).

Table 8: Principal component analysis proportions of variance by each component and corresponding Eigen values.

	PCA Statistics					
	Component 1	Component 2	Component 3	Component 4	Component 5	Component 6
Proportions	0.97	0.02	0.01	0	0	0
Eigen Values	5.81	0.11	0.04	0.03	0.01	0.01

Table 9: Accuracy assessment for PCA.

Clim PCA Accuracy Assessment			
$p < 0.01$ **Overall Accuracy = 0.88** **$\hat{k} = 0.75$**		Reference	
		Unirrigated	Irrigated
Mapped	Unirrigated	37	6
	Irrigated	3	27

Products

    Irrigated area, center pivot and other method areal estimates vary by analysis. Further,

forested areas are misclassified as irrigated in all Irrig/Unirrig products (Figure 31). Finally,

when interpreted visually, CP/OM analyses are unreliable on an analysis-area scale but

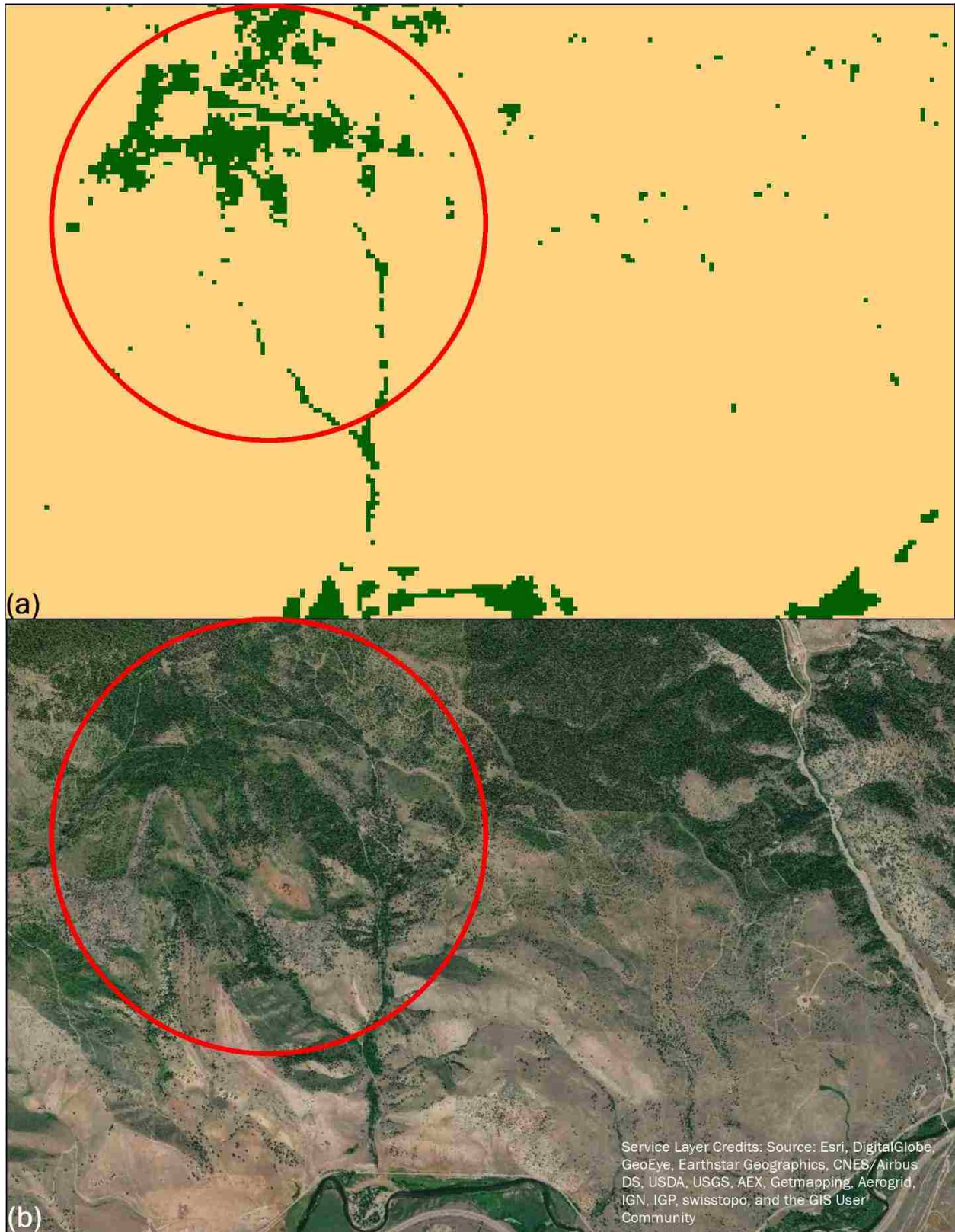inconsistently reliable at the scale of individual fields.

Figure 31. Misclassified forested areas: (a) Irrig/Unirrig Random Forest product irrigated area (misclassified); (b) forested area misclassified as irrigated by Random Forest model.

Random Forest

Products were generated from six Random Forest analyses. Irrigated area estimates increased with size of the analysis area. The train NoClim & classify NoClim analysis yielded a total irrigated area estimate of 340 km^2 (Figure 32a), an estimated 90 km^2 under center pivot systems and 250 km^2 under other methods of irrigation (Figure 32b). The train NoClim & classify Clim analysis yielded a total irrigated area estimate of 422 km^2 (Figure 33a), an estimated 91 km^2 under center pivot systems and 332 km^2 under other methods of irrigation (Figure 33b). The train Clim & classify Clim analysis yielded a total of irrigated area estimate of 467 km^2 (Figure 34a), an estimated 122 km^2 under center pivot systems and 345 km^2 under other methods of irrigation (Figure 34b). The six-class train Clim & classify Clim analysis yielded a total irrigated area estimate of 448 km^2 when the threshold method was applied to assign irrigated/unirrigated status (Figure 35a) and 600 km^2 when the highest-position method was applied. Finally, when post-classification masking with a 3 x 3 moving modal window was applied to the train Clim & classify Clim product, irrigated area was estimated at 327 km^2 (Figure 35b).

Visually, the train Clim & classify Clim irrigated area product closely matches the extent of irrigated area observed in the high-resolution imagery (Figure 36) except for forested areas on the edge of the analysis area (Figure 31). However, CP/OM models correctly classify some individual fields, but they do not correctly classify entire analysis areas (Figure 37).

Decision Tree

The Decision Tree used in a train NoClim & classify NoClim analysis was generated using the C4.5 algorithm (Figure 38). The algorithm constructed the decision-rule nodes using

the day 145, 177, 241 and 257 time-step variables. The Decision Tree model produced an

irrigated area estimate of 440 km^2 (Figure 39).

PCA

The PCA model generated a product from Clim data. The estimated irrigated area of the

PCA product is 493 km^2 (Figure 39).

Irrigated Area: 340 square kilometers

(a)

Unirrigated
Irrigated

Other Methods: 250 square kilometers
Center Pivot: 90 square kilometers

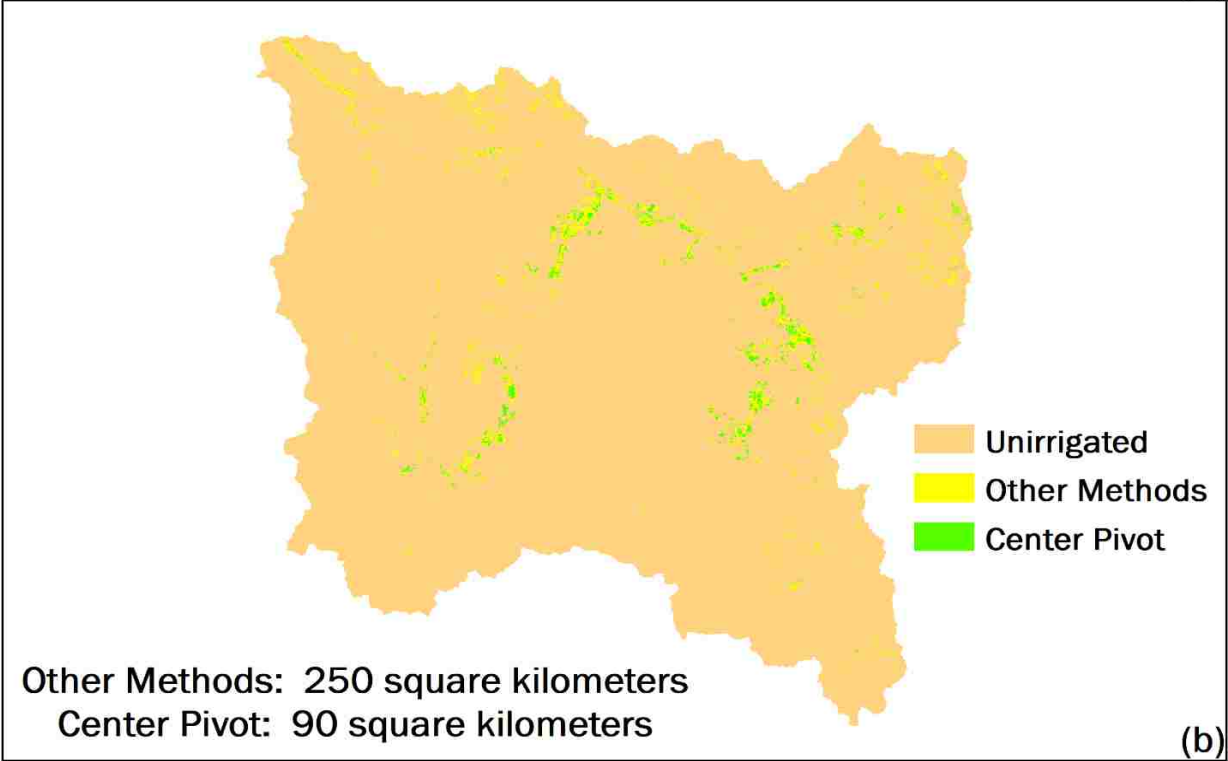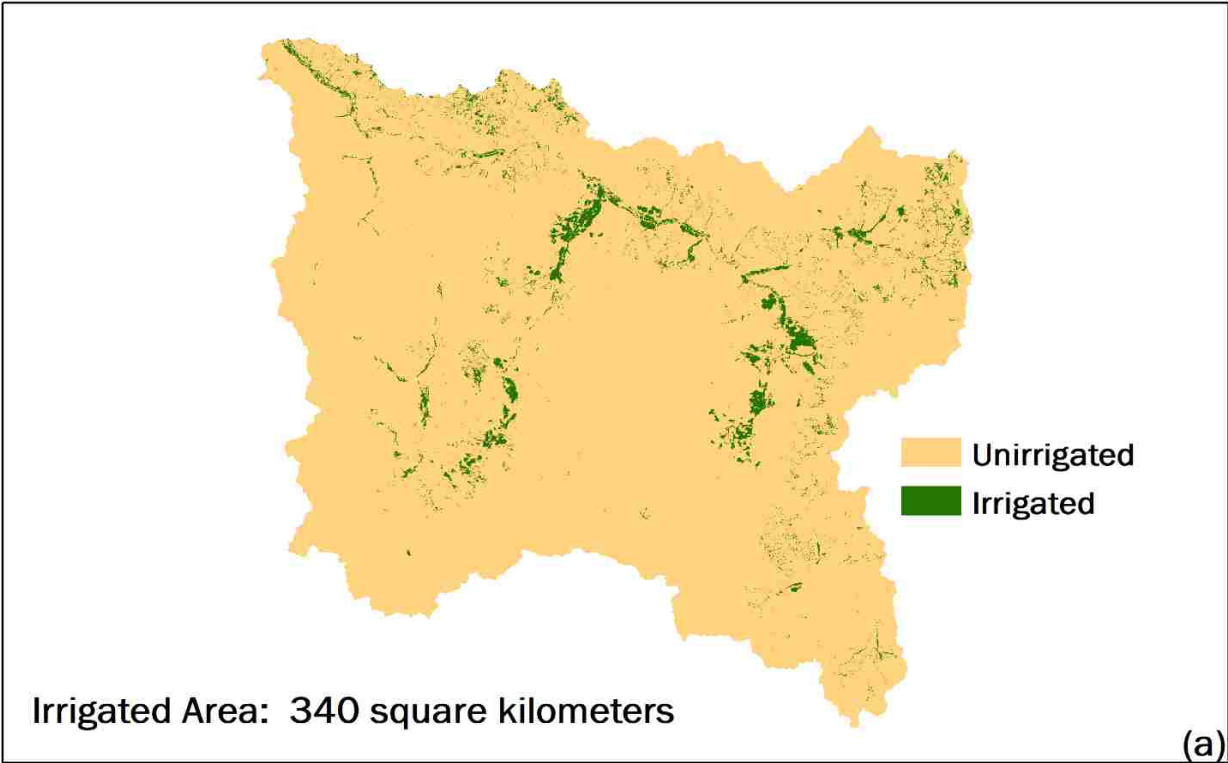(b)

Unirrigated
Other Methods
Center Pivot

Figure 32. Train NoClim & classify NoClim Random Forest products: (a) Train NoClim & classify NoClim irrigated product; (b) train NoClim & classify NoClim CP/OM product.

Irrigated Area: 422 square kilometers

(a)

Unirrigated
Irrigated

Other Methods: 332 square kilometers
Center Pivot: 91 square kilometers

(b)

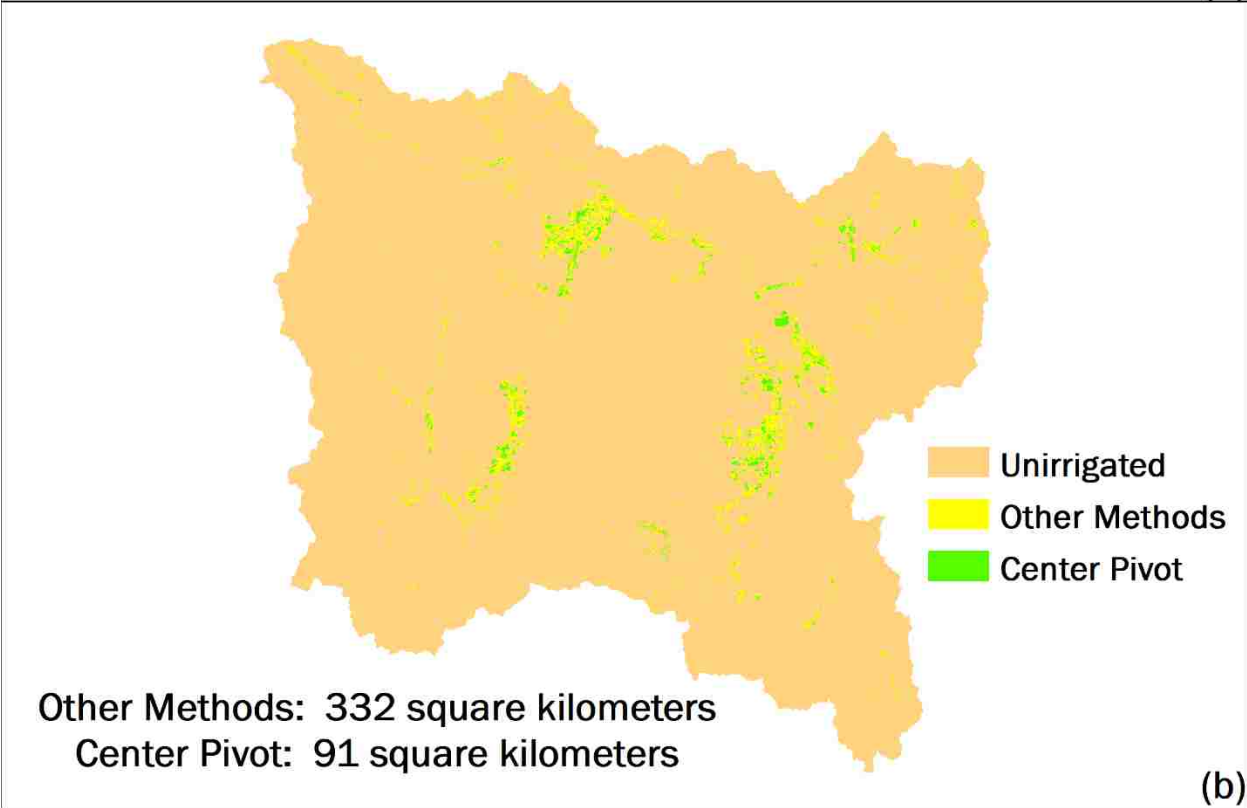Unirrigated
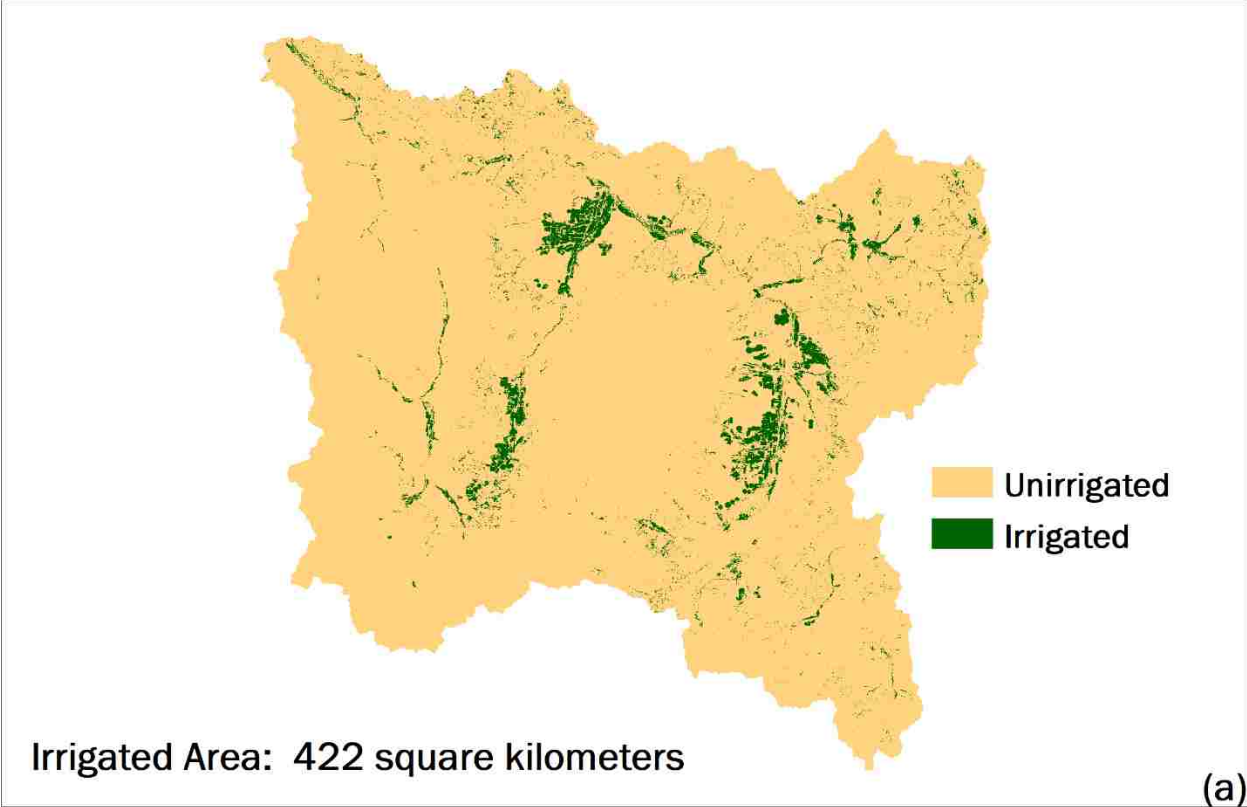Other Methods
Center Pivot

Figure 33. Train NoClim & classify Clim Random Forest products: (a) Train NoClim & classify climatology irrigated product; (b) train NoClim & classify climatology CP/OM product.
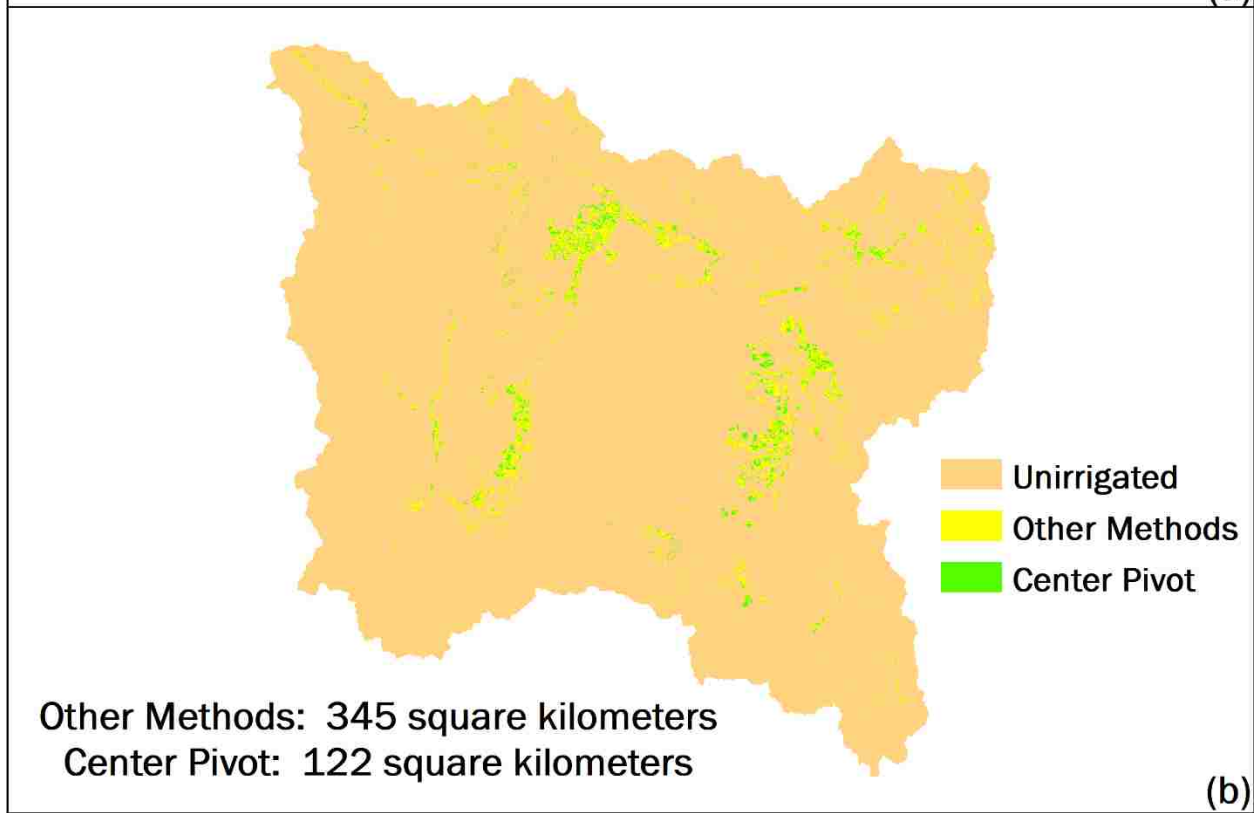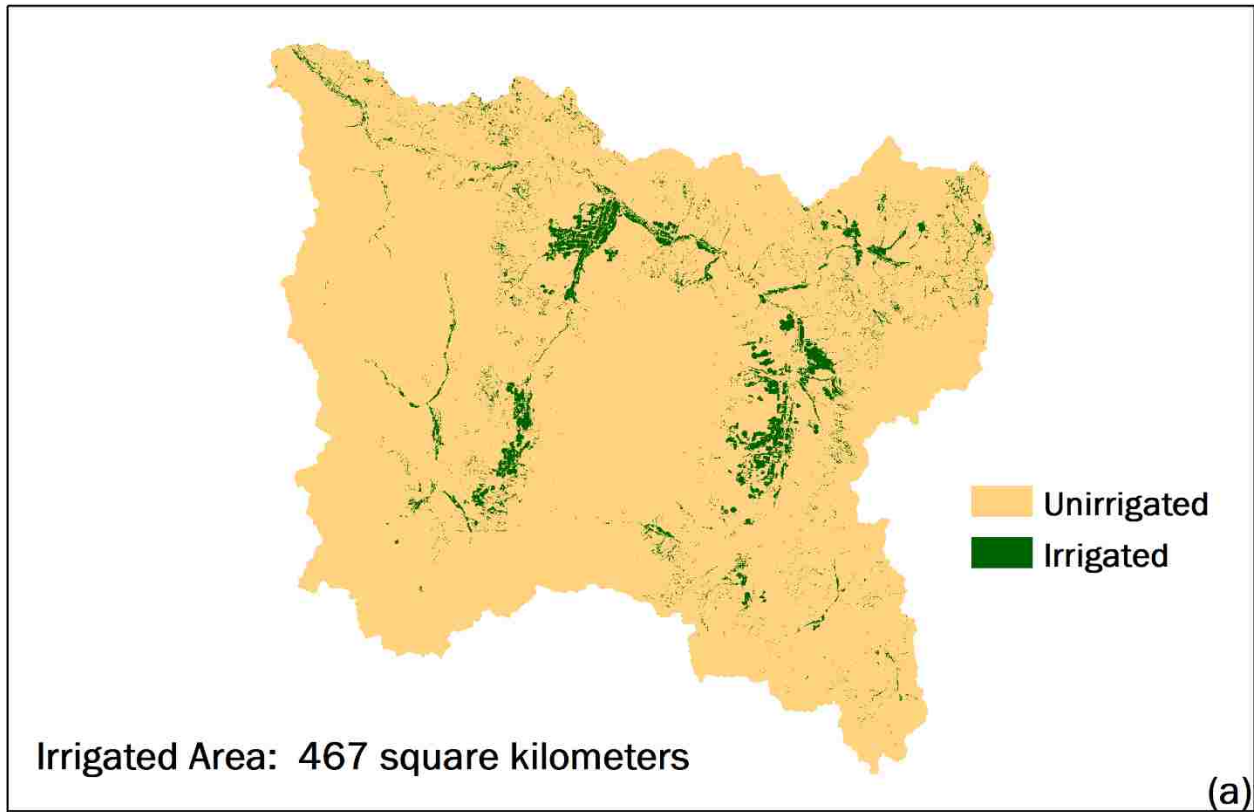
Figure 34. Train Clim & classify Clim Random Forest products: (a) Train Clim/classify Clim irrigated product; (b) train Clim/classify Clim CP/OM product.

Irrigated Area: 448 square kilometers

(a)

Irrigated Area: 327 square kilometers
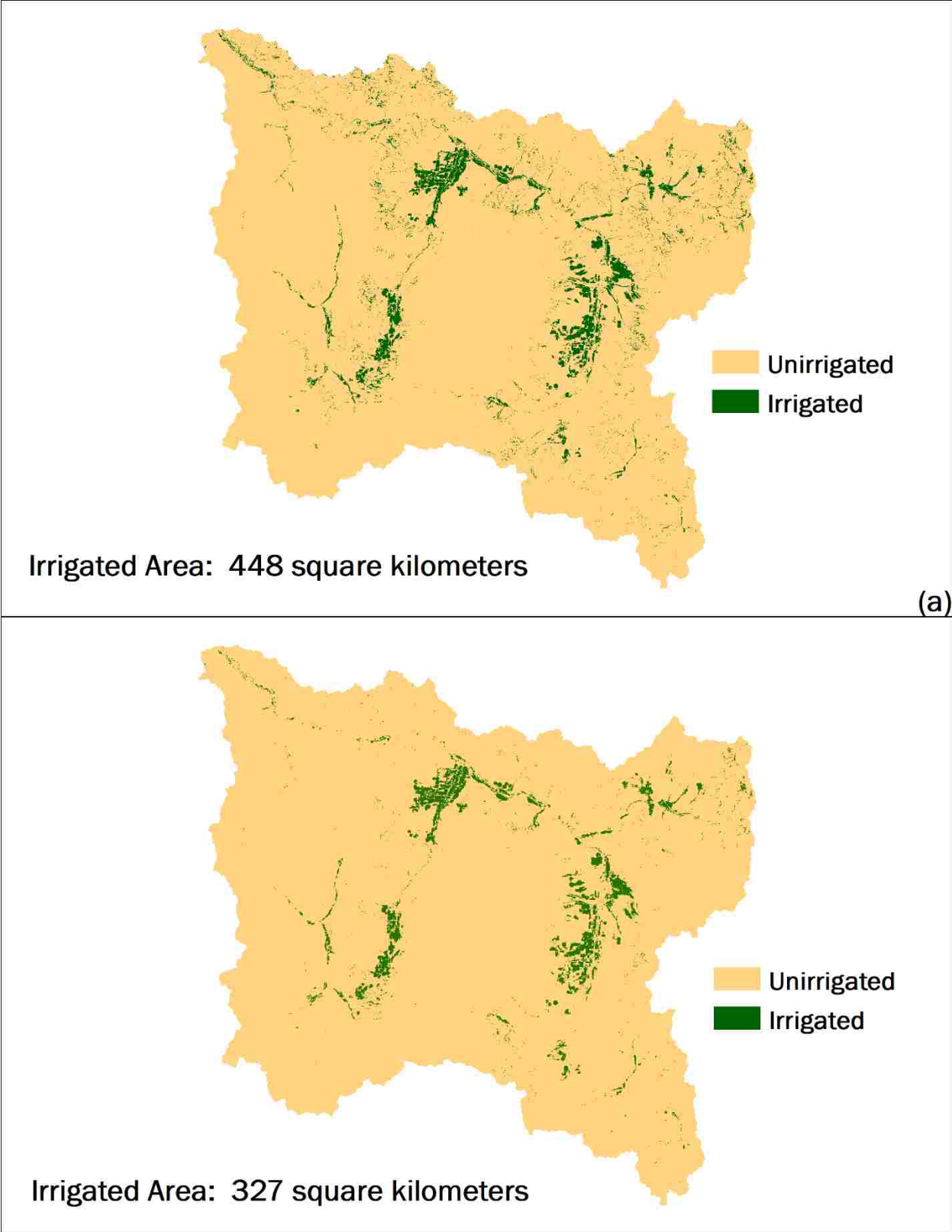
Figure 35. Products created to address classification errors: (a) Train Clim/classify Clim six-class product; (b) train Clim/classify Clim following post-classification land cover masking.
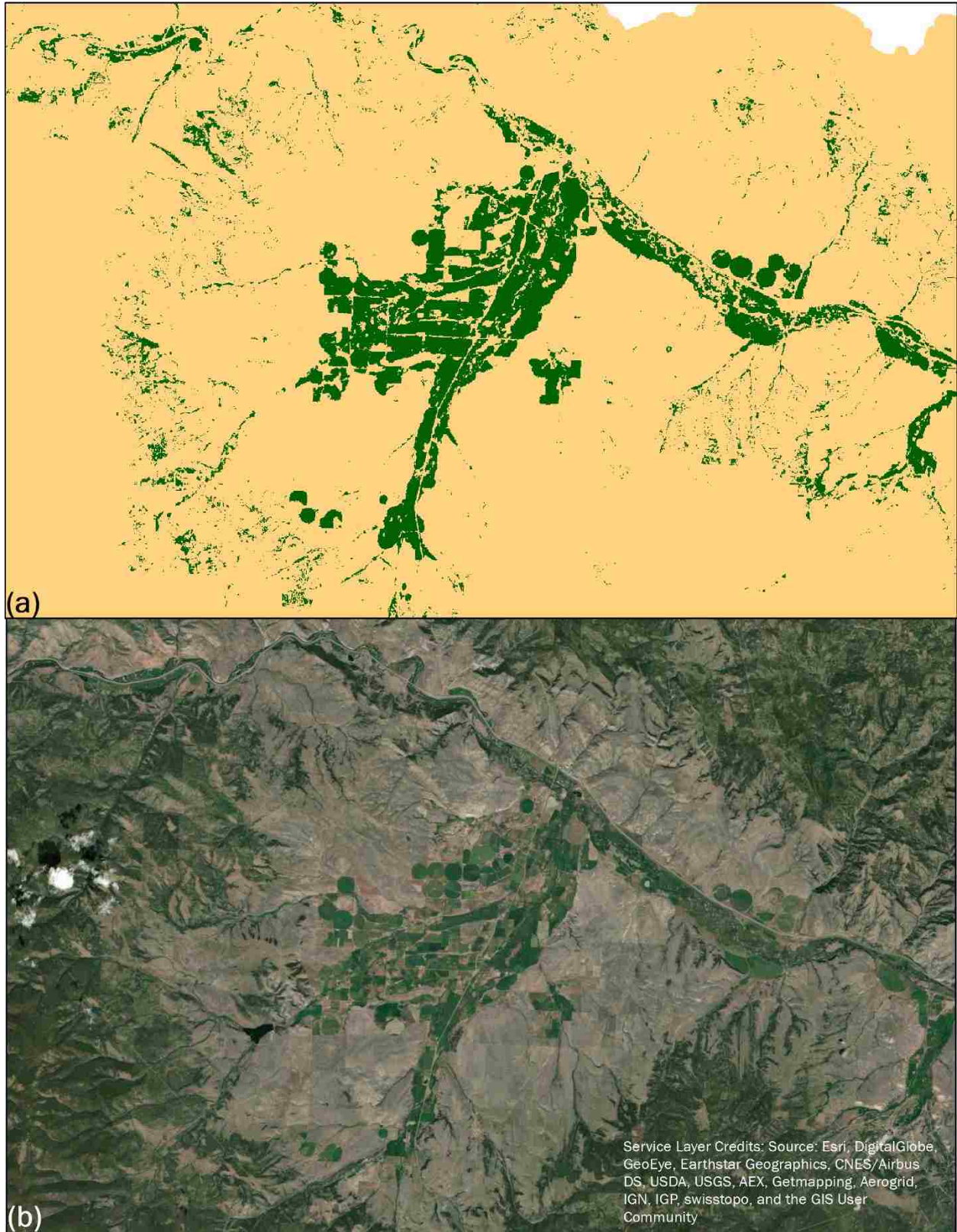
Figure 36. Irrigated/Unirrigated comparison: (a) Random Forest Irrig/Unirrig product; (b) high resolution imagery.
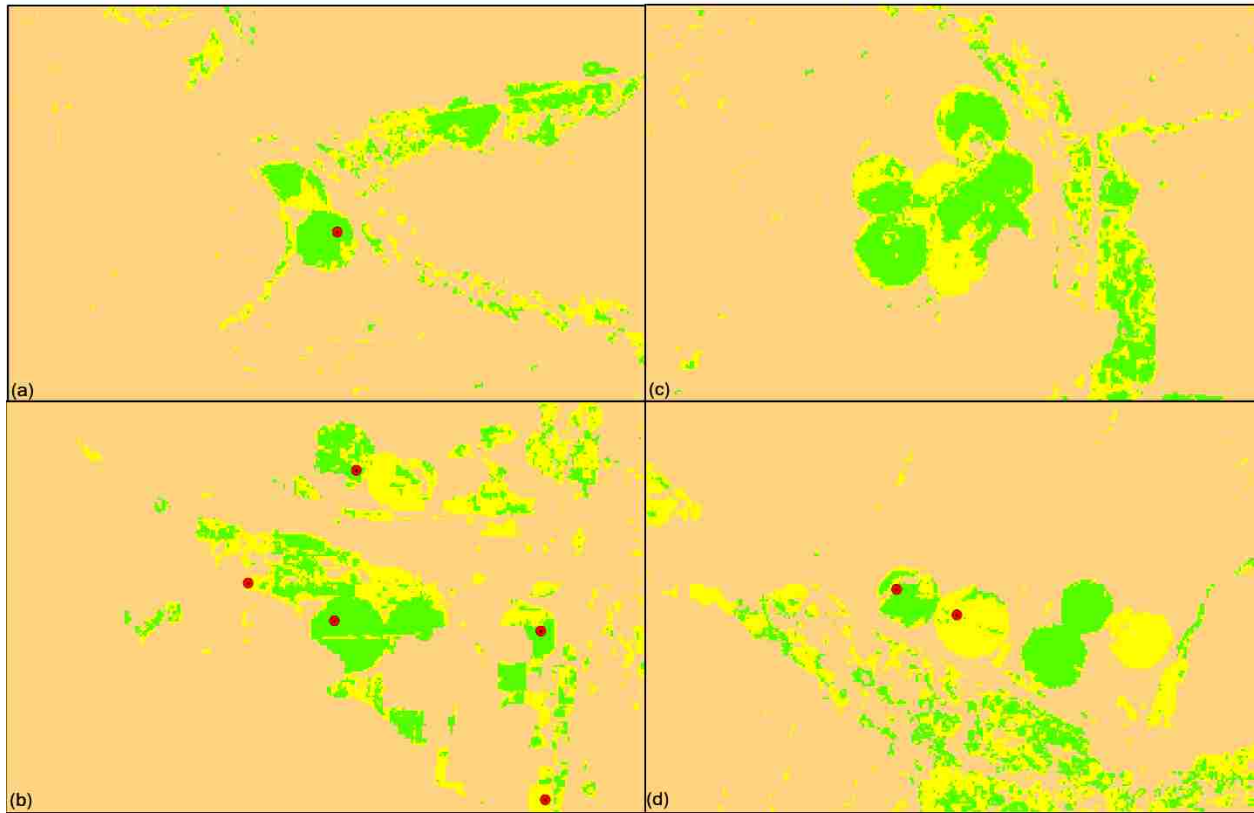
Figure 37. Center pivot/other method NoClim analysis center pivot comparisons: (a) Center pivot field with a training point on it; (b) a mixture of center pivot fields and fields under other irrigation methods, with at least two center pivot fields with training points on them; (c) cluster of center pivot fields with no training points on them; (d) two center pivot fields with training points, one mostly classified as center pivot and one most classified as other method.
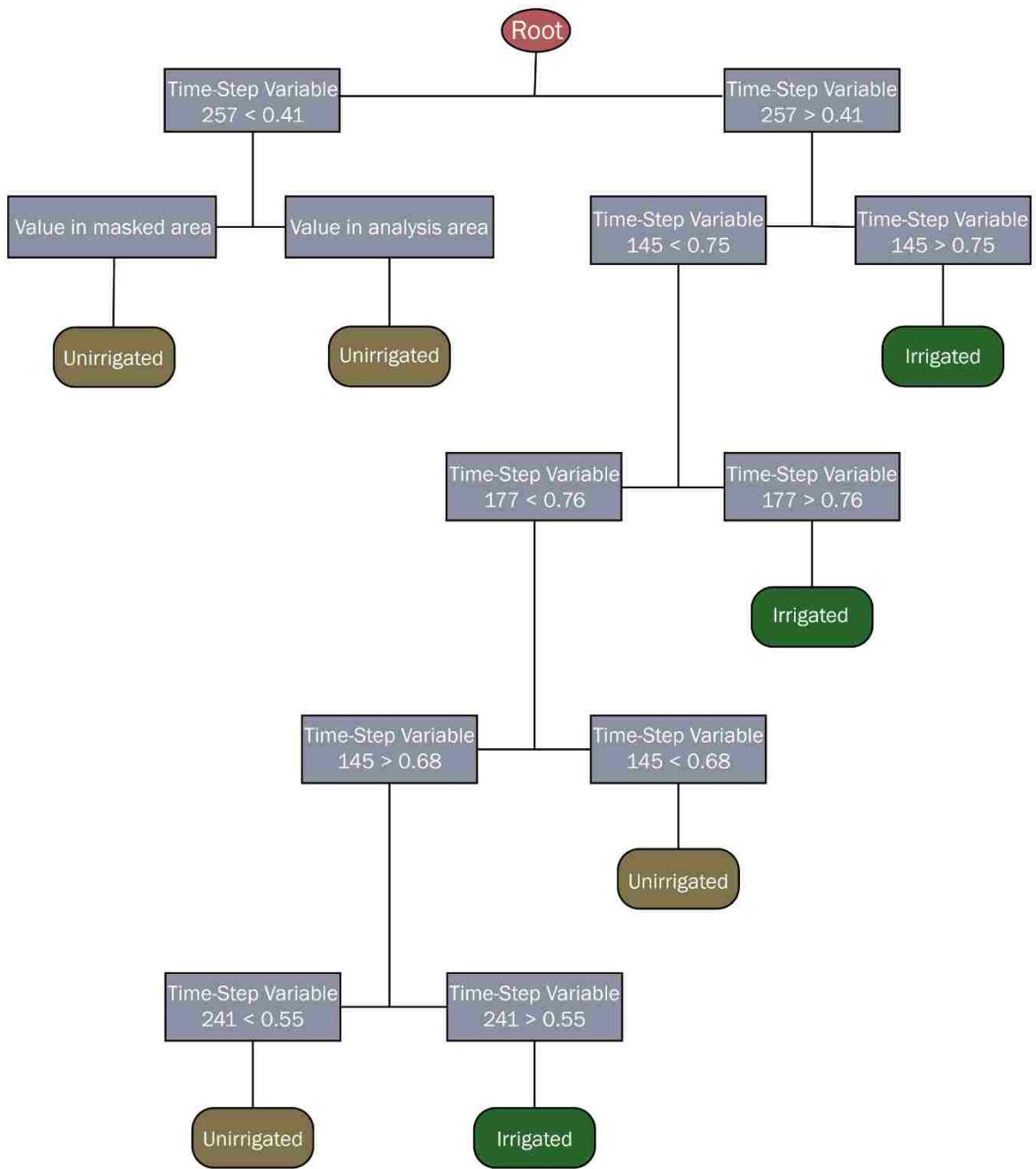
Figure 38: Decision tree, constructed by the C4.5 algorithm, used for classification.

Irrigated Area: 440 square kilometers

Unirrigated
Irrigated

Figure 39: Decision tree product.

Figure 40: Principal Component Analysis results compared with Random Forest and Decision Tree results.

DISCUSSION

Examinations of NDVI distributions reveals that two or three land cover classes may exist within the Irrig/Unirrig analysis areas. Certainly, one of these classes is irrigated land cover. However, NDVI distributions of certain shrubland, sagebrush steppe, grassland, disturbed forest and riparian areas seem to overlap with irrigated land ND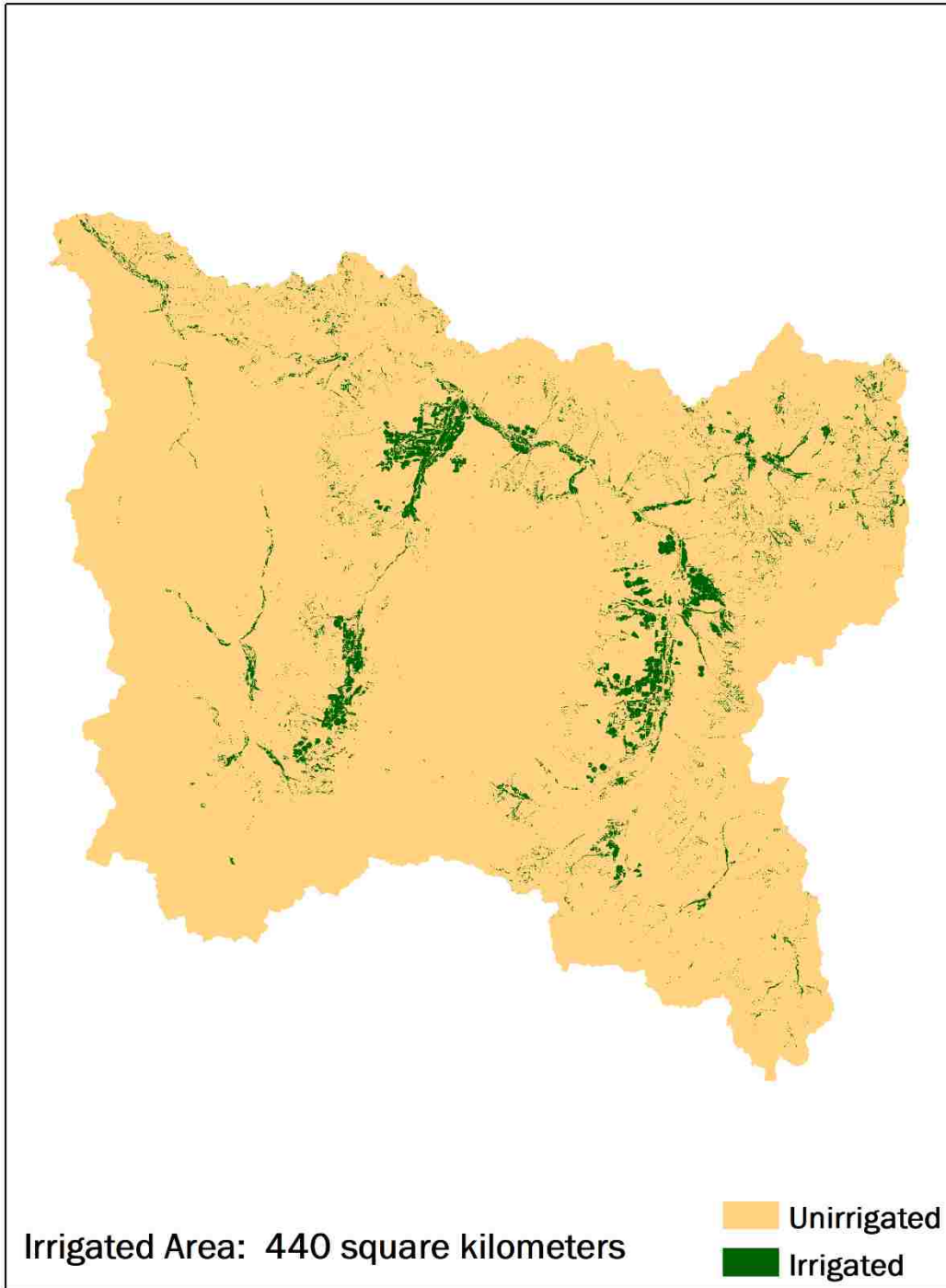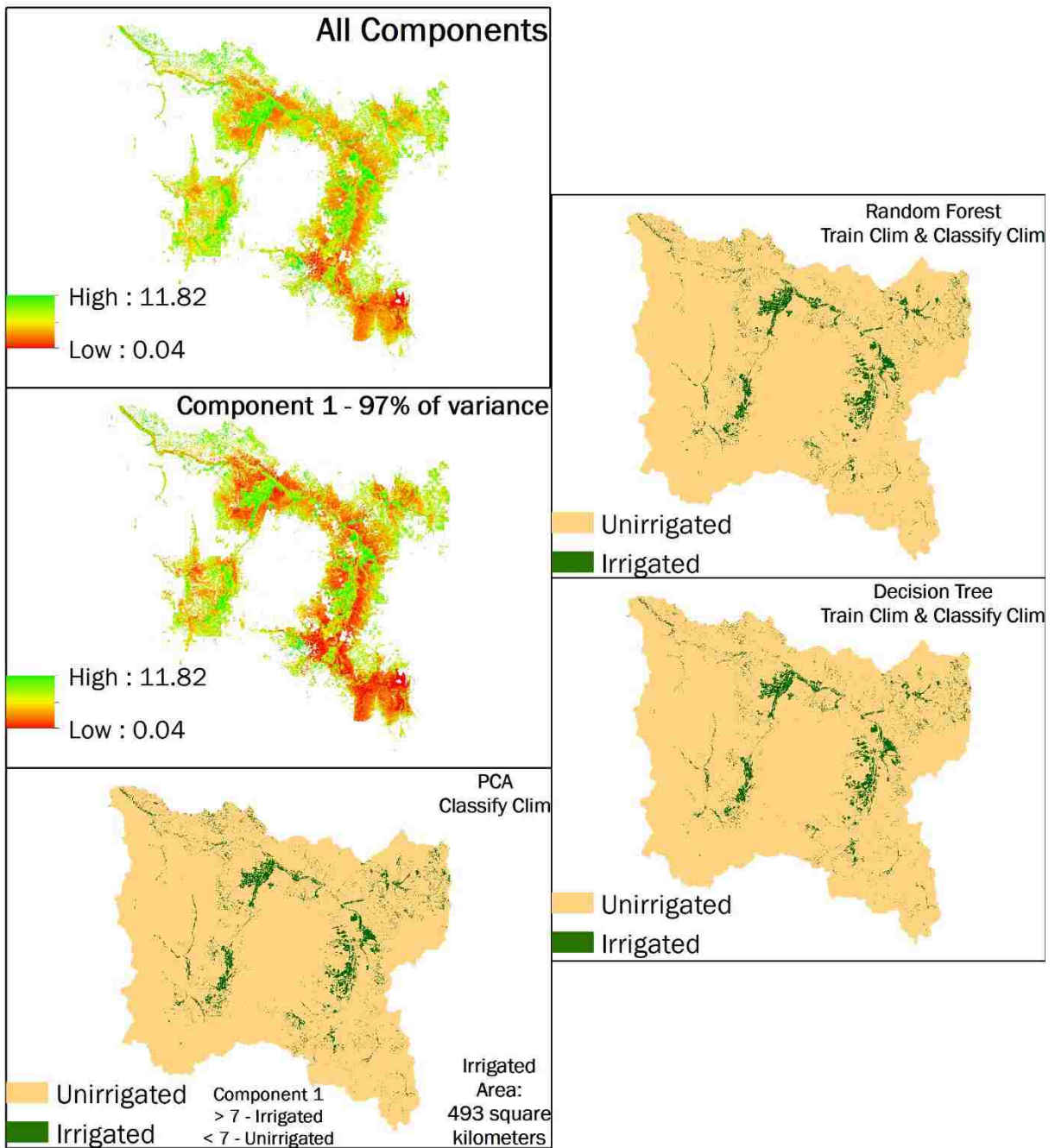VI distributions, since small patches of these areas on the edges of analysis areas are mistakenly classified as irrigated by the models.

Within areas classified as irrigated during the first stage of each analysis, NDVI distributions are expectedly narrower, and a bimodal pattern is not apparent (Figure 29 and Figure 30). Additionally, probability distribution graphs for CP/OM models demonstrate that smaller proportions of trees classify pixels as center pivot or other method when compared with the probability distribution graphs of Irrig/Unirrig models. This difference in confidence between the Irrig/Unirrig models and CP/OM models suggests that NDVI temporal profiles alone may not adequately train models to distinguish between center pivot irrigated land cover and other methods. However, average spectro-temporal profiles of center pivot and other method classes (Figure 21) suggest the formation of two classes within irrigated land cover.

Variable importance examination also revealed that the number of training points and/or sampling scheme plays a considerable role in development of models. For the Irrig/Unirrig analyses, two models were trained on the same NoClim analysis areas by randomly selecting 79 of 126 points (63%) from the same 2018 training and validation point set for each model (Figure 16). However, for the train NoClim & classify NoClim analysis, only removal of time-step variable 257 created error greater than saturation error, but for the train NoClim & classify Clim analysis, days 145 and 161 were the most important model variables, and both of these models

78

were trained with 63% of the 2018 TVPs. Increasing the number of points and the size and

extent of the sampling and classification area for the train Clim & classify Clim analysis created

a more robust Irrig/Unirrig model (Table 5 and Table 6), suggesting this inconsistency in

variable importance among models trained with the same NoClim analysis areas and proportion

of points could be attributed to the extent and size of analysis areas. The NoClim analysis area

covers 1,477 km^2, 15% of the study area (Figure 7a-b), and NoClim training utilized 79 points

(Figure 16a, c), while the Clim analysis area covers 2,636 km^2, 28% of the study area (Figure

7c), and Clim training utilized 123 points (Figure 16e), suggesting that an increase in sample size

and sampling area created a more robust model. Finally, changing the sampling scheme to a

pure stratified random sampling approach for irrigated points, like the approach used for

unirrigated points, would likely require a reduced standard for ground truthing irrigated land

cover. The standard for irrigated points in this study required that active irrigation was observed

and marked in a TVPs layer exactly where it was observed. Due to the daily and seasonal timing

of active irrigation, observing active irrigation at stratified random pre-selected points would be

rare, if adhering to the strict, observed active irrigation sampling standard, thus substantially

reducing the number of irrigated points and affecting the representation of different irrigation

methods within the sample. To retain enough irrigated points, standards would need to be

loosened, and irrigation validation at points would usually require inference, rather than direct

observation. Fields with higher greenness relative to their surroundings with evidence of

irrigation infrastructure would meet the criteria of "irrigated," regardless of the presence of

active irrigation at the time of observation. For a study area where most agricultural areas are

irrigated, this is perhaps acceptable, but for study areas where rainfed crops represent a

substantial proportion of agricultural production, standards for irrigated point validation should

remain strict, thus requiring a modified approach to the stratified random sampling method for irrigated points validation.

For Irrig/Unirrig analyses, results are promising. Although, additional land cover masking or model training with more classes could mitigate misclassification of certain areas and increase accuracy. This was explored, and masking problem land cover classes produced better results, but training with more classes did not mitigate the issue of misclassified pixels on analysis area edges. However, the lack of sampling for training points on analysis area edges where no public, drivable roads exist could explain why the issue was not mitigated by increasing the number of classes. Random sampling for training points without a roads bias would provide better representation of classes that spectrally resemble the irrigated class, and this may lead to a better product that does not overestimate irrigated land cover. Due to bias created by only sampling along roads, accuracy assessments are not fully accounting for the misclassification of pixels on the edges of analysis areas. Due to the difficulty of accessing areas at considerable distances from roads, using a high-resolution imagery validation approach for unirrigated points comfortably outside agricultural areas could reduce bias. However, this would require using separate strategies for irrigated and unirrigated points, thus introducing a bias created by using two considerably different sampling methods. Finally, using high-resolution imagery without field verification to validate irrigated points creates a bias of uncertainty.

Results from CP/OM analyses are less promising. At the scale of individual fields, accuracy is inconsistent (Figure 37), but at the analysis-area scale, accuracy is non-existent. Field-level accuracy is perhaps attributable to variation in average spectro-temporal profiles of center pivot and other method irrigated land cover, but this is not certain. Training points on individual fields could train models to classify similar fields based on the spectral variation

80

produced by different crop species or seed mixtures. Most of the UCFRB crop species are hay or

forage, but percent grass/alfalfa mixtures are highly variable, and barley composes a small

percentage of crop production. Alternatively, since these analyses are temporal, timing of water

application (not necessarily based on irrigation system) could also explain accurate classification

of some center pivot fields. Regardless, small variations in center pivot systems and other

methods may not exist at larger scales. As scale of the analysis area increased, CP/OM model

error increased, and product accuracy declined considerably (Table 5 and Table 6).

CONCLUSION

The aims of this study were: (1) determine which classification model worked best for

irrigation classification in the UCFRB of western Montana, (2) develop a simple method for

classifying irrigated land cover in semi-arid western Montana, and (3) attempt classification of

irrigation by method using only time-series NDVI data. All three aims were achieved, but

results were not completely satisfactory. When trained and run on Clim data, the Random Forest

model was the most robust method (classification error = 0.04, overall accuracy = 92% and $\hat{k}$ =

0.83), and accuracy and agreement of that analysis increased with post-classification masking

(overall accuracy = 94% and $\hat{k}$ = 0.88). However, the Decision Tree model produced accurate

results as well (overall accuracy = 0.89 and $\hat{k}$ = 0.78. Random Forests and Decision Trees are

suitable for this semi-arid river basin, and they have been proven suitable in the American West

for other studies. The PCA analysis also yielded strong results, but due to the arbitrary nature of

threshold selection from a unitless range of values and the inability to train a PCA model, it is

not recommended for irrigation classification. Irrigation classification was successful, but there

is room for improvement, and lack of variable importance consistency among models trained

without Clim data is likely mitigated by increasing the analysis area to include Clim data and

more training points. Training a Random Forest model with more classes or further masking could provide the best solution. However, this makes products more dependent on the accuracy of land cover products. Adjustments in masking will produce a sufficient binary, Irrig/Unirrig product in semi-arid river basins of western Montana and adjusting the number of training classes may as well. Further, introduction of climate data into the classification process reduces ambiguity in identifying irrigation using only remotely-sensed inputs on the continental scale (Ozdogan and Gutman 2008) and potentially reduces ambiguity on smaller scales but is likely unnecessary on smaller scales for most purposes. Further, the potential for model error leading to misclassification of isolated pixels or clusters of isolated pixels within otherwise homogenous areas might increase at higher resolutions. Finally, the green index has shown promise as a better alternative to NDVI (Ozdogan and Gutman 2008) and should be included in future analyses.

The methodology and workflow developed for irrigated area classification is simple, reproducible and implementable in ArcGIS, a widely utilized GIS program. Further, the climatology-interpolated NDVI dataset produced by Robinson et al. (2017) is suitable for irrigation classification as demonstrated by the low model error and high model accuracies generated from running analyses on areas including Clim data. The increase in irrigated area estimates, decline in model error, increase in accuracy, and increase in agreement associated with the inclusion of Clim data suggests that temporal classifications utilizing only clear pixels/NoClim data are impractical. The viability of this dataset makes 30-meter Landsat SR products better suited for similar spectro-temporal analyses for which NDVI is a suitable index. The methodology developed in this study is simple and at least applicable across western Montana and probably across the American West with one or a few adjustments. Increasing the

number of classes or further masking or some combination of those potential solutions should reduce the problem of misclassified areas on the edges of analysis areas. However, to apply this approach to other river basins in western Montana or the American West, field-verified points for each basin are important, since spectro-temporal profiles change as climate, irrigation timing and crop type varies.

Finally, subclassification of irrigated areas by method was attempted but unsuccessful. The best models for CP/OM classification were those trained with NoClim data (Table 5 and Table 6), but error and accuracies were insufficient for the those models, and probability distributions for important variables demonstrate that a consistently smaller proportion of trees classified pixels as center pivot or other method when compared with Irrig/Unirrig analyses, suggesting a problem with model confidence for the CP/OM analyses. Evapotranspiration data coupled with spectral data transformed to the green index and machine learning algorithms trained to classify rearranged classes (e.g., sprinkler and flood) may produce better results.

REFERENCES

Ambika, Anukesh Krishnankutty, Brian Wardlow, and Vimal Mishra. 2016. "Remotely Sensed High Resolution Irrigated Area Mapping in India for 2000 to 2015." *Scientific Data* 3 (December): 1-13. https://doi.org/10.1038/sdata.2016.118.

Anderson, J. R., E. E. Hardy, J. T. Roach, and R. E. Witmer. 1976. *A Land Use and Land Cover Classification System for Use with Remote Sensor Data*, US Department of the Interior. US Geological Survey. US Geological Survey Circular 671. Washington: US Government Printing Office.

Barbosa, P. M., M. A. Casterdad, and J. Herrero. 1996. "Performance of Several Landsat 5 Thematic Mapper (TM) Image Classification Methods for Crop Extent Estimates in an Irrigation District." *International Journal of Remote Sensing* 17, no. 18: 3665-3674.

Biggs, T. W., P. S. Thenkabail, M. K. Gumma, C. A. Scott, G. R. Parthasaradhi, and H. N. Turral. 2007. "Irrigated Area Mapping in Heterogenous Landscapes with MODIS Time Series, Ground Truth and Census Data, Krishna Basin, India." *International Journal of Remote Sensing* 27, no. 19 (October): 4245-4266.

Boucher, O., G. Myhre, and A. Myhre. 2004. "Direct Human Influence of Irrigation on Atmospheric Water Vapouir and Climate." *Climate Dynamics* 22: 597-603.

Breiman, Leo. 2001. "Random Forests." *Machine Learning* 45: 5-32.

Brown, Jesslyn F., and Md Shahriar Pervez. 2014. "Merging Remote Sensing Data and National Agricultural Statistics to Model Change in Irrigated Agriculture" *Agricultural Systems* 127: 28-40.

Bruinsma, Jelle, ed. 2003. *World Agriculture: Towards 2015/2030 An FAO Perspective*. London: Earthscan Publications Ltd.

Chen, Yaoliang, Lu Dengsheng, Luo Lifeng, Yadu Pokhrel, Kalyanmoy Deb, Jingfeng Huang, and Youhua Ran. 2018. "Detecting Irrigation Extent, Frequency, and Timing in a Heterogeneous Arid Agricultural Region using MODIS Time Series, Landsat Imagery, and Ancillary Data." *Remote Sensing of Environment* 204: 197-211.

Dappen, Patti. 2003. *Using Satellite Imagery to Estimate Irrigated Land: A Case Study in Scotts Bluff and Kearney Counties: Summer 2002*. Lincoln, Nebraska: University of Nebraska – Lincoln, Center for Advanced Land Management Information Technologies.

Deines, J.M., A.D. Kendall, and D.W. Hyndman. 2017. "Annual Irrigation Dynamics in the US Northern High Plains Derived from Landsat Satellite Data" *Geophysical Research Letters* 44: 9350-9360.

Eckhardt, David W., James P. Verdin, and Gordon R. Lyford. 1990. "Automated Update of an Irrigated Lands GIS Using SPOT HRV Imagery" *Photogrammetric Engineering and Remote Sensing* 56, no. 11 (November): 1515-1522.

Food and Agriculture Organization. International Fund for Agricultural Development. United Nations International Children's Emergency Fund. World Food Program. World Health Organization. 2018. *The State of Food Security and Nutrition in the World 2018: Building Climate Resilience for Food Security and Nutrition*. Rome: Food and Agriculture Organization.

Heimes, Frederick J., and Richard R. Luckey. 1980. *Evaluating Methods for Determining Water use in the High Plains in Parts of Colorado, Kansas, Nebraska, New Mexico, Oklahoma, South Dakota, Texas and Wyoming; 1979*, US Department of the Interior. US Geological Survey. Water-Resources Investigations 80-111. Denver, Colorado: US Geological Survey, Water Resources Division.

Hill, Robert W., and Ivan A. Walter. 2003. "Irrigation Impact on River Flows." In *Encyclopedia of Water Science*, edited by B. A. Stewart, and Terry A. Howell, 473-477. New York, Marcel Dekker, Inc.

Hogland, J., and N. Anderson. 2017. "Function Modeling Improves the Efficiency of Spatial Modeling Using Big Data from Remote Sensing." *Big Data and Cognitive Computing* 1, no. 3: 1-14.

Howell, Terry A. 2003. "Irrigation Efficiency." In *Encyclopedia of Water Science*, edited by B. A. Stewart, and Terry A. Howell, 467-472. New York: Marcel Dekker, Inc.

Intergovernmental Panel on Climate Change. 2014. *Climate Change 2014: Synthesis Report: Contribution of Working Groups I, II and III to the Fifth Assessment Report of the Intergovernmental Panel on Climate Change*, by The Core Writing Team, R.K. Pachauri, and L.A. Meyer. Geneva, Switzerland: IPCC.

Irmak, Suat, Lameck O. Odhiambo, William L. Kranz, and Dean E. Eisenhauer. 2011. "Irrigation Efficiency and Uniformity, and Crop Water Use Efficiency." Biological Systems

Engineering: Papers and Publications. Accessed March 6, 2018.
https://digitalcommons.unl.edu/biosysengfacpub/451.

Kearney, John. 2010. "Food Consumption Trends and Drivers." *Philosophical Transactions:
Biological Sciences* 365, no. 1554 (September): 2793-2807.

Lauffenburger, Zachary H., Jason J. Gurdak, Chris Hobza, Duane Woodward, and Cassandra
Wolf. 2018. "Irrigated Agriculture and Future Climate Change Effects on Groundwater
Recharge, Northern High Plains Aquifer, USA." *Agricultural Water Management* 204:
69-80.

Lutz, Wolfgang, and Samir KC. 2010. "Dimensions of Global Population Projections: What do
We Know about Future Population Trends and Structures?" *Philosophical Transactions:
Biological Sciences* 365, no. 1554 (September): 2779-2791.

Montana Department of Natural Resources and Conservation (DNRC). Water Rights Bureau.
Change Applications. 2013. *Change Application – Historic Use*. ch. 36.12, rule no. 1902
(2013).

Montana DNRC. 2018. "Survey Books." Water Rights Bureau. Accessed September 23, 2018.
http://dnrc.mt.gov/divisions/water/water-rights/records-unit/survey-books.

Montana State Library. 2018a. "Geographic Information Clearinghouse." Accessed October 22,
2018. http://geoinfo.msl.mt.gov/.

——. 2018b. *Montana Ground-Water Atlas*. Accessed October 10, 2018.
http://geoinfo.msl.mt.gov/geography/water_information_system/groundwater/groundwat
er_maps.aspx.

Ozdogan, Mutlu, Curtis E. Woodcock, Guido D. Salvucci, and Hüseyin Demir. 2006. "Changes
in Summer Irrigated Crop Area and Water Use in Southeastern Turkey from 193 to 2002:
Implications for Current and Future Water Resources." *Water Resources Management*
20: 467-488.

Ozdogan, Mutlu, and Garik Gutman. 2008. "A New Methodology to Map Irrigated Areas using
Multi-Temporal MODIS and Ancillary Data: An Application Example in the Continental
US." *Remote Sensing of Environment* 112: 3520-3537.

Peña-Arancibia, Jorge L., Mohammed Mainuddin, John M. Kirby, Francis H.S. Chiew, Tim R.
McVicar, and Jai Vaze. 2016. "Assessing Irrigated Agriculture's Surface Water and

Groundwater Consumption by Combining Satellite Remote Sensing and Hydrologic Modelling." *Science of the Total Environment* 542: 372-82.

Pervez, Md. Shahriar, and Jesslyn F. Brown. 2010. "Mapping Irrigated Lands at 250-m Scale by Merging MODIS Data and National Agricultural Statistics." *Remote Sensing* 2: 2388-2412.

Pervez, Md. Shahriar, Michael Budde, and James Rowland. 2014. "Mapping Irrigated Areas in Afghanistan over the Past Decade using MODIS NDVI." *Remote Sensing of Environment* 149: 155-165.

Planet Labs. 2018. "Planet Explorer." Accessed October 22, 2018. https://www.planet.com/.

Postel, Sandra L. 2003. "Securing Water for People, Crops, and Ecosystems: New Mindset and New Priorities." *Natural Resources Forum* 27: 89-98.

Quinlan, J. Ross. 1993. *C4.5: Programs for Machine Learning*. San Francisco: Morgan Kaufman.

Rask, Kolleen J., and Norman Rask. 2011. "Economic Development and Food Production-Consumption Balance: A Growing Global Challenge." *Food Policy* 36: 186-196.

Robinson, Nathaniel P., Brady W. Allred, Matthew O. Jones, Alvaro Moreno, John S. Kimball, David E. Naugle, Tyler A. Erickson, and Andrew D. Richardson. 2017. "A Dynamic Landsat Derived Normalized Difference Vegetation Index (NDVI) Product for the Conterminous United States." *Remote Sensing* 9, no. 8: 63-877.

Sala, Osvaldo E., F. Stuart Chapin III, Juan J. Armesto, Eric Berlow, Janine Bloomfield, Rodolfo Dirzo, Elisabeth Huber-Sanwald, Laura F. Huenneke, Robert B. Jackson, Ann Kinzig, Rik Leemans, David M. Lodge, Harold A. Mooney, Martin Oesterheld, N. LeRoy Poff, Martin T. Sykes, Brian H. Walker, Marilyn Walker, and Diana H. Wall. 2000. "Global Biodiversity Scenarios for the Year 2100." *Science* 287, no. 5459 (March): 1770-1774.

Salmon, J. Meghan, Mark A Friedl, Steve Frolking, Dominik Wisser, and Ellen M. Douglas. 2015. "Global Rain-fed Irrigated, and Paddy Croplands: A New High Resolution Map Derived from Remote Sensing, Crop Inventories and Climate Data." *International Journal of Applied Earth Observation and Geoinformation* 38: 321-334.

Schürkmann, A. K., A. Biewald, and S. Rolinksi. 2014. "A Global Approach to Estimating the Benefit-Cost Ratio of Water Supply Measures in the Agricultural Sector." In *the Global Water System in the Anthropocene: Challenges for Science and Governance*, edited by

Anik Bhaduri, Janos Bogardi, and Sina Marx, 73-87. Switzerland: Springer International Publishing.

Schwartz, Mark D. 1994. "Monitoring Global Change with Phenology: The Case of the Spring Green Wave." *International Journal of Biometeorology* 38: 18-22.

Thelin, Gail P., and Frederick J. Heimes. 1987. *Mapping Irrigated Cropland from Landsat Data for Determination of Water Use from the High Plains Aquifer in Parts of Colorado, Kansas, Nebraska, New Mexico, Oklahoma, South Dakota, Texas, and Wyoming*, US Department of the Interior, US Geological Survey. US Geological Survey Professional Paper 1400-C. Washington: US Government Printing Office.

Thenkabail, Prasad S., Mitchell Schull, and Hugh Turral. 2005. "Ganges and Indus River Basin Land Use/Land Cover (LULC) and Irrigated Area Mapping Using Continuous Streams of MODIS Data." *Remote Sensing of Environment* 95: 317-341.

Thenkabail, Prasad S., Chandrashekhar M. Biradar, Praveen Noojipady, Xueliang Cai, Venkateswarlu Dheeravath, Yanjie Li, Manohar Velpuri, MuraliKrishna Gumma, and Suraj Pandey. 2007. "Sub-pixel Area Calculation Methods for Estimating Irrigated Areas." *Sensors* 7: 2519-2538.

Thenkabail, Prasad S., Chandrashekhar M. Biradar, Praveen Noojipady, Venkateswarlu Dheeravath, Yuanjie Li, Manohar Velpuri, Muralikrishna Gumma, Obi Reddy P. Gangalakunta, Hugh Turral, Xueliang Cai, Jagath Vithanage, Mitchell A. Schull, and Rishiraj Dutta. 2009. "Global Irrigated Area Map (GIAM) Derived from Remote Sensing, for the End of the Last Millenium." *International Journal of Remote Sensing* 30, no. 14 (July): 3679-3733.

Thenkabail, Prasad S., and Zhuoting Wu. 2012. "An Automated Cropland Classification Algorithm (ACCA) for Tajikistan by Combining Landsat, MODIS, and Secondary Data." *Remote Sensing* 4: 2890-2918.

The World Bank. 2018. "Water in Agriculture." Understanding Poverty. Accessed September 24, 2018. https://www.worldbank.org/en/topic/water-in-agriculture.

Tian, Yong, Hongjie Xie, and Randy Keller. 2007. "Suitable Remote Sensing Method and Data for Mapping and Measuring Active Crop Fields." *International Journal of Remote Sensing* 28, no. 2 (January): 395-411.

Tucker, Compton J. 1979. "Red and Photographic Infrared Linear Combinations for Monitoring Vegetation." *Remote Sensing of Environment* 8: 127-150.

US Department of Agriculture (USDA). National Agricultural Statistics Service (NASS). 2014. *2012 Census of Agriculture: Farm and Ranch Irrigation Survey (2013)*, November.

USDA. 2018. "Census of Agriculture." NASS. Accessed January 4, 2018. https://www.agcensus.usda.gov/.

US Department of the Interior (USDI). US Geological Survey (USGS). 2018a. *Product Guide: Landsat 4-7 Surface Reflectance (LEDAPS) Product*, March.

⸺. 2018b. *Product Guide*: *Landsat 8 Surface Reflectance Code (LaSRC) Product*, March.

USGS. 2018. "TNPDownload *(V1.0).*" The National Map. Last Modified October 19, 2018. Accessed October 22, 2018. https://viewer.nationalmap.gov/basic/.

Wada, Yoshihide, Dominik Wisser, Stephanie Eisner, Martina Flörke, Dieter Gerten, Ingjerd Haddeland, Naota Hanasaki, Yoshimitsu Masaki, Felix T. Portmann, Tobias Stacke, Zachary Tessler, and Jacob Schewe. 2013. "Multimodel Projections and Uncertainties of Irrigation Water Demand under Climate Change." *Geophysical Research Letters* 40: 4626-4632.

Wang, J., P. M. Rich, and K. P. Price. 2003. "Temporal Responses of NDVI to Precipitation and Temperature in the Central Great Plains, USA." *International Journal of Remote Sensing* 24, no. 11: 2345-2364.

Weare, Bryan C., and Hui Du. 2008. "Modelling Regional Climate Changes: Influences of Recent Global Warming and Irrigation in California." *International Journal of Climatology* 28: 1201-1212.

Wiegand, C. L., J. H. Everitt, and A. J. Richardson. 1992. "Comparison of Multispectral Video and SPOT-1 HRV Observations for Cotton Affected by Soil Salinity." *International Journal of Remote Sensing* 13, no. 8: 1511-1525.

Winter, Thomas C., Judson W. Harvey, O. Lehn Franke, and William M. Alley. 1998. *Ground Water and Surface Water: A Single Resource*, US Department of the Interior. US Geological Survey. US Geological Survey Circular 1139. Denver, Colorado: US Geological Survey.